A COMPOSITE GEOPHYSICAL INVESTIGATION OF BURUM DOLOMITIC MARBLE DEPOSIT, FEDERAL CAPITAI TERRITORY, NIGERIA

BY

SYLVANUS CHUKWUMA ANEKE, B.Sc (Hons) Unife

Ihesis submitted to the Ahmadu Bello University in partial fulfillment of the requirements for the award of the degree of Master of Science in Applied Geophysics.

Department of Physics
Faculty of Science
Ahmadu BPLLO University, Zaria

November, 1988

DECLARATION

It is hereby declared that:

. the report presented in this thesis is the result of the original research carried out by the author under the supervision of Dr. C.O. Ajayi;

'. this thesis has not been submitted in whatever form to any other Institution, organization or body other than Ahmadu Bello University, Zaria, Nigeria, for the award of any Degree;

!. the work of others cited is duly acknowledged and referenced.

(S.C. ANEKE)
Author

(DR. C.O. AJAYI)
Supervisor

A. B. U. ZARIA

NOVEMBER 1988

CERTIFICATION

This Thesis entitled - A Composite Geophysical Investigation of Burum Dolomitic Marble Deposit, Federal Capital Territory, Nigeria, by S.C. Aneke meets the regulations governing the award of the degree of Master of Science of Ahmadu Bello University, and is approved for its contribution to knowledge and literary presentation.

.....	.....
Dr. C.O. Ajayi	Date
Chairman, Supervisory Committee.	
.....	.....
Dr. I.B. Osazuwa	Date
Member, Supervisory Committee.	
.....	.....
Dr. J. Adetunji	Date
Head of Department	
.....	12-1-96
Prof. D.I. Sapor	Date
Dean, Post-graduate School	

DEDICATION

This Thesis is dedicated to my Wife and Children for their patience and understanding.

ACKNOWLEDGEMENT

I hereby express my profound gratitude to my supervisor Dr. C.O. Ajayi of Physics Department. His keen interest and immeasurable contributions to the successful completion of this project is highly appreciated. I also appreciate with thanks, the very useful contributions of my Co-supervisor Dr. I.B. Osazuwa. My thanks also go to Dr. S.B. Ojo and Mr. M.N. Umego for their inspiration and brotherly advice.

My special thanks also go to Mr. A.D. Famuboni, the Director and Chief Executive, Steel Raw Materials Exploration Agency, Kaduna, Mr. O.E. Okeudo Assistant Director (Operations), SRMEA and Mr. A. George, the Head of Geophysics Section SRMEA, for making available the funds, men and material with which this project was executed. I am also grateful to Mr. E.A. Mogekwu of National Water Resources Institute, Kaduna for allowing me to make use of their Computer for the interpretation of my field data. The co-operation and assistance of Mr. Owolabi during the interpretation is highly appreciated. My sincere thanks also go to Ogbuibor Petrus Agballah, Messrs G.N. Akubue, F.A. Otako and T. Oyinloye for their interest, encouragement and support during the execution of this project.

I am also highly indebted to my colleagues, who provided vital information or contributed in one way or the other, to the successful completion of this work. They include Messrs O. Fagbe, E. Emelis, E. Oguike, C. Awak, F. Williams, O. Achohwora and Lecky Yusuf.

Finally, I wish to appreciate with thanks the roles of Mr. Neboh Emmanuel of AREWA METAL CONTAINERS LIMITED (ARMECO) for typing this project and Mr. A.B. Fagbemi for tracing all the figures.

A B S T R A C T

A composite geophysical investigation was carried out on the Dolomitic marble deposit at Burum. In the Federal Capital Territory. The aim was to delineate the lateral extent of the deposit, provide a preliminary estimate of its' quantity and to identify the geotechnical and hydrogeological conditions of the deposit. Ihe Electrical Resistivity Profiling, Vertical Electrical Sounding and VLF (EM) Methods were employed for the investigation.

There is a close match and striking agreement between the outlines of the marble deposit (fig. 4.1) as obtained from the resistivity profiling (fig. 2.8) and VLF (EM) data (figs 2.11, 2.12 and 2.13). The figures show that the deposit extends laterally for about 950m in the NNE - SSW direction with an average width of about 120m.

Based on geophysical (VES) and borehole data, the shape of the deposit has been approximated to that of an inverted triangular-prism with a rectangular top model (fig. 4.2). It has a variable central axial thickness with an average of about 61m. The minimum ore reserve of the deposit was consequently calculated to be about 9.74 mi11ion tonnes.

The VES results indicate four geoelectric layers with resistivities of 250 to 2000 Ohm - m *for* the firsl layer, 25 Lo 60 Ohm - m for the second layer, 65 to 96 Ohm - m for the third and 1950 to 4000 Ohm - m for the fourth layer. The Third layer is replaced in some regions by a geoelectric unit with resistivity of 105 to 130 Ohm - m.

The results show a thickness varying from 0.4 to 0.9 for the first layer, 2 to 20m for the second layer, 10 to 46m for the third layer. The other geoelectric unit which replaced the third layer in some regions has a thickness varying between 39.5 and 102m, while the fourth layer is of infinite thickness. These results are in agreement with those deduced from borehole data from the area.

The first two geoelectric layers constitute the overburden whose thickness varies between 0 and 25m within the project *area.* The total volume of the overburden overlying the deposit is estimated to be about 0.137 x 10^6 m^3.The region bounding the deposit to the north has comparatively lower apparent resistivity values (18 - 60 Ohm - m) than the region bounding it to the south (with apparent resistivity values of 100 to 400 Ohm - mV Using the results of the investigations, comparatively weak zones have been identified and some pre-mining and hydrogeological conditions of the deposit have been highlighted.

TABLE OF CONTENT

TITLE			PAGE
Acknowledgement	....	....	v
Abstract	....	....	vi
Table of Content	....	....	viii
List of Tables	....	....	xi
List of Figures	....	....	xii
List of Appendices	....	....	xiv
Abbreviations, Glossaries and Symbols	....	....	xv
CHAPTER 1: INTRODUCTION			01
1.1 Location of study area	....	....	01
1.2 Climate, Topography and Drainage	....	....	01
1.3 Geology of the area	....	....	03
1.4 Properties and uses of marble	....	....	06
1.5 Previous works	....	....	06
1.6 Aims of the present work	....	....	07
1.7 Choice of the geophysical methods used	....		07
CHAPTER 2: PRINCIPLES OF METHODS USED, DATA COLLECTION AND REDUCTION			11
2.1 Principles and theories of methods used	....		11
2.1.1 The Electrical Resistivity Methods	....		11
2.1.2 The VLF (EM) Method	....	....	19
2.2 Data Collection	....	....	20
2.2.1 Instrumentation	....	....	20
2.2.2 Horizontal Resistivity Profiling	....	....	22

2.2.3 Vertical Electrical Sounding 24

2.2.4 VLF (EM) Survey 26

2.3 Data Reduction and Interpretation 28

2.3.1 The Horizontal Resistivity Profiling data 28

2.3.2 The Vertical Electrical Sounding data 31

2.3.3 The VLF (EM) data 36

2.3.4 Limitations 42

CHAPTER 3: R E S U L T S 44

3.1 Results from Resistivity Profiling 44

3.1.1 Profile L_4 44

3.1.2 Profile L_5 44

3.1.3 Iso-resistivity Contour map 45

3.1.4 Deductions from Resistivity Profiling Results ... 45

3.2 Results from VLF Survey 46

3.2.1 VLF Profile across P_0 47

3.2.2 VLF Profile across P_2 47

3.2.3 VLF (EM) Contour map 47

3.2.4 Deductions from results of the VLF Survey 48

3.3 Results of the Vertical Electrical Soundings 49

3.3.1 Geoelectric Section for Traverse Line L_6 (AA') 49

3.3.2 Geoelectric Section for Traverse Line L_4 (BB') 51

3.3.3 Geoelectric Section for Traverse Line L_2 (CC') 53

3.3.4 Geoelectric Section for Profile DD' 55

3.3.5 Geoelectric Section for Profile P_3 (EE') 55

3.3.6 Geologic sections from borehole data 58

3.3.7 Correlating the Geoelectrical and Geologic sections 60

CHAPTER 4:

D I S C U S S I O N S 64

4.1 Outline of the Marble deposit 64

4.2 Preliminary Estimation of the Quantity of the Marble deposit 64

4.3 Pre-mining conditions of the deposit 69

4.4 Present hydrogeological conditions 72

CHAPTER 5:

CONCLUSIONS AND RECOMMENDATIONS 73

5.1 Conclusions 73

5.2 Recommendations and suggestions for future work 76

References 77

Appendix I 81

Appendix II 85

List of Tables

TABLE	TITLE	PAGE
2.1	Typical Resistivity Sounding Field and Computed Data.....	34

List of Figures

FIGURE			PAGE
1.1	:	Simplified geologic map of Nigeria showing the project area	02
1.2	:	A Topographic map of the study area showing locations of Data stations	04
2.1	:	The Spherical Co-ordinates	14
2.2	:	Scheme of Simple Field Apparatus for Resistivity Measurements	16
2.3	:	The Schlumberger Electrode Configuration	18
2.4	:	Block diagram of EM 16 VLF Equipment	23
2.5	:	A Base map showing the location of the VES points, geoelectric sections and Boreholes	25
2.6	:	Resistivity profile across L_4	29
2.7	:	Resistivity profile across L_5	30
2.8	:	Iso-resistivity contour map at AB/2=20m	32
2.9	:	Resistivity Depth Sounding curve for VES 30	33
2.10a	:	The initial Model fed into the Computer for VES 6	37
2.10b	:	The Final Intepreted Model Obtained for VES 6	37
2.11	:	Stacked VLF (EM) Data showing the In-phase and quadrature components	38
2.12	:	Contour Map of Filtered VLF Data (In-phase components)	40
2.13	:	Contour Map of First Derivatives of the VLF Data (In-phase components)	41
3.1	:	Geoelectric and Geologic section for Traverse Line L_6 (AA')	50
3.2	:	Geoelectric and Geologic section for Traverse Line L_4 (BB')	52

FIGURE			PAGE
3.3	:	Geoelectric and Geologic Section across Line L_2 (CC')	54
3.4	:	Geoelectric and Geologic Section Section for Profile DD'	56
3.5	:	Geoelectric and Geologic Section across Profile P_3 (EE')	57
3.6a	:	Geologic Section from BH.2	59
3.6b	:	Geologic Section from BH.11	59
3.7a	:	Geoelectric and Geologic Section Beneath L_4 P_0	62
3.7b	:	Geoelectric and Geologic Section Beneath L_7 P_{-1}	62
4.1	:	A Geologic Map of the Project site showing the Delineated Marble Deposit.....	65
4.2	:	A 3-Dimensional sketch of the Marble deposit	67
4.3	:	A contour map showing the thickness of the Marble Deposit	68
4.4	:	A contour Map of the Total Overburden Thickness	70

List of Appendices

APPENDIX	TITLE	PAGE
I	Geologic sections from Borehole data...	81
II	Interpreted VES Field curves.....	85

ABBREVIATIONS, GLOSSARIES AND SYMBOLS

SYMBOL/ABBREVIATION		MEANING
A.C.	-	Alternating current
D.C.	-	Direct Current
E	-	East
W	-	West
N	-	North
S	-	South
VES	-	Vertical Electrical Sounding
VLF	-	Very Low Frequency
EM	-	Electromagnetic
Km	-	Kilometer
mm	-	Millimeter
m	-	Meter
%	-	Percent
^{o}C	-	Degrees centigrade
Kg	-	Kilogram
ρ	-	Resistivity
ρ_a	-	Apparent resistivity
KHz	-	Kilohertz
m/s	-	Meter per second
Ω-m	-	Ohm - meters

CHAPTER 1

INTRODUCTION

1.1 Location of the Study Area

The geophysical investigations discussed in this work were carried out at a site located about 2km west of Burum Village. Burum is located 25km South-East of Abuja, in the Federal Capital Territory. The study area which covers an area of about 0.58 km^2, approximately lies on longitude $7.50^{O}E$ and latitude $9^{O}N$ (fig. I.1).

Burum is a small and sparsely populated village. The inhabitants are mostly Gwaris, although increasing economic activities at the Federal Capital Territory has attracted Nigerians from different parts of the Country to the Village.

1.2 Climate, topography and Drainage

The study area lies within the Savannah belt of West Africa and it is, therefore, essentially a grassland with patches of semi-deciduous forests along streams and depressions. It has a wet season from April to October which is followed by a dry season from November to March. From November to early March, the North-East trade wind, known as the "Harmattan", keeps the humidity extremely low.

Meteorological data obtained over a six-year period (1981-1987) at the Lower Usman Dam, Abuja, about 40km north of Burum, show that the monthly rainfall varies - from 0 to 400mm, with an average of 132.59mm. The humidity ranges from about 24% in January to about 87% in August.

YASHIM IBRAHIM LIBRARY

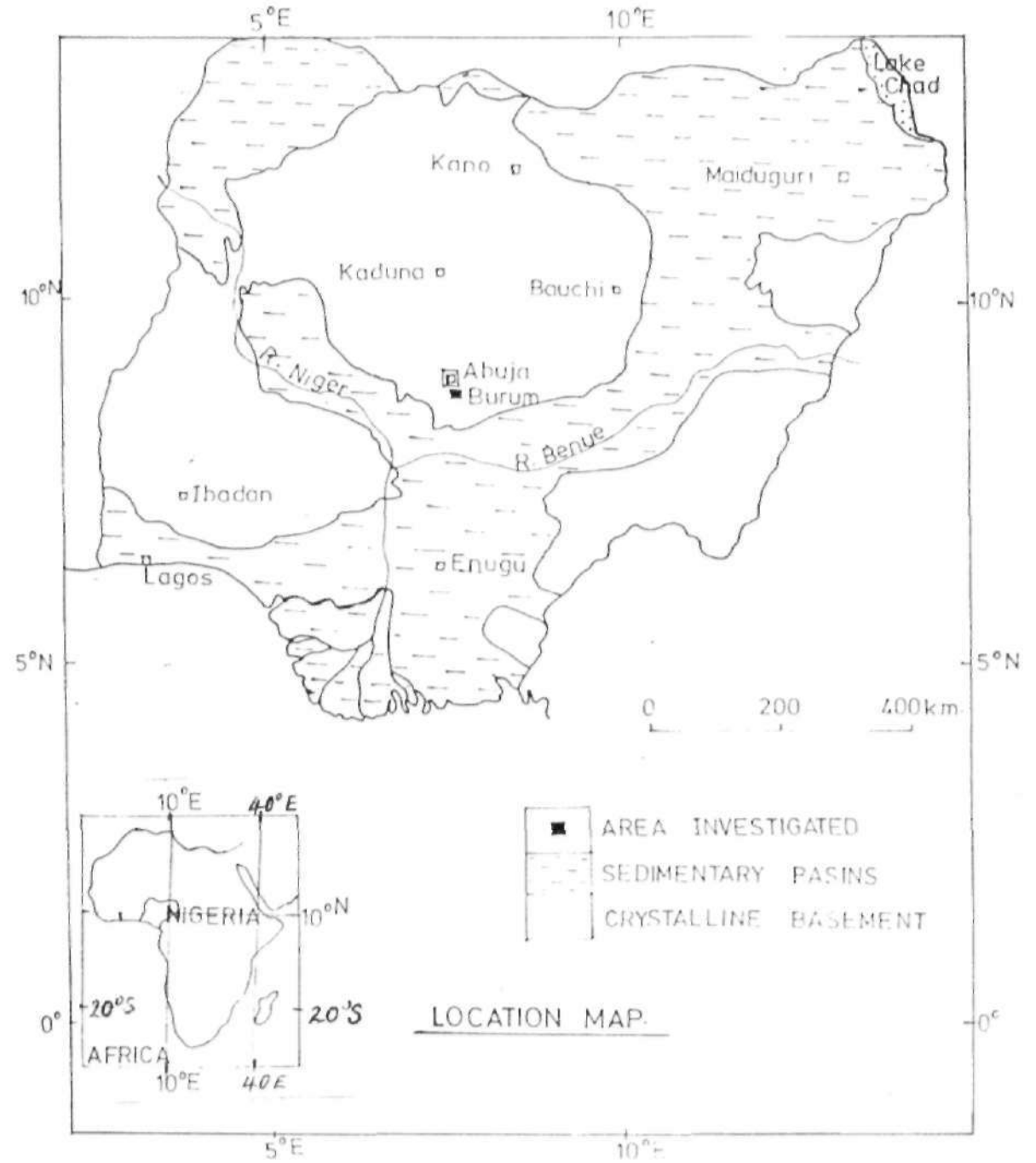


Fig. 1.1 MAP OF NIGERIA SHOWING THE PROJECT AREA (Insert Map of Africa)

Daily temperatures vary between about 24^{O}C in July to about 30^{O}C in March.

The monthly evaporation is lowest in August with a value of about 38.50mm and highest in March with a value of about 399mm. The meteorological information obtained from Abuja Airport, located 30km West of Burum are not quite different from those collected from the Lower Usman Dam.

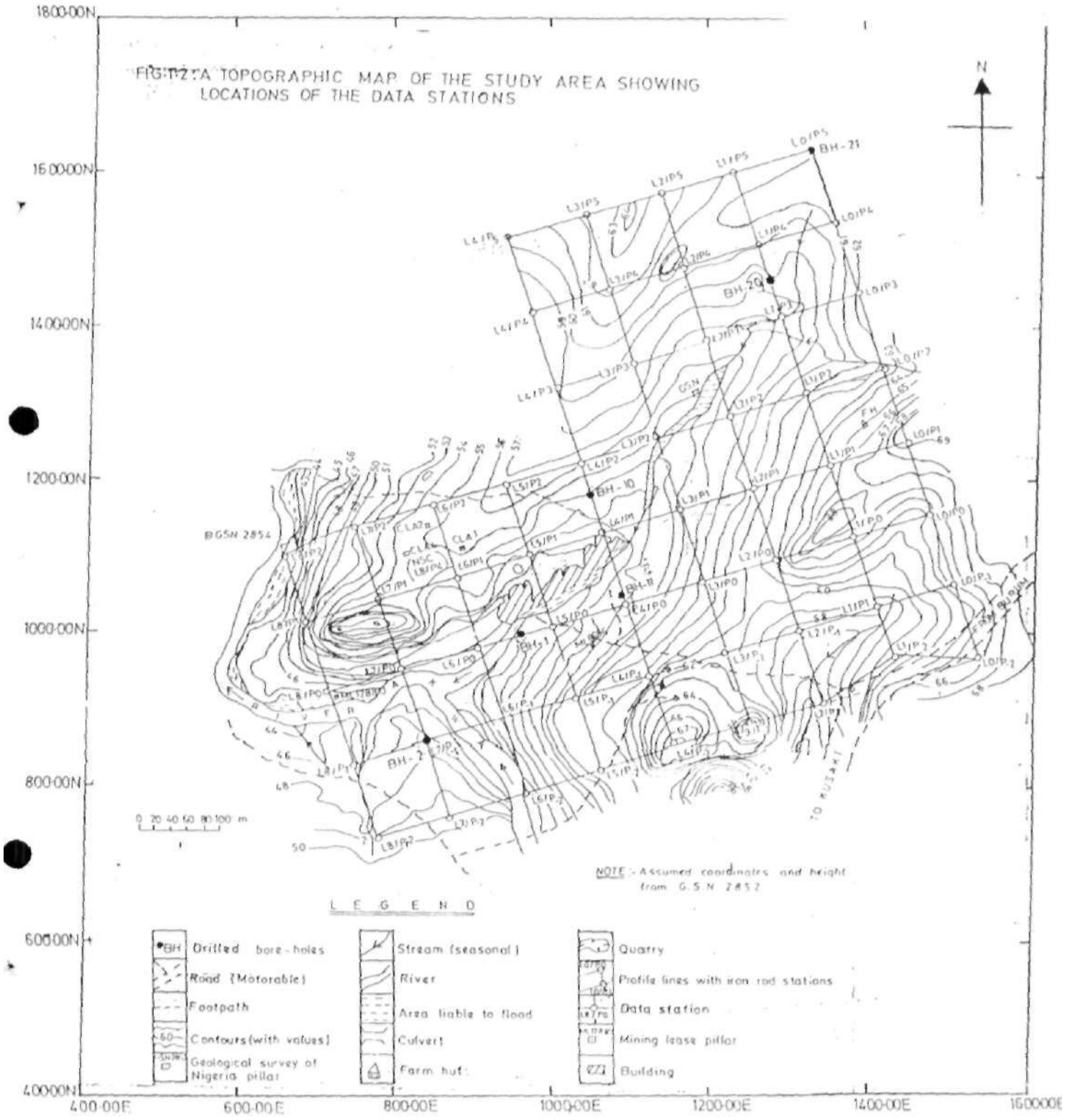
Burum is surrounded by a number of isolated hills such as the Buru, Kusaki and Tarka Lafia hills. The area of interest is, however, a gently undulating broad Valley, which is flanked by these elongated hills. A perennial stream which flows in the NE - SW direction flows through the valley into River Tarkwa which constitutes the major drainage channel in the area (fig. 1.2).

1.3 Geology of the Area

Burum area lies within the southern extremity of the N.W. Nigerian (Birnin Gwari) schist belt which was deposited on the migmatite - gneiss basement complex during the Pan African Orogeny (Grant, 1978).

The Basement complex which constitutes the oldest exposed rocks in Nigeria is the end product of at least two major orogenic cycles (Oyawoye, 1964). The later of these cycles is generally believed to have extended from Late Precambrian to Lower Paleozoic. According to Ofomata et el (1973), these rocks have a long history during which they suffered varying degrees of alteration by heat and pressure. They were subsequently folded, crumpled and raised into mountain ranges and then eroded. The basement complex comprises the remnants of an ancient sedimentary series - the metasediments which have been transformed into anatectic migmatites and granites (Ofomata et el, 1973).

FIG: 1.2 : A TOPOGRAPHIC MAP OF THE STUDY AREA SHOWING LOCATIONS OF THE DATA STATIONS



The metasediments include quartzo - feldspathic, biotite and hornblende - gneisses, schists, quartzites, marbles and calc-silicate rocks (Wright and McCurry, 1970).

The rock types exposed within the area of investigation include different varieties of schists, ranging from fine grained, thinly laminated green schists, through medium grained, layered grey schists to hard, massive black schists (Awak, 1988). The presence of fine grained laminated schists suggests a quiet water condition of sedimentation (Fitcher et el, 1985). These schists may have been derived from argillitic rocks such as siltstone, mudstone or shales, which have metamorphosed in the low green schist facies. These sediments might date to Pan - African events and were most likely deposited in the early Precambrian Basement (Turner, 1983).

Other rock types in the area include quartzo - feldspathic rocks, pegmatites, granite gneiss, light grey to black amphibolite Gneiss, mylonites, dolomitic marble and quartzites. The schists and pegmatites are micaeous and contain a lot of quartz veins.

Trustwell and Cope (1963) and Ajibade (1971) reported from their respective structural analysis of the Birnin Gwari schist belt, a complex tectonic history in terms of deformation stages. It is, therefore, likely that Burum area had its' due share of this complex geological history. This is supported by the strike and dip measurements taken in the area (Achelwora,1988). The general trend of the rocks in the area, as indicated by 68.5% of the strike measurements taken in the area is N 30^{O}E. About 15% of the measurements indicated trends of between N 15^{O}E and N 20^{O}E while 16.5% showed strikes of between N 45^{O}E and N 50^{O}E.

Dips of between 70^{O} and 85^{O} were recorded. 57.5% of the dip measurements were eastwards while westward dips accounted for 42.5%.

1.4 Properties and Uses of Marble

Marble is a granoblastic, fine to coarse grained, calcerous metamorphic rock derived from the recrystallization of limestone to produce a granular mosaic of calcite and/or dolomite crystals (Deeson, 1973). From results of laboratory tests carried out at Steel Raw Materials Exploration Agency, Kaduna, Burum marble is dolomitic and shows a streaky alteration of light and dark patches. It has an average density of 2.8×10^{3} Kg/M^{3}, and a hardness of between 3.5 and 4 in Mohs scale. Its resistivity values range between 100 and 150 Ohm - m. Dolomitic marbles commonly contain magnesium bearing silicates such as pyroxenes, amphiboles and serpentine (Read and Watson, 1973).

Dolomitic marble is required for use as a fluxing material for the sintering plant at Ajaokuta Steel complex. It is also in great industrial demanddue to its use in cement factories, manufacture of ceramics, tiles and as ornamental and statuary stones.

1.5 Previous Works

No known earlier geophysical investigation has been carried out in the project area. However, a number of trenches exist within the area. This suggests that Messrs W.P. Syndicate, the Mining Company currently working the deposit of interest, may have carried out some pre-mining geological investigation in the area.

On the other hand, it is certain that the Steel Raw Materials Exploration Agency (National Steel Council, Kaduna) has carried out some intensive geological and hydrogeological studies of the area. The Agency is currently undertaking some exploratory drilling within the area.

1.6 Aims of the Present Work

The present geophysical investigation, which is at the instance of my employers - The Steel Raw Materials Exploration Agency (National Steel Council, Kaduna), is aimed at:

i) Delineating the boundary of the Burum marble deposit within the host rock.

ii) Estimating the ore reserve of the deposit.

iii) Identifying geologic structures such as faults, fractures or joints and/or weak and weathered zones within the deposit, in order to determine the Pre-mining, structural and hydrogeological conditions of the deposit.

1.7 Choice of Geophysical Methods Used

Physical properties of ore bodies such as density, magnetic susceptibility, elasticity, electrical conductivity etc, generally differ from those of the host rocks within which they occur. Consequently, each of the four main methods of geophysical prospecting; gravity, magnetics, seismic and electrical methods is capable of furnishing useful information in a geophysical investigation of an ore deposit, using the contrast between specific parameters of the ore and the host rocks. The choice of geophysical methods to be employed in any investigation will, therefore, depend among other factors, on which of these physical parameters of the ore that show appreciable contrasts with those of the host rocks.

The choice of the geophysical methods used in this investigation was, therefore, largely influenced by considerations of the contrasts between the physical properties of marble and those of the host rocks (granites, gneiss, schists etc.)

The gravity method is a rapid method of determining the gross configuration of sub-surface structures where good density contrasts exist between the sub-surface materials. The method could not be used for this work because the density of marble (2.8×10^3 Kg.m^{-3}) lies within those of the host rocks (Granite - 2.78×10^3 Kg m^{-3}, Gneiss - 2.72×10^3 Kg m^{-3}, and Schist - 2.85×10^3 Kg m^{-3}). Hence, it would be difficult to differentiate the gravity anomalies due to density contrast between the marble and granite from that between schist and granite, as both have positive density contrasts.

The magnetic method on the other hand, involves measurement of the direction, gradient or intensity of the earth's magnetic field and the interpretation of variation in these quantities due to contrasts in magnetic susceptibilities of the rocks within the area. It had been hoped that the magnetic method would be very useful in the present investigation because of the significantly higher magnetic susceptibilities of the host rocks (granite - 200×10^6 emu; gneiss - 10 - 2000×10^6 emu; schist - 120×10^6 emu) compared with that of the marble (Dolomite - $0\text{-}75 \times 10^6$ emu). However, this method had to be abandoned due to the poor quality of the data obtained. The magnetic data was marred by a lot of noise. The noise may have been due to inhomogeneity in the rock which resulted in variable magnetic susceptibility.

The seismic method basically involves the timing of artificially generated pulses of elastic energy propagated through the ground and picked up by electromagnetic transducers operating as detectors. The parameters of interest are the propagation velocities and the geometry of the propagation path. The partition of energy of compressional waves, incident on an interface between two media, into a reflected and a refracted part is governed by the difference in the acoustic impedances of the media. The compressional acoustic impedance of a medium is the product of the longitudinal wave velocity and the density of the medium. The compressional wave velocities of rocks similar to those in the area and published in Parasnis (1971) are as follows:

- Marble (3,750 - 6,940 m/s), Granite (4,750 - 6,000 m/s), Gneiss (3,500 - 7,500 m/s) and Schist (4,900 m/s).

The compressional wave velocities of the various units are, therefore, quite variable and lie within the same order of magnitude. Seismic refraction method was not attempted for this investigtion due to non-availability of functional refraction equipment.

In the electrical methods, the observed electric anomalies of sub-surface conductors depend upon the electric resistivity contrast between the conductors and the host rocks. Electric resistivity is one of the most variable of all physical properties of rocks. The causes of this variability are numerous.

The conductivities and mode of distribution of the conducting minerals in a rock sample have a dominating effect on the resistivity of a sample, but other factors such as fractures, water content, inter-facial resistance between crystals etc, also come into play. In polycrystalline aggregates, the resistivity is also affected by the grain size. The coarser the grain size, the higher the resistivity, other things being equal.

According to Telford, et al (1976), the resistivity ranges (in ohm - meters) of the various rock units similar to those found in the project area are as follows:

- Marble (10^2 - 2.5×10^8), Granite (3×10^2 - 10^6), Gneiss (6.8×10^4 - 3×10^6) and Schist (20 - 10^4).

In spite of the variability and the over-laping nature of resistivity of these rocks, a preliminary investigation revealed an appreciable resistivity contrast between the Burum marble and the host rocks. The electrical resistivity method was, therefore, considered and employed as one of the most appropriate geophysical methods for the present investigation.

The electromagnetic (VLF) method involves measurement of intensity, direction and phase difference between a primary field and the resultant field due to a secondary field produced by a time varying electromagnetic field. Any variation in the conductivity of sub-surface materials will give rise to an inhomogeneity in the resultant electromagnetic field observed on the surface. Since the preliminary investigation revealed signifi cant resistivity (and hence conductivity) contrast, the VLF (EM) Method was considered and employed as another appropriate geophysical method for the present investigation.

CHAPTER 2

PRINCIPLES OF METHODS USED, DATA COLLECTION AND REDUCTION

2.1 Principles and Theories of Methods Used

As discussed above, the electrical properties of the sub-surface can be explored using the electrical and/or the electromagnetic methods of geophysical prospecting. In most rocks, electrical conduction is mainly electrolytic because most rocks are insulators and therefore, their grains cannot conduct electronically. Rather, conduction takes place through interstitial water which is usually present and contains some dissolved salts. The resistivity of a formation, therefore, often depends on the resistivity of the contained electrolyte which is inversely related to the porosity and degree of saturation of the formation (Vingoe, 1972). In crystalline rocks with relatively low porosities, conduction is mainly along cracks and fissures. The degrees to which these are present usually determine the resistivity of the formation (Vingoe, 1972).

The principles of the two methods used in the investigation are briefly discussed below.

2.1.1 The Electrical Resistivity Methods

Basically, if a direct or low frequency alternating current is introduced into the ground, any sub-surface variation in conductivity alters the current flow within the earth. This alteration, is also affected by the distribution of the anomalous electric potential.

The degree to which the potential at the surface is affected depends upon the size, location, shape and conductivity of the material within the ground. Consequently, measurements of the electric potential at the surface yields information about the sub-surface distribution of this material.

In resistivity surveys, the normal practice is to pass current into the ground by means of two electrodes and to measure the potential difference due to this current between a second pair of electrodes placed in line between them. From the value of the potential difference, the current applied and the electrode separation, the apparent resistivity of the sub-surface can be calculated as will be shown later in the text.

One of the principal advantages of the electrical resistivity method is that it has great resolving power. It uses an artificial source of energy, rather than the natural fields of force such as are used in the gravity and magnetic methods. Consequently, the source - detector separation can be altered to achieve the optimum Separation which effectively controls the depth of measurement.

The simplest approach to the theoretical study of the earth resistivity measurements is to consider the case of a completely homogeneous, isotropic earth. The equation giving the potential about a single point source can be developed from two basic considerations as shown below:

(i) From Ohm's Law we have

$$\bar{E} = \rho \bar{J} \quad \ldots\ldots\ldots\ldots\ldots\ldots\ldots\ldots\ldots\ldots (1)$$

where $\bar{E}$ = the electric field intensity

$\bar{J}$ = the current density

and ρ = the resistivity of the medium

(ii) From the divergence condition, we have

$$\nabla \cdot \bar{J} = 0 \quad \ldots\ldots\ldots\ldots\ldots\ldots\ldots\ldots\ldots\ldots (2)$$

That is, all the current going into a piece of material must leave through the other side, unless there is a current source or sink within that piece of material.

Therefore, the divergence of the current density vector $\bar{J}$ must be zero everywhere except at the current source. The $\bar{E}$ in (1) is related to the scaler potential function U as follows:

$$\bar{E} = -\nabla U \quad \ldots\ldots\ldots\ldots\ldots\ldots\ldots\ldots\ldots\ldots (3)$$

Combining equation (1) and (3) we have

$$\bar{J} = -\frac{1}{\rho}\nabla U \quad \ldots\ldots\ldots\ldots\ldots\ldots\ldots\ldots\ldots\ldots (4)$$

It follows from equation (2) that

i.e $$\nabla \cdot \left(\frac{1}{\rho}\nabla U\right) = 0 = 0 \quad \ldots\ldots\ldots\ldots\ldots\ldots\ldots\ldots\ldots\ldots (5)$$

If ρ remains constant, as is the case in homogeneous medium, then (5) gives the Laplace's equation:

$$\nabla^2 U = 0 \quad \ldots\ldots\ldots\ldots\ldots\ldots\ldots\ldots\ldots\ldots (6)$$

In spherical co-ordinates, the laplace equation is

$$\frac{\partial}{\partial r}\left(r^2 \frac{\partial U}{\partial r}\right) + \frac{1}{r^2 \sin\theta}\frac{\partial}{\partial \theta}\left(\sin\theta \frac{\partial U}{\partial \theta}\right) + \frac{1}{r^2 \sin^2\theta}\frac{\partial^2 U}{\partial \varphi^2} = 0 \quad \ldots\ldots (7)$$

where the spherical co-ordinates r, φ, θ are related to the cartesian co-ordinates as follows:

$x = r \cos\psi \sin\theta$

$y = r \sin\psi \sin\theta$

$z = r \cos\psi$

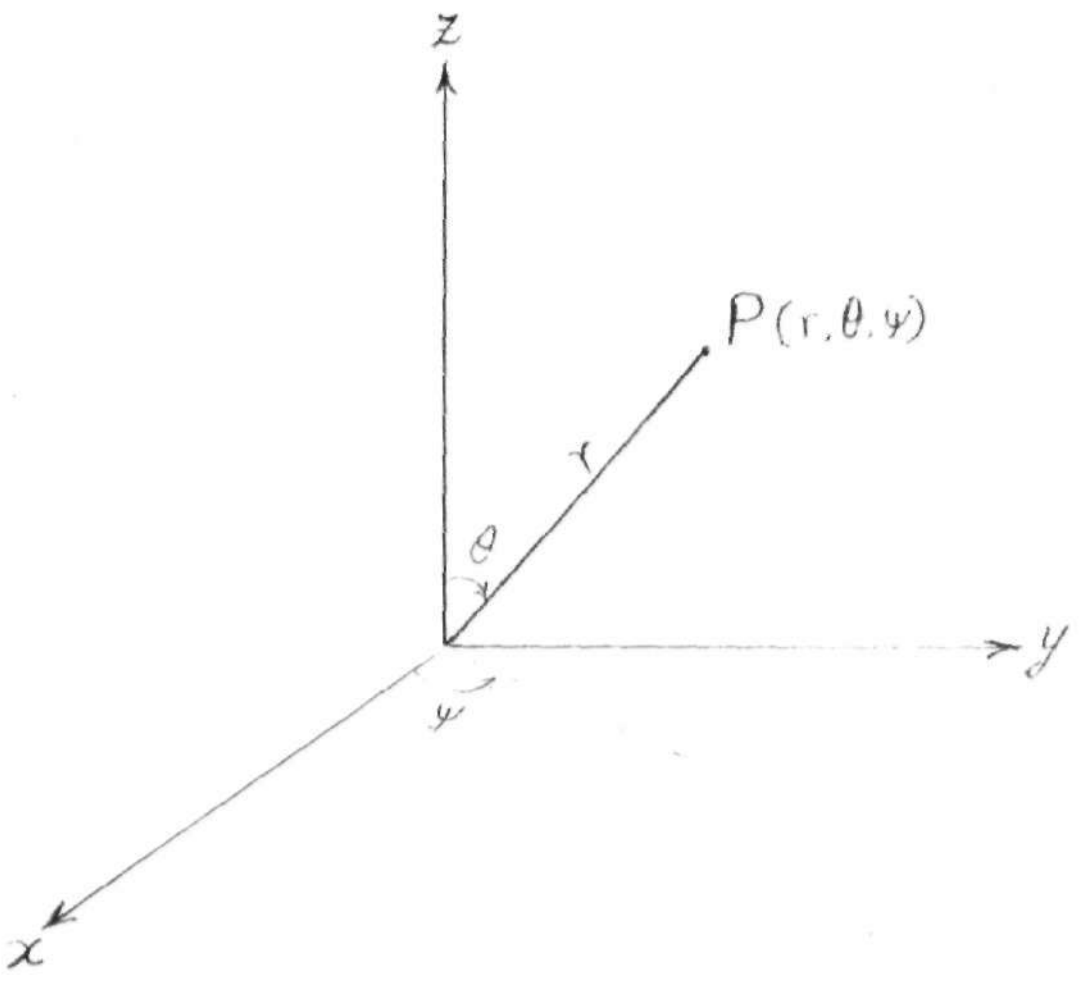


Fig. 2.1: The Spherical Co-ordinates

If only a single current source is considered, complete symmetry of current flow with respect to the ψ and θ directions may be assumed. For a current I introduced into an infinite homogeneous medium, the potential at a distance r from a point will only be a function of r. Hence, equation (7) becomes:

$$\frac{d^2U}{dr^2} + \frac{2}{r}\frac{dU}{dr} = 0 \qquad \text{.....(8)}$$

Which,after integration and elimination of the constant of integration, has a solution given as:

$$U = \frac{I\rho}{2\pi}\cdot\frac{1}{r} \qquad \text{.....(9)}$$

When we have several sources of current as against the single source assumed so far, the total potential at an observation point is calculated by adding the potential distribution from each source considered independently. So for n sources of current, equation (9) becomes:

$$U_n = \frac{\rho}{2\pi}\left(\frac{I_1}{r_1} + \frac{I_2}{r_2} + \text{-----} + \frac{I_n}{r_n}\right) \text{.....(10)}$$

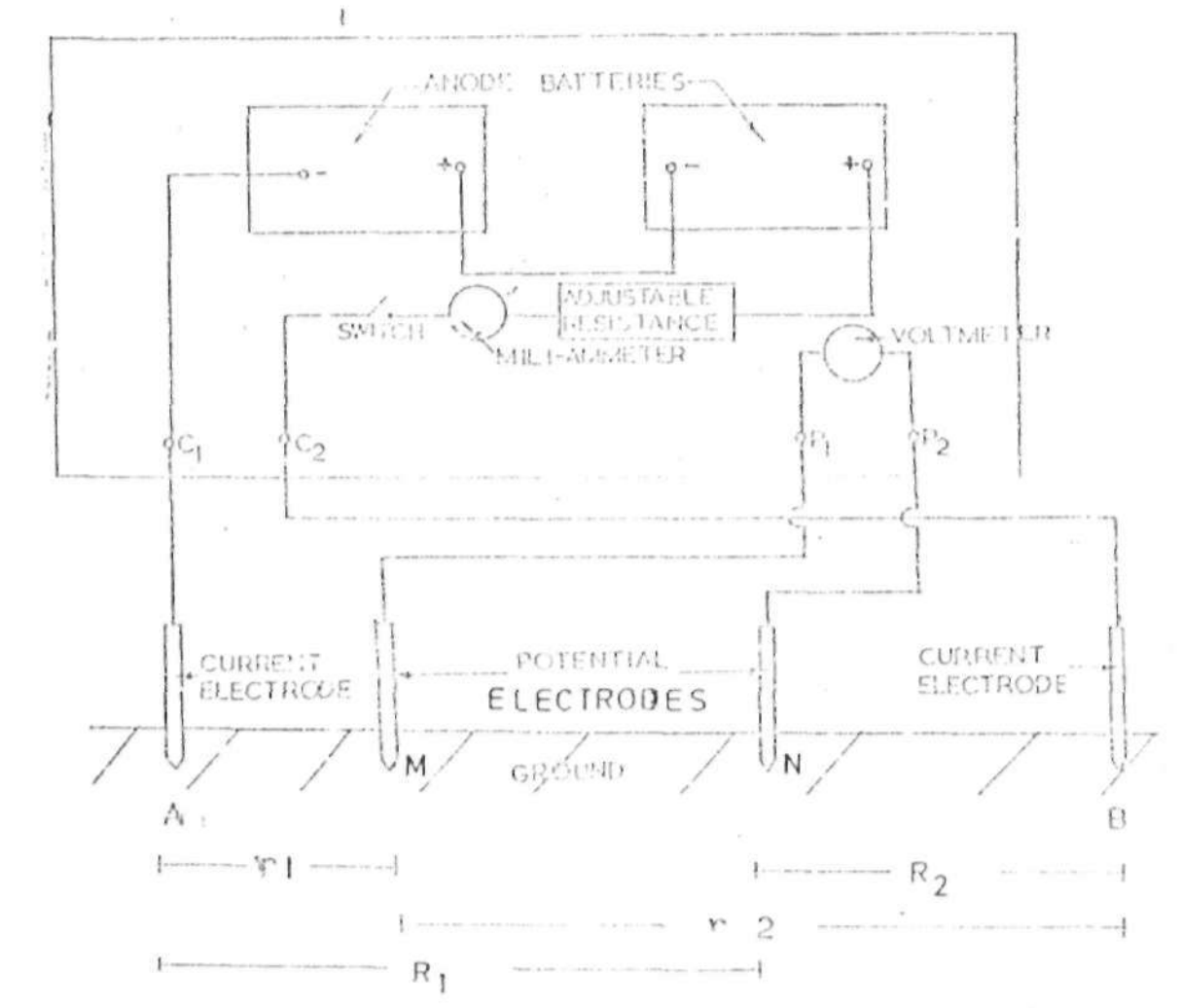
Let us consider a semi infinite solid with uniform resistivity ρ and assume that a current I is introduced into this material through electrodes A and B respectively, on its surface (fig. 2.2.). Assuming also that the potential gradient associated with this current is measured across two electrodes at M and N on the same surface, the potential at electrode M will be.

$$V_M = \frac{I\rho}{2\pi}\left(\frac{1}{r_1} - \frac{1}{r_2}\right) \text{ - - .....(11)}$$

Where r_1 is the distance from potential electrode M to current electrode A and r_2 is the distance of the same potential electrode to the current electrode B.

Similarly, the potential at N is

$$V_N = \frac{I\rho}{2\pi}\left(\frac{1}{R_1} - \frac{1}{R_2}\right) \qquad \text{.....(12)}$$



FIG·2·2: SCHEME OF SIMPLE FIELD APPARATUS FOR RESISTIVITY MEASUREMENTS
(AFTER PARASNIS 1973)

Where R_1 is the distance from the potential electrode N to A and R_2 is the distance from N to the current electrode at B.

The potential difference ΔV measured by the potentiometer across electrodes M and N is simply Vm - Vn. Therefore from equations (11) and (12),

$$\Delta V = \frac{I\rho}{2\pi}\left(\frac{1}{r_1} - \frac{1}{r_2} - \frac{1}{R_1} + \frac{1}{R_2}\right) \quad \ldots\ldots\ldots\ldots(13)$$

and consequently, the resistivity (apparent) can be found as follows:

$$\rho = \frac{2\pi\Delta V}{I}\left(\frac{1}{\frac{1}{r_1} - \frac{1}{r_2} - \frac{1}{R_1} + \frac{1}{R_2}}\right) \quad \ldots\ldots\ldots\ldots\ldots\ldots(14)$$

which can be generally represented as

$$\rho = \frac{2\pi\Delta V}{I} \cdot K \quad \ldots\ldots\ldots\ldots\ldots\ldots(15)$$

where K is the geometric factor as it depends on the electrode configuration used during the field measurements.

For a homogeneous medium, the value of the resistivity, is independent of the positions of the electrodes and is not affected when the current and potential electrodes are interchanged. However, the effective resistivity as computed from equation (14) is termed the apparent resistivity and, varies with the position of the electrodes. This change in ρ with electrode spacing makes it possible in most cases to determine the variation of resistivity with depth (Dobrin, 1976).

Apparent resistivity represents the resistivity which the ground would have if it were homegenous (Grant and West, 1965). It does not represent the average resistivity and it can be lower than the lowest or higher than the highest resistivity within the sub-surface to which it pertains (Jain, 1980).

A number of different electrode configurations have been proposed and used in electrical prospecting. They include, among others, the Wenner array, the Schlumberger array, the Dipole - Dipole array and the Threee - point array. However, only the Schlumberger array was used for the present investigation and hence described below:

In the Schlumberger configuration (fig. 2.3), the distance AB (2L) between the current electrodes is large compared with the distance MN (2L) between the potential electrodes. For the Schlumberger array, the apparent resistivity as given by equation (14) reduces to:

$$\rho_a = \frac{\pi}{2l}\left(L^2 - l^2\right)\frac{\Delta V}{I} \qquad \text{.....(16)}$$

When L >> 10l, the above relation can be approximated to

$$\rho_a = \frac{\pi}{2l} L^2 \frac{\Delta V}{I} \qquad \text{.....(17)}$$

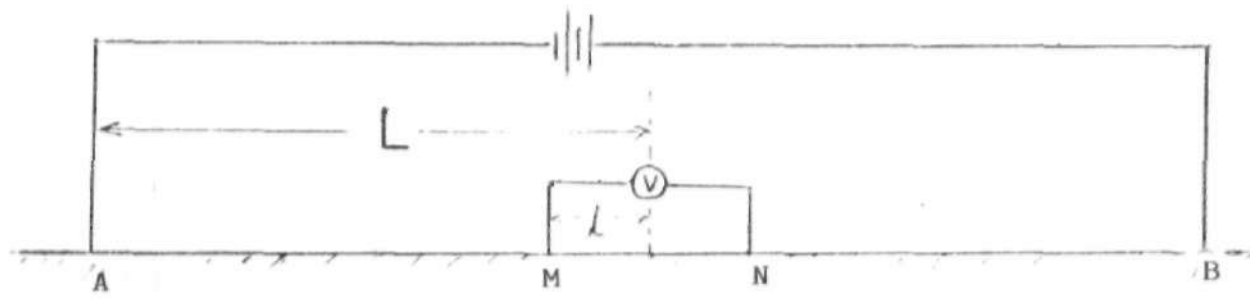


Fig. 2.3: The Schlumberger electric configuration

2.1.2 **The VLF - EM Method**

If a time varying electromagnetic field is produced on the surface of the ground, currents will flow in sub-surface conductors whose strikes are parallel to the bearings of the VLF stations, in accordance with the laws of electromagnetic induction. These currents give rise to secondary fields which distort the primary field observed at any point on the surface. In general, the resultant field due to the effect of these conductors, which can be picked up by a suitable receiver (search coil), will differ from the primary field in intensity, phase and direction. Consequently, inhomogeneities in the electromagnetic field observed on the ground surface would indicate variations in the conductivity below the surface and suggest the presence of anomalous masses in the sub-surface.

In the VLF method, the sources of the time varying electromagnetic field are powerful radio transmitters, situated in different parts of the World, which transmit unmodulated carrier waves either continuously or with Morse code signals for purposes of Military communications, on frequencies in the band 15-25 KHz (Very Low Frequencies).

The VLF - transmitting stations have vertical antenna. The antenna current is therefore vertical, creating concentric horizontal magnetic field around them. When these magnetic fields meet conductive bodies in the ground, there will be secondary fields radiating from these bodies. The VLF equipment measures the resultant electromagnetic field which is a combination of two waves of the same frequency but different amplitudes and phases.

One of these components of the resultant waves is in phase with the primary field and its amplitude is called the in-phase or real component of the resultant field. The other component into which the resultant field is split is displaced exactly 90^{o} and its amplitude is termed the Out-of-phase or quadrature or the imaginary component of the resultant field.

Since the area to be investigated is normally small and of considerable distance from the transmitting stations, the primary field is uniform in the area so that a conductor in the area will be subjected to a homogeneous horizontal magnetic flux density, allowing rather simple mathematics to be used in anomaly prediction and analysis (Parasnis, 1968).

2.2 Data Collection

2.2.1 Instrumentation

The ABEM AC Terrameter model SAS 300 was used to collect the resistivity data while the EM 16 VLF equipment (by GEONIC LTD) was used for the VLF Survey.

The Terrameter is made up of two units. The T-Box which is the Transmitter or Power source and the R-Box which is the Receiver and Meter unit. The T and R - Boxes are assembled in rugged aluminium boxes that withstand rough handling and give excellent protection to the electronic circuitry and instrument. The instrument is completely weather-proof and the casing is sealed against dust and damp. It has a dial which is used to balance the resistivity of the ground set up due to the passage of current. The dial is varied in such a way as to balance a preset milliameter reading which was set for a given voltage output. The meter acts like a galvanometer in a potentiometer experiment where the earth resistance is balanced with an unknown resistance when the milliameter is nulled. This low frequency AC Terrameter has an advantage over the DC type because small voltages such as those obtained over highly conductive ground or ores can easily be amplified by means of electronic amplifiers. Moreover, self potentials need not be compensated since they are steady potentials which will not be picked up by AC instrument (Parasnis, 1968) Other necessary components used for the resistivity survey include round stainless steel (current) electrodes and brass (potential) electrodes, insulated flexible wire wound on portable reels, hammers etc.

The EM 16 VLF equipment is simply a sensitive receiver covering the frequency band of the VLF transmitting stations with means of measuring the vertical field components. The receiver measures a tilt angle and quadrature component by means of two mutually perpendicular coils wound on ferrite cores. The signal of the second coil is shifted in phase by 90^{o}. The amplitude of this signal is adjustable on the quadrature dial, which reads percent plus or minus. A clinometer on the instrument allows tilt angle measurement. By tilt and quadrature adjustments, a good minimum is obtained. The receiver amplifier incorporates two plug-in units tuned to the frequencies of two VLF stations which can be detected from the survey area. There is a world wide net work of high-power VLF stations for marine navigation located such that at least two stations can be detected anywhere over the earth's surface. The stations used for this investigation were NAA (Cutler, U.S.A.) transmitting on a frequency of 17.8 KHz and FUO (Bordeaux, France) which transmits on a frequency of 15.1 KHz. Fig. 2.4 shows the block diagram of the principal component parts of the VLF Receiver used.

2.2.2 **Horizontal Resistivity Profiling**

The resistivity profiling technique furnishes information on the lateral variation in the resistivity of the ground. The Schlumberger electrode configuration was used with AB/2 = 20m and MN/2 = 1m, see fig. 2.3. The choice of the spread was based on results of some preliminary soundings earlier carried out in the area. The preliminary investigations indicated that the average overburden thickness in the area is about 10m.

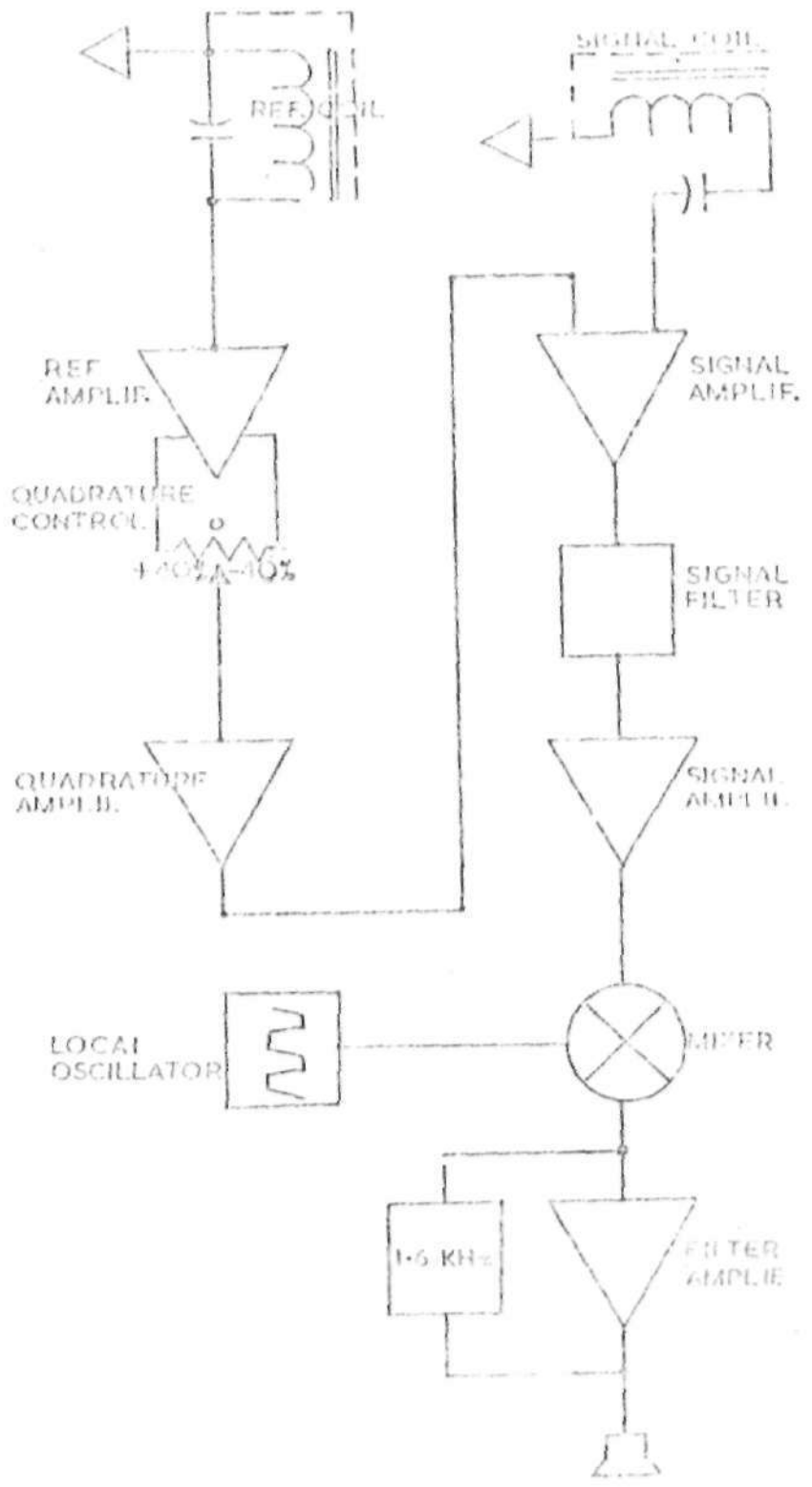


FIG. 2·4: BLOCK DIAGRAM OF EM16 VLF-EM
(GEONICS LTD.)

Two sets of survey lines were laid for the investigations. The first set termed "profiles", are the nine lines with azimuth of 075° and numbered P_{-2} to P_6, while the second set, termed "travesse lines" are perpendicular to the first set and are numbered L_0 to L_8 (See figs 1.2 and 2.5). Both the profiles and traverse lines are located at an interval of 100m. The direction of the traverse lines cuts obliquely across the suspected general trend of the marble deposit making an angle of approximately 65° with it.

Stations for obtaining the horizontal profiling data were sited on all the traverse lines at intervals of 20m but the interval was reduced to 10m around the marble/basement rock contact. After each resistivity measurement, the array was moved as a whole to the next station along the survey line, while maintaining the same electrode spacings. The mid-point of each spread was located at the station of interest.

2.2.3 Vertical Electrical Sounding

The electrical sounding technique is based on the fact that the fraction of the electric current put into the ground which penetrates below any particular depth, increases with an increase in the separation of the current electrodes. The depth of investigation, therefore, increases generally with increasing electrode spacing.

Forty-five stations were sounded within the area (Fig. 2.5), using the Schlumberger electrode configuration.

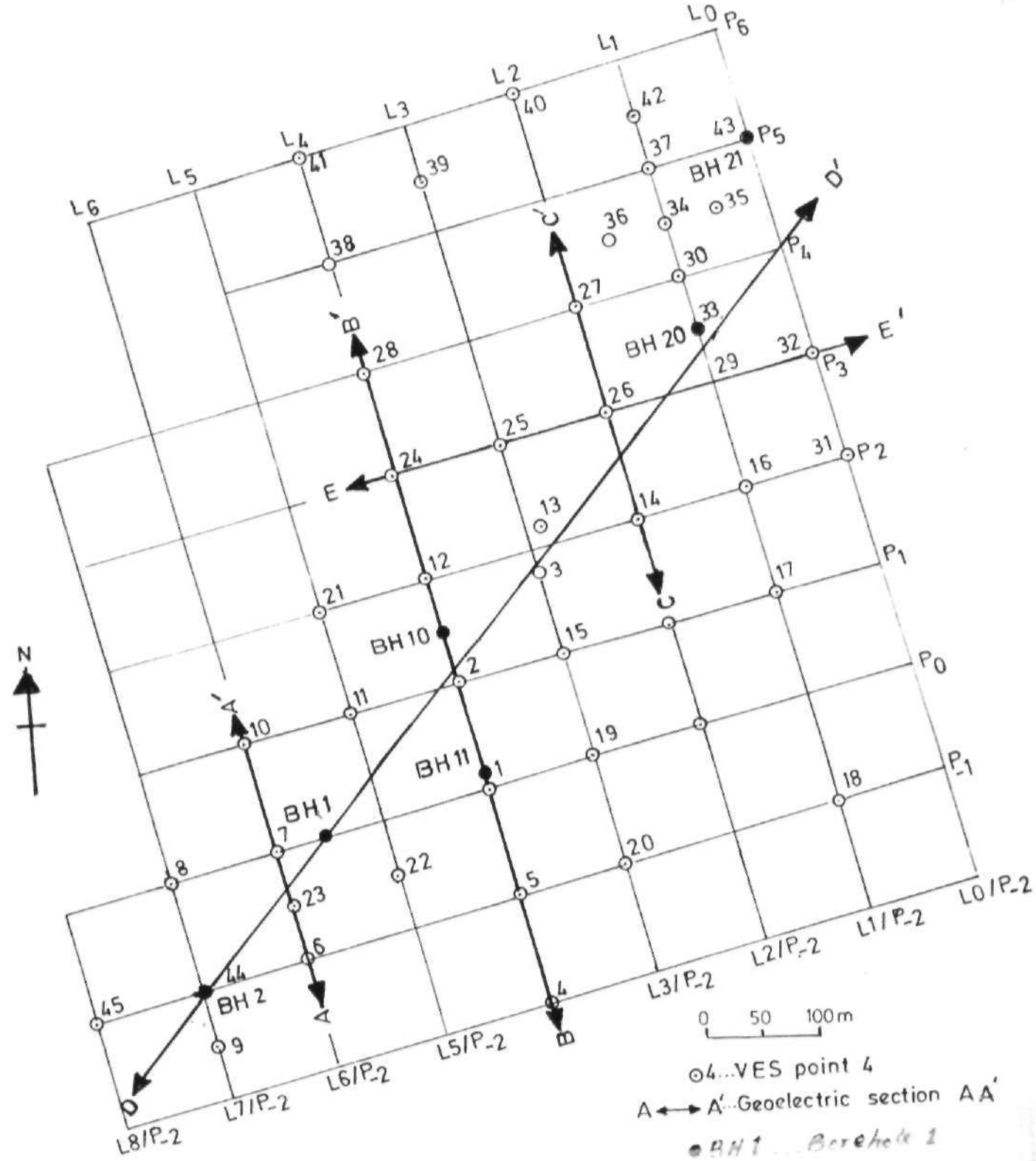


FIG.2-5: A BASE MAP SHOWING THE LOCATION OF THE VES POINTS AND GEOELECTRIC SECTIONS

The azimuths of the spreads were generally along the profiles (azimuth 075^{o}). At each of the sounded stations, the potential electrodes were fixed symmetrically about the station while the current electrode spacing was expanded symmetrically about the centre of the spread, from AB/2 = 1m to AB/2 = 200m. At stages when the potential difference between the potential electrodes became too small to be measured accurately, the potential electrode spacing was increased accordingly and measurements continued. The potential electrode separation (MN) was therefore, varied from 0.6m to 20m during the investigation. The data obtained from this method were used to obtain information on the vertical succession of the various conducting zones, their individual thicknesses and true resistivities.

2.2.4 VLF - EM Survey

As earlier mentioned, the VLF field observations were based on primary signals from both NAA (Cutler) and FUO (Bourdeaux) stations. The choice of these stations was based on the fact that they provide fields that are approximately parallel to the traverse direction. That is, their fields are nearly perpendicular to the expected strike of the marble deposit.

Before each measurement, the instrument was turned sideways until minimum signal was obtained to determine the azimuth of the transmitter relative to that of the profile. To obtain the readings, the reference coil was oriented along the magnetic lines.

The instrument was swung back and forth for a minimum intensity in the speaker. The volume control was used to adjust the sound level for comfortable listening. Then the quadrature component dial was adjusted to further minimize the sound. After obtaining the minimum signal strength on both adjustments, the readings were noted.

The exact position at which the noise level is minimum may not easily be obtained precisely, when taking readings. This is due to the fact that an error in the range of 20 - 35 percent may be introduced in the measurement if a station having $\pm 45^{o}$ to the direction of the strike line is selected for the target body (George, 1976).

Both in-phase and quadrature component readings were taken along all the nine profiles at station intervals of 20m. Westward orientation was maintained throughout the survey to avoid reversal of polarity of the readings.

2.3 Data Reduction and Interpretation

The interpretation of geophysical data involves expressing in geological terms, the information deduced from the obtained field data. A successful interpretation requires considerable practical experience with the geophysical method and a sound knowledge of the geology of the area under consideration. Therefore, all available geological information on the project area were taken into consideration in interpreting the data collected.

2.3.1 Horizontal Resistivity Profiling

The aim of resistivity profiling is to detect the lateral variation in (apparent) resistivity of the sub-stratum within a predetermined depth range. Under normal conditions, the effective depth of penetration of the current is roughly considered to be between one-third and half of the current electrode separation (Rao, 1980). However, due to the non-homogeneous nature of the sub-surface, this assumption may not always be true. So the depth of penetration could be more or less than the given range.

The values of the apparent resistivity at each of the resistivity profiling (RP) stations were obtained by multiplying the meter reading at the station by the corresponding Schlumberger geometric factor (equation 17). The values were plotted on the ordinate, against the RP stations on the abscissa. Such plots for profile L4 and L5 are shown in Figs. 2.6 and 2.7 respectively.

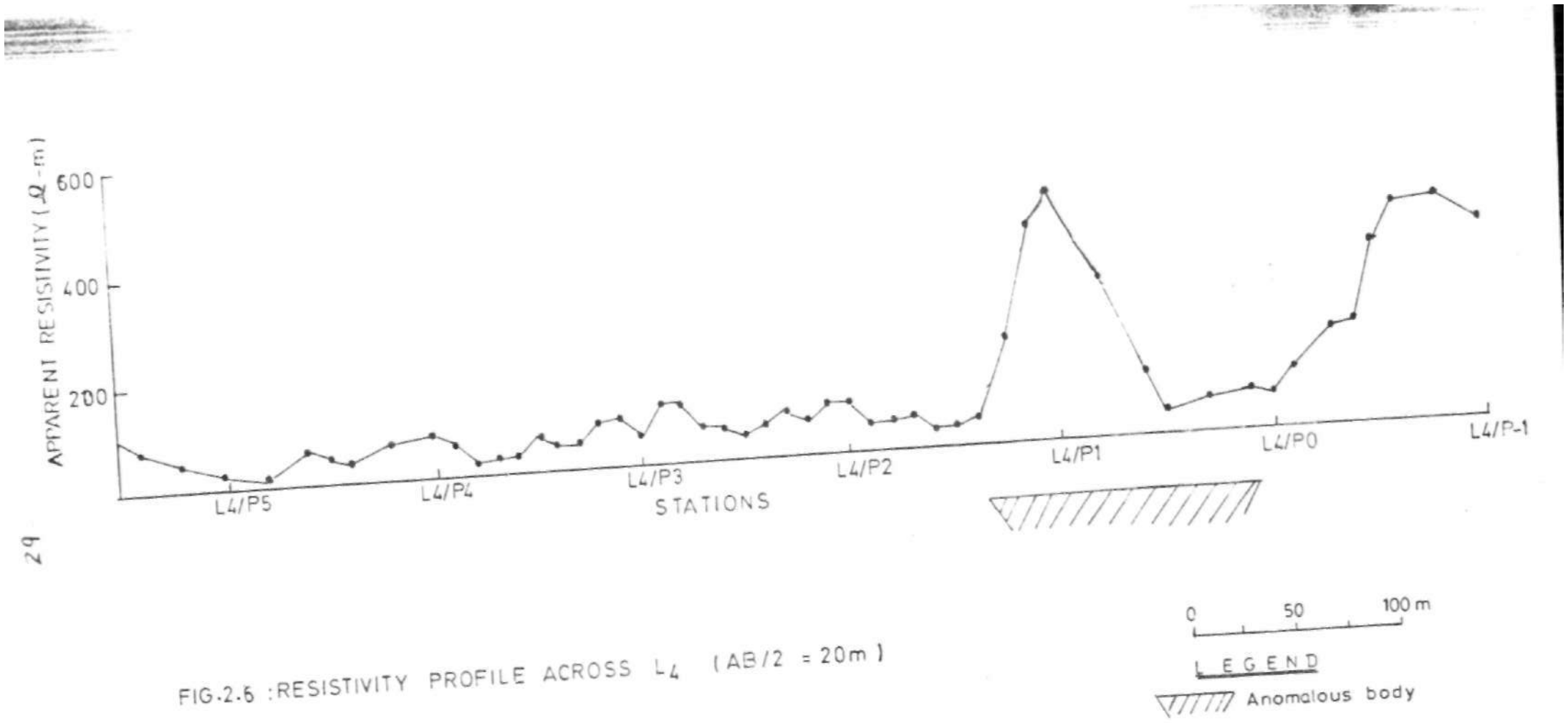
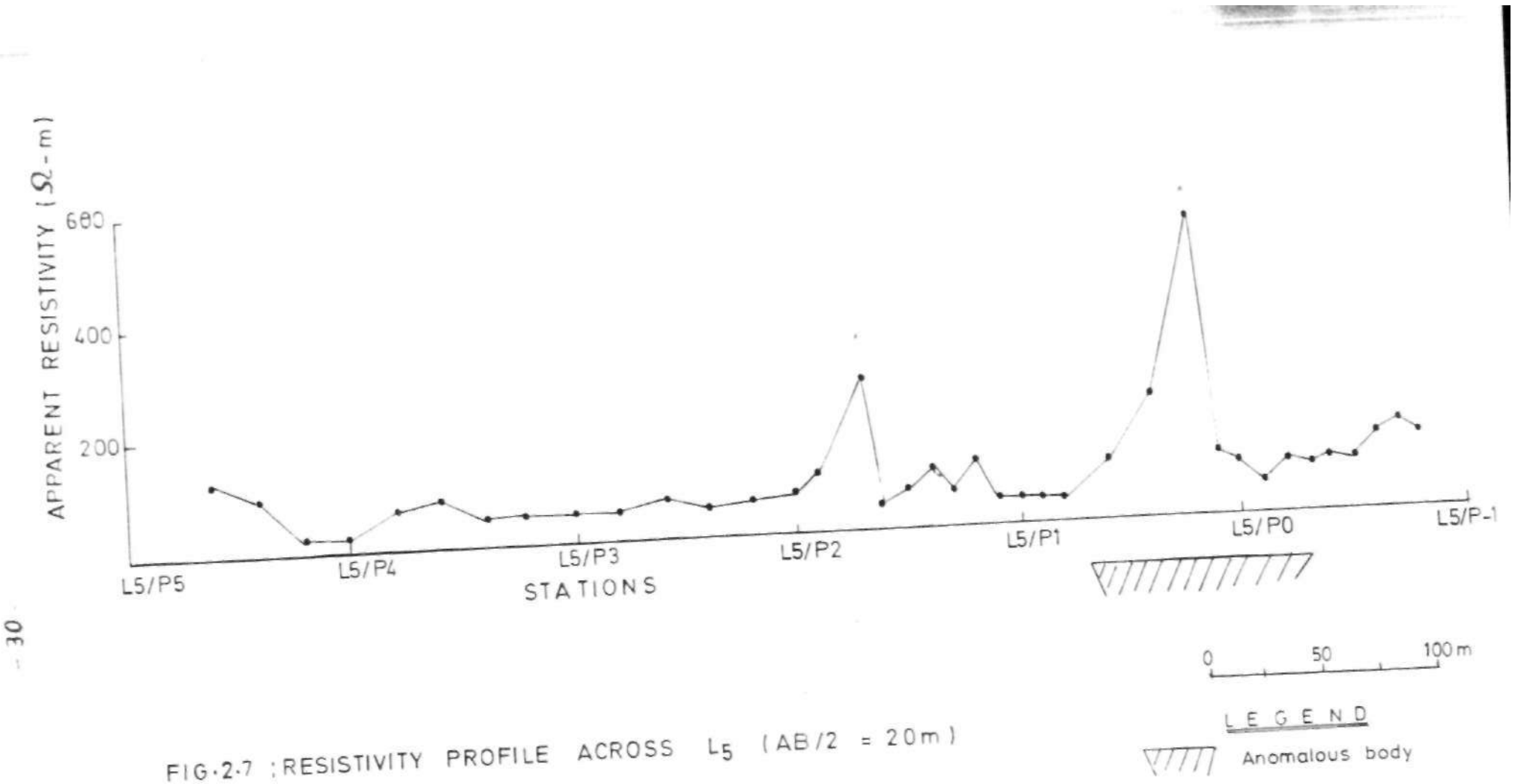


FIG.2.6 :RESISTIVITY PROFILE ACROSS L4 (AB/2 = 20m)



FIG·2·7 ; RESISTIVITY PROFILE ACROSS L_5 (AB/2 = 20m)

The figures show the lateral variation in apparent resistivity along the two traverse lines at a depth of about 15m. Furthermore, in order to get a complete picture of the variation in apparent resistivity within the depth of interest, the profiling data for all the stations in the project area were contoured to give fig. 2.8.

2.3.2 The Vertical Electrical Sounding (VES) data

The apparent resistivity values for each spread were computed using equation (17). Resistivity curves were plotted on bi-logarithmic paper with the computed apparent resistivity values on the ordinate and half the current electrode separation (AB/2) as abscissa. A typical example of the resistivity curves (obtained for VES 30) is shown in fig. 2.9, while its field and computed data are shown in table 2.1.

Preliminary interpretation of the field curves, which were generally of the H - A types, were done by partial curve matching technique (Keller, et al 1966) using two layer standard curves and auxilliary curves designed by Orellana and Mooney (1966). This preliminary interpretation provided the parameters of the initial model (number of layers, resistivity values, and thickness of each layer) fed into a computer for the second phase of the interpretation. The first phase was necessary in order to minimize the number of iterations the computer would have to carry out.

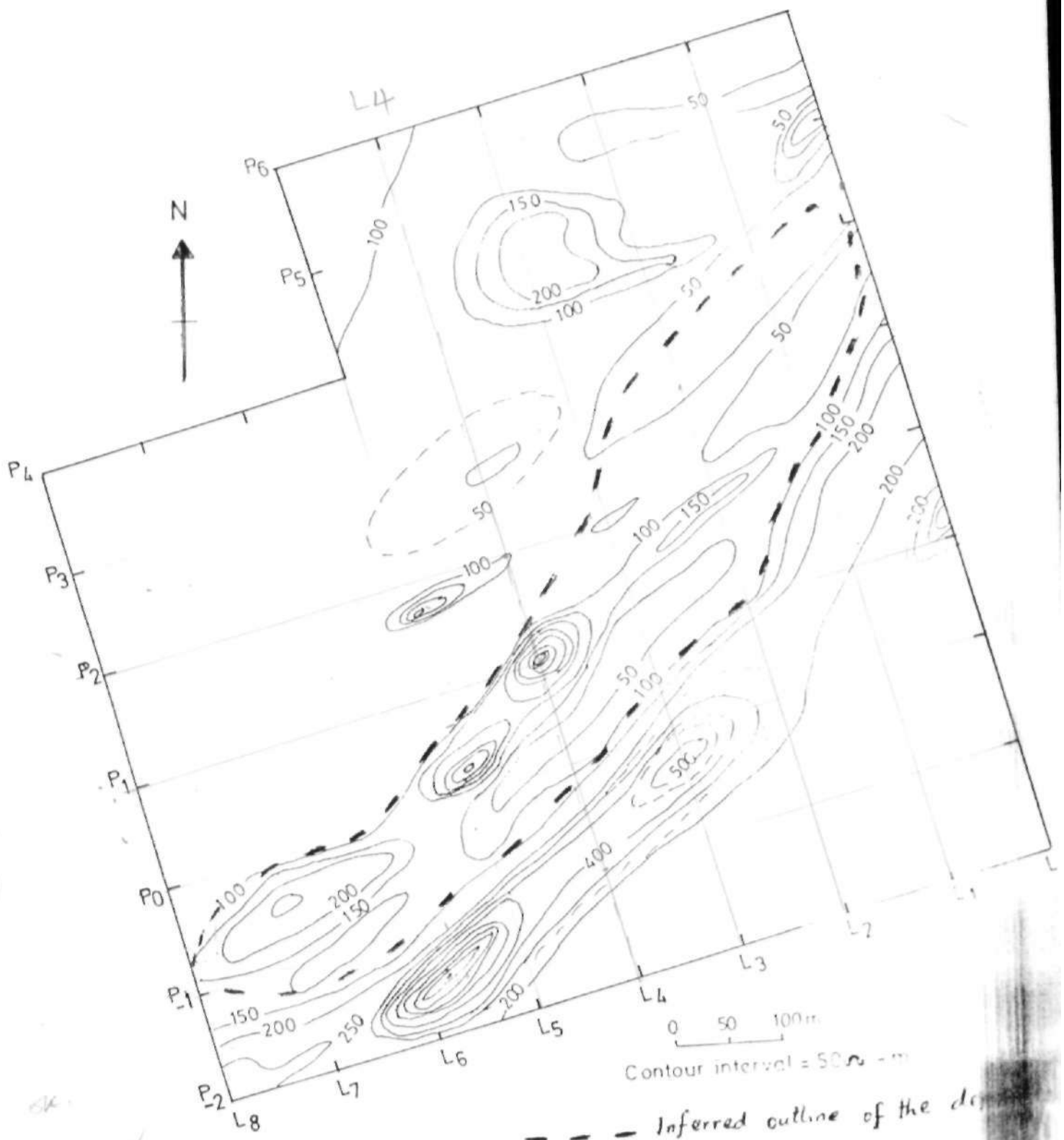


FIG. 2·8 : ISO - RESISTIVITY CONTOUR MAP AT AB/2 = 20m
(Using Horizontal Profiling Data)

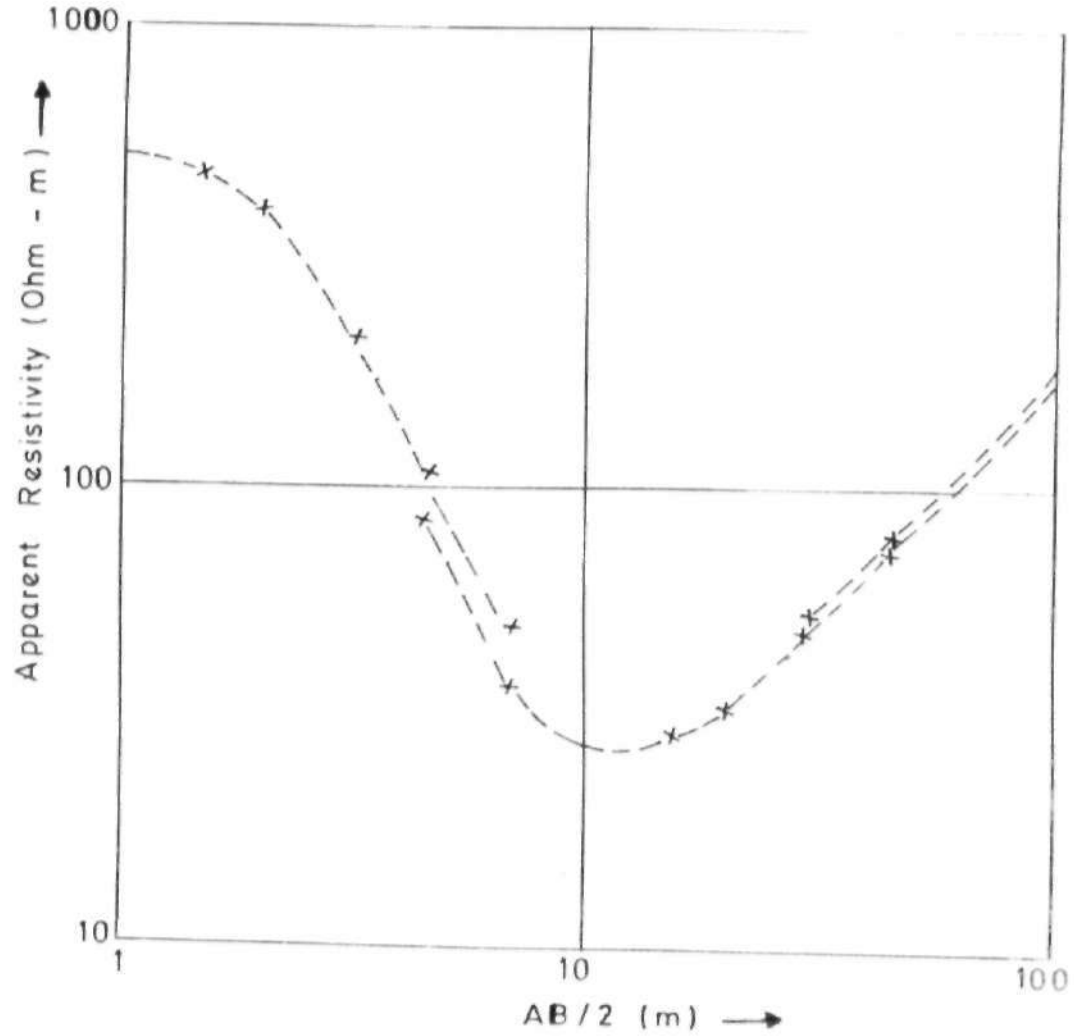


FIG-2.9:RESISTIVITY DEPTH SOUNDING CURVE FOR VES 30

TABLE 2.1: TYPICAL RESISTIVITY SOUNDING FIELD AND COMPUTED DATA

V.E.S. No. 30 Date - 01.12.87

LOCATION - L_1 P_4 Instrument: ABEM AC Terrameter

Electrode Configuration - Schlumberger

S/R	AB/2 (m)	MN/2 (m)	K - Factor	Meter Reading R = V/I (Ohms)	Computed Apparent Resistivity ρ_a (Ohm - meter)
1	1	0.3	4.8	110	528
2	1.5	0.3	11.3	44	497.2
3	2	0.3	20.5	20	410
4	3	0.3	46.7	4.4	206
5	4.5	0.3	105.6	10	106
6	4.5	1	30.2	295	89
7	7	0.3	256.1	0.2	51
8	7	1	75.4	0.5	38
9	10	1	155.5	0.18	28
10	15	1	351.9	0.085	30
11	20	1	626.7	0.055	35
12	30	1	1412.2	0.038	54
13	30	5	274.9	186	51
14	45	1	3179.3	0.026	83
15	45	5	628.3	0.122	77
16	70	5	1531.5	0.078	120
17	70	10	754	0.156	118
18	100	5	3133.7	0.061	191
19	100	10	1555.1	0.117	182
20	150	5	7060.7	-	-

A BBC Mini - computer (which displays on a Toshiba TV screen) belonging to the Federal Department of Water Resources, Kaduna was used for the interpretation. The use of this computer became necessary because the A.B.U.'s CDC Cyber 72 Computer was completely out of order during the period the data were processed and interpreted (February - March, 1988).

The basic procedure followed in the interpretation were:

i. Assumption of a trial model,

ii. Computing the theoretical field curve expected from the trial model,

iii. Comparison of the computed curve with the observed field curve,

iv. Modifying the model where necessary to improve the agreement between the computed and the observed data until the 'best' possible agreement has been achieved.

The program used the trial model fed in by the interpreter to compute a theoretical apparent resistivity curve. This curve when displayed on the screen was compared with the field curve (also displayed on the screen) and the layer parameters were modified accordingly (by the interpreter) until the 'best' fit was obtained between the computed and observed resistivity values. The layer paremeters for this fit were considered the 'best' for the interpreted model of the causative body beneath the VES point.

A typical interpretation using the above described method is shown in figs 2.10a and 2.10b. The field data for the VES point were put into the computer. An initial four layers model whose parameters are shown in fig.2.10a was also fed into the computer. The parameters of the initial model were obtained from the preliminary interpretation by partial curve matching. The computer in turn, displayed the resultant theoretical curve, which did not fit the field curve (fig. 10a). The parameters were subsequently varied until what was considered the 'best' possible fit between the field and the theoretical curves was obtained (see fig. 2.10b). The parameters of this final model give the individual thicknesses and "true" resistivities of the various conducting zones for that VES point. As shown in fig.2.10b four geoelectric layers were distinguished. The first layer has a resitivity ρ_1 = 1650 Ohm - m and a thickness t_1 = 0.40m. The second layer with a resistivity of 30.0 Ohm-m has a thickness of 2.5m. The third layer has a resistivity of 66 Ohm-m and is 12.5m thick. The last layer with a resistivity of 2800 Ohm - m has an infinitely large thickness that could not be determined in this work.

All the VES data were interpreted following the above procedure and the obtained results are shown in Appendix II.

2.3.3 The VLF - EM data

The obtained VLF data (both in-phase and quadrature components) were plotted and stacked on the field profiles, to give fig. 2.11.

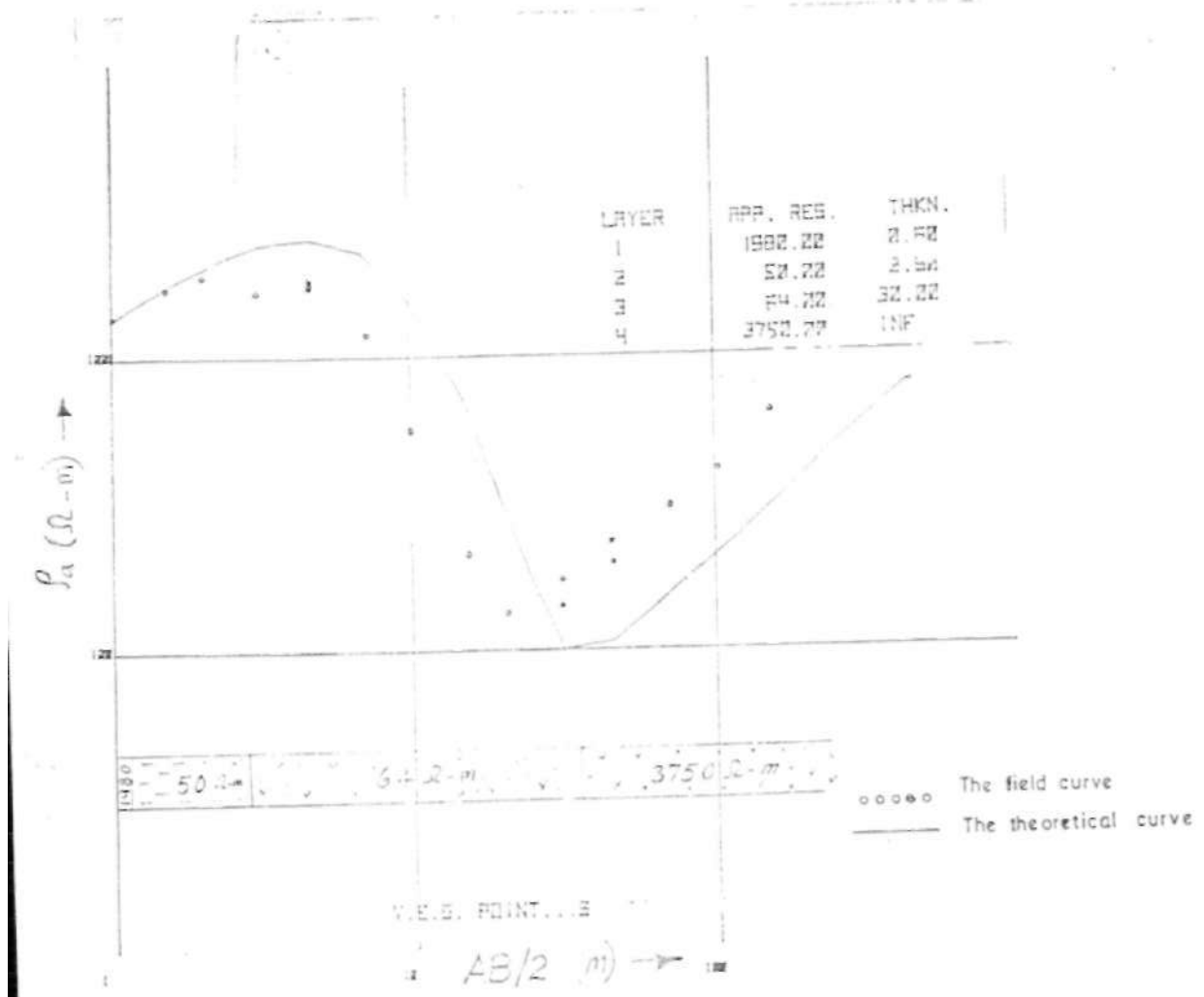


Fig. 2.10a: THE INITIAL MODEL FED INTO THE COMPUTER FOR VES 6

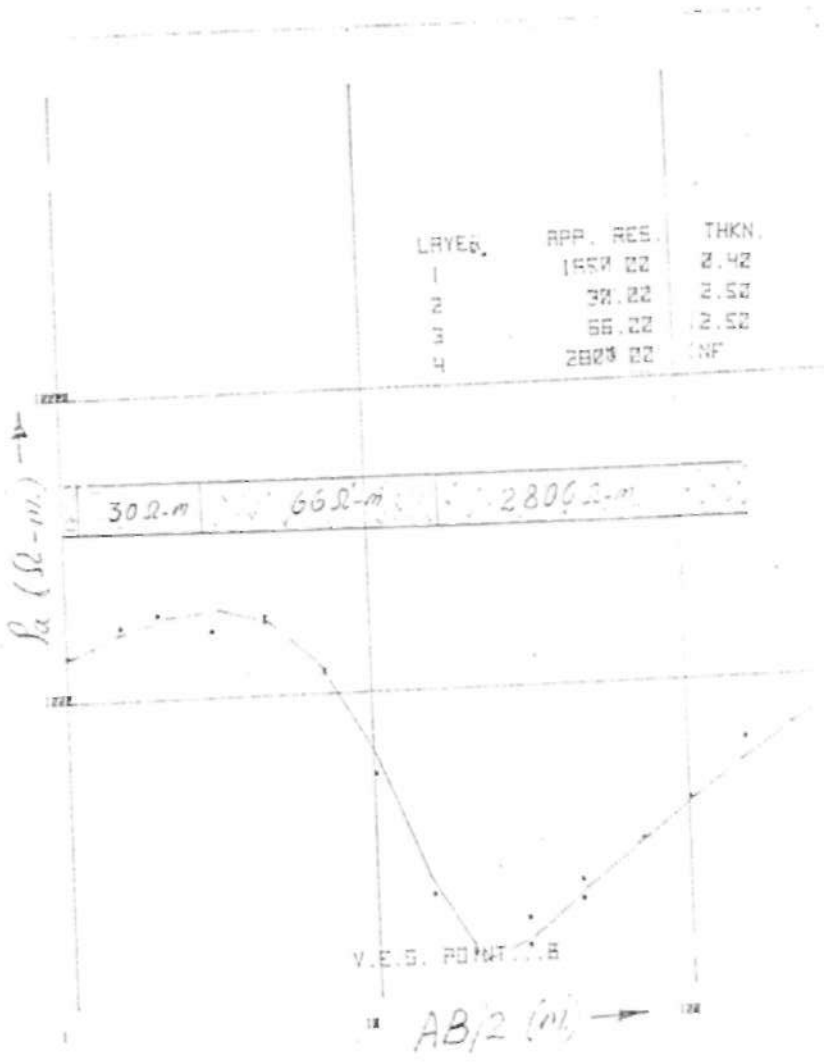


Fig. 2.10b: THE FINAL INTERPRETED MODEL OBTAINED FOR VES 6



FIG. 2.11 STACKED VLF (EM) DATA SHOWING THE IN-PHASE AND QUADRATURE COMPONENTS

The VLF in-phase data were filtered and contoured using a method proposed by Fraser (1969) to give fig. 2.12. In this method, the plotted function is:

$$f2.5 = (M_4 + M_3) - (M_2 + M_1) \quad \text{.....(18)}$$

where M_1, M_2, M_3 and M_4 are four consecutive data points and f2.5 is plotted mid-way between M_2 and M_3. The negative values were ignored during the contouring, since, according to Fraser (1969), the negative values are not contoured as they are caused by dip angle flanks and therefore, do not aid interpretation but rather only confuse the picture. The filtering of the VLF data has a smoothing effect which reduces the large geologic noise caused by the relatively high frequencies of the transmitting stations. For example, FUO, Bordeaux transmits at 15.1 KH_z while NAA, Cutler operates at 17.8 KH_z.

The first derivative of the in-phase data were also computed and contoured using the derivative method proposed by Whittle (1969). The in-phase derivative function is given by:

$$f1.5 = \frac{M_2 - M_1}{\times} \quad \text{.....(19)}$$

where $\times$ = the station interval and f1.5 is plotted mid-way between M_1 and M_2 data points. The contoured map of the filtered VLF data is shown in fig. 2.12 while that of the first derivative is shown in fig. 2.13.

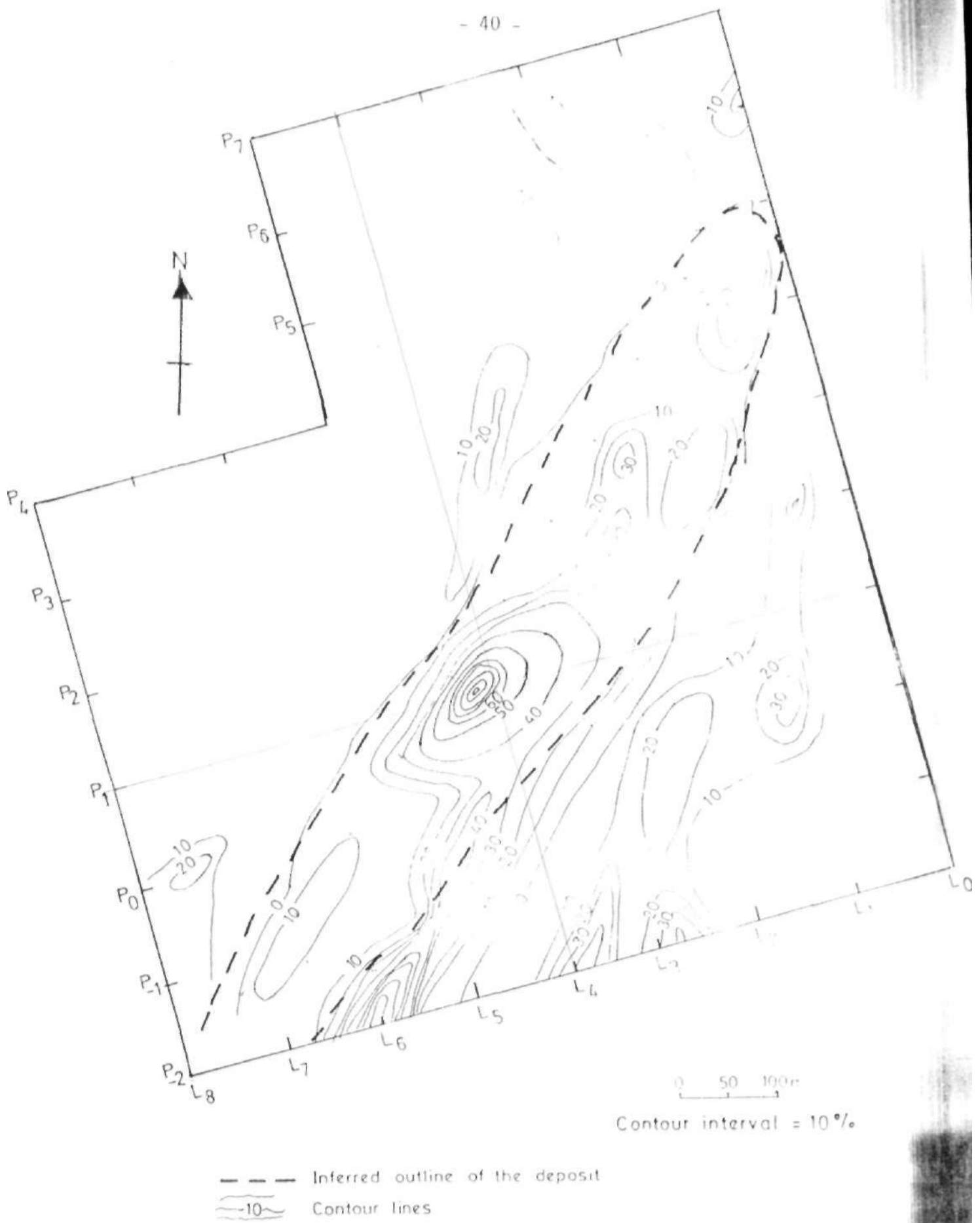
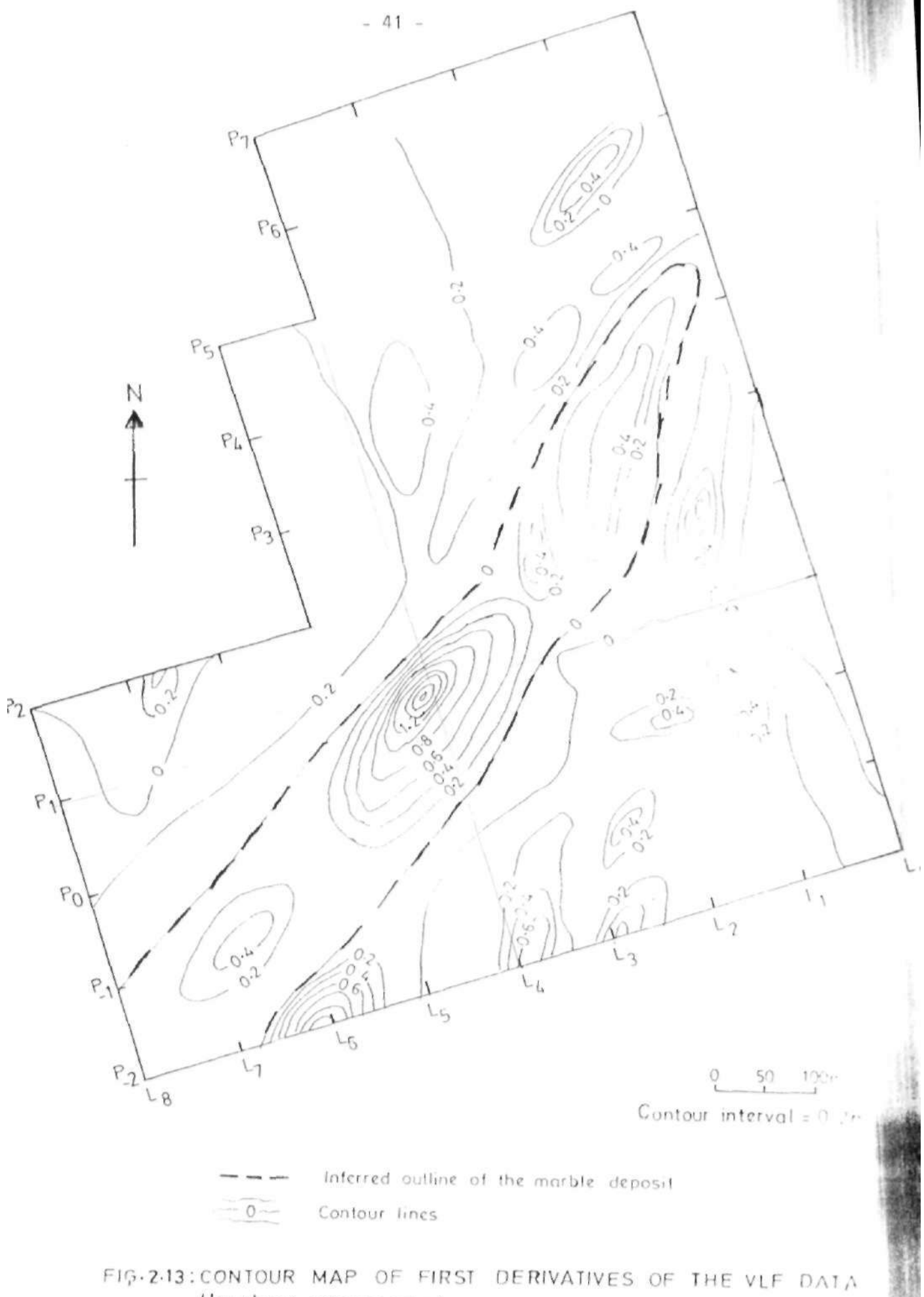


FIG. 2-12 : CONTOUR MAP OF FILTERED VLF DATA (In-phase components)



FIG·2·13: CONTOUR MAP OF FIRST DERIVATIVES OF THE VLF DATA
(In-phase components)

2.3.4 Limitations

Quantitative interpretations of geophysical data generally have some limitations. Some of these limitations relevant to this work are highlighted below:

a. Non - unique Solutions

The curve matching method of interpretation of VES data is an inverse problem which may admit several possible solutions. Different combination of values of resistivity and thickness of a three-layer section may lead to apparent resistivity curves similar to each other within the accuracy of observations. This lack of uniqueness is referred to as the "Principle of equivalence". For types H and A curves (i.e. when $\rho_1 > \rho_2 < \rho_3$ or $\rho_1 < \rho_2 < \rho_3$), the curve remains virtually the same, if within certain limits (usually 5%), the values of h_2 (thickness of the middle layer) and ρ_2 (resistivity of the middle layer) are multiplied by the same factor. Consequently, the H and A type layered sections are equivalent within certain limits, if $h_2/\rho_2 = S$, remains constant - Keller and FreschKnecht (1966).

For K or Q type sections (i.e. $\rho_1 < \rho_2 > \rho_3$ or $\rho_1 > \rho_2 > \rho_3$), the form of the curve does not change significantly if h_2 is increased or decreased by a certain factor and ρ_2 is correspondingly decreased or increased by the same factor.

Therefore K and Q type sections are equivalent if

$h_2 \cdot \rho_2$ = T remains constant.

b. Presence of non-horizontal layer boundaries

The computed (theoretical) curves are based on the assumption that the sub-surface layers are horizontal. In most cases, this assumption may not be true and this will introduce some error into the interpretation. The effect of dipping beds was, however, considerably reduced in the present investigation by orienting the sounding line approximately paralled to the geological strike of the rocks in the area.

c. Lateral Variation in resistivity of the Layers

It was assumed in the interpretation that the layers are electrically homogeneous. However, lateral variation in resistivity within a geoelectric layer is common and is a possible source of error in the interpretation of resistivity soundings.

In view of the above limitations, a maximum error of about 5% may possibly have been introduced into the results of this interpretations. However, correlation of this VES results with borehole data show that the error is less than 3%.

CHAPTER 3

RESULTS

3.1 Results from Resistivity Profiling

Horizontal resistivity profiles showing the lateral variation in resistivity values along traverse lines L_4 and L_5 are shown in figs. 2.6 and 2.7 respectively. A contoured iso-resistivity map of the area is also shown in fig. 2.8. These results are discussed below:

3.1.1 Profile L_4

The resistivity profile across traverse line L_4 (fig. 2.6) shows that there is a gentle variation of apparant resistivity along the profile with values ranging between 25 and 110 Ohm-m. The maxima of values 445 and 413 Ohm-m are observed at L_4P_1 and $L_4P_{-0.8}$ respectively.

3.1.2 Profile L5

The resistivity profile across traverse line L_5 (fig. 2.7) shows that the apparent resistivity values generally varied uniformly between 50 and 130 Ohm-m along the traverse line.

Apart from the kink at L_5 $P_{1.7}$ where an apparent resistivity value of 270 Ohm-m was recorded, there was a general increase in the apparent resistivity values between L_5 $P_{0.7}$ and L_5 $P_{-0.1}$ with a maximum of 530 Ohm-m at L_5 P_0.

3.1.3 **The Iso-resistivity Map**

The contoured iso-resistivity map of the area (fig. 2.8) shows that the values of apparent resistivity obtained within the deposit ranged generally between 90 and 200 Ohm-m, although values as high as 400 Ohm-m were recorded in regions where marble either outcrops to the surface (between $L_{5.5}$ P_0 and L_4 P_1) or is covered by relatively thin overburden (around $L_{6.5}$ $P_{-0.5}$). The region bounding the deposit to the south has a relatively higher resistivity range (200 - 650 Ohm-m) while the region bounding it to the north has a relatively lower resistivity range (50 - 100 Ohm-m).

3.1.4 **Deductions from Resistivity Profiling results**

The resistivity profiles (figs 2.6 and 2.7) show qualitatively, the lateral variation in apparent resistivity values within the project area, at an approximate depth of between 15 and 20m. The apparent resistivity values were generally low (30 - 100 Ohm-m) within the project area and relatively higher (90 - 445 Ohm-m) across the marble deposit.

The exceptions are some isolated regions within which the basement rocks (Pegmatite , gneiss, schist, granite etc) either outcrop or are covered by relatively thin overburden. In such regions, particularly the area bounding the deposit to the south (between $L_6\ P_{-1.6}$ and $L_{2.5}\ P_0$), the resistivity values were relatively higher (250 - 700 Ohm - m) than those obtained over the marble deposit.

The resistivity anomaly shown in the profile across L4 (fig 2.6) suggests that the marble deposit probably occurs between $L_4 P_{1.4}$ and $L_4\ P_{0.5}$. The high resistivity values obtained between $L_4\ P_{0.5}$ and $L_4\ P_{-0.1}$ are probably due to outcrops of Hornblende gneiss within that region. The kink at $L_5\ P_{1.7}$ on the profile across L_5 (fig. 2.7) may have been due to outcrops of schist at that point. The resistivity anomaly on this profile suggests that the marble occurs between $L_5\ P_{0.7}$ and $L_5\ P_{0.1}$. The closures and elongation of the iso-resistivity contours were used to infer the outline of the marble deposit (fig. 2.8). The inferred outline suggests that the deposit trends in the NNE - SSW direction with an average width of about 120m and a length of about 950m.

3.2 **Results from VLF Survey**

VLF profiles and contour maps obtained from the results of the VLF survey are discussed below.

3.2.1 VLF Profile across P_o

The in-phase values across P_o are included in fig. 2.11. The figure shows that the values vary between -16% and +18%. Negative values were obtained between L_oP_o and $L_{4.4}P_o$ and between $L_{5.8}P_o$ and L_8P_o while the values were positive between $L_{4.4}P_o$ and $L_{5.8}P_o$. The figure also shows that the quadrature component ranges between -10% and +16%. The negative values were obtained between $L_{4.4}P_o$ and $L_{5.8}P_o$ while positive values were obtained over the remaining portion of the profile.

Cross-over points on this profile occur at $L_{5.8}P_o$, $L_{4.4}P_o$, $L_{1.8}P_o$ and $L_{1.5}P_o$.

3.2.2 VLF Profile across P_2

The in-phase values across profile P_2 are included in fig. 2.11. The figure shows that the values vary from -14% to +13%, while the quadrature component also vary between -12% and +4%.

3.2.3 VLF (EM) Contour Maps

A contour map derived from the filtered VLF data (positive in-phase values) is shown in fig. 2.12. The map shows that the VLF data vary between 0 and 102% within the project area, with a maximum at L_4 P_1. The contours have a general elongation in the NNE - SSW direction.

Furthermore, the first derivatives of the VLF data were contoured to give fig. 2.13. The values vary between 0 and 1.8% within the project area, with a maximum of 1.8% around L_4 P_1. As can be seen in the figure, the contours are again elongated in the NNE - SSW direction, as in the case of the iso-resistivity and the VLF (filtered data) contour maps.

3.2.4 Deductions from results of the VLF Survey

The VLF profile across P_{-1} (fig. 2.11) shows that the values of the in-phase component remained negative along the profile from L_0 P_{-1} until around $L_{5.5}$ P_{-1}, after which the values became positive between $L_{5.5}$ P_{-1} and $L_{7.8}$ P_{-1}. This observation tends to suggest the presence of a material whose conductivity is different from that of the host rock within the region between $L_{5.5}$ P_{-1}, and $L_{7.8}$ P_{-1}. Along profile P_0, this "anomalous region" occurs between $L_{4.4}$ P_0 and $L_{5.8}$ P_0. The possible existence of this region was further highlighted by the occurence of cross-overs at these two points. This "anomalous region" was similarly identified on profile P_1 between L_3 P_1 and $L_{4.6}$ P_1; on profile P_2 between $L_{1.2}$ P_2 and $L_{3.5}$ P_2; on profile P_3 between $L_{0.8}$ P_3 and $L_{2.6}$ P_3 and along profile P_4 between $L_{0.6}$ P_4 and $L_{1.7}$ P_4.

Cross over points are often related to vertical contacts between sub-surface materials of different conductivities (Telford et el, 1976).

However, the cross-over points could not be used to infer the outline of the deposit due to the occurence of several other cross over points within the study area.

From the contoured map of the filtered VLF data (positive in-phase component only), the outline and trend of the marble deposit was inferred using the peaks and the zero contour which "brackets the anomaly" (Fraser, 1969). Similarly, the peaks, elongation and zero contour were used to infer the outline of the deposit from the contour map of the first derivatives of the VLF data (fig. 2.13).

3.3 Results of the Vertical Electrical Sounding

Geoelectric section along the profiles of interest were obtained using the interpreted models at the VES points along the corresponding traverse lines/profiles. To obtain each section, the topographic section was first drawn. Then the resistivity boundaries beneath each VES point were drawn. The resulting geoelectric sections for the five profiles/traverse lines of interest are described below:

3.3.1 Geoelectric Section for Traverse Line L6 (AA')

The geoelectric section obtained for traverse line L6 is shown in fig. 3.1. It can be seen from the figure, that four geoelectric layers can be identified across the traverse line except at VES 23 where only three geoelectric layers were distinguished.

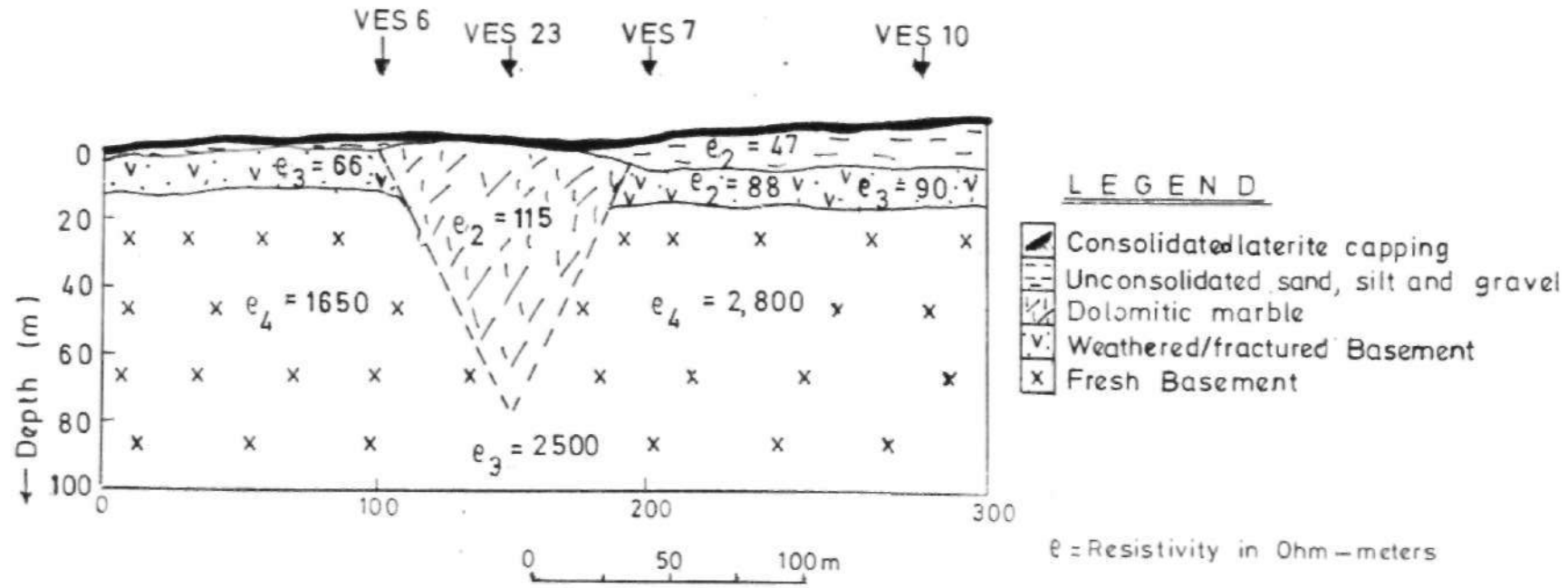


FIG.3-1 : GEOELECTRIC AND GEOLOGIC SECTION FOR TRAVERSE LINE L_6 (AA')

The first layer which is very thin (<1m), has a relatively high resistivity value (250 - 600 Ohm-m). This upper layer is underlian by a relatively thicker layer (2.5 - 14m) with a resistivity value of about 47 ohm-m. The third layer has a resistivity in the range 66 - 90 Ohm-m and a thickness varying between 10.5 and 12.5m. The fourth layer, of infinite thickness, has a relatively much higher resistivity value (1950 - 2800 Ohm - m).

At VES 23, only three layers were distinguished. These consist of a very thin upper layer with a resistivity value of 1000 Ohm-m and a second layer with a thickness of about 82.1m and a resistivity value of 110 Ohm - m. This second layer, in turn, overlies the third layer, of infinite thickness, which has a resistivity value of 2000 Ohm - m.

3.3.2 Geoelectric Section of Traverse Line L4 (BB')

Four geoelectric layers were again distinguished for this traverse line as was the case for L6 (AA'). As shown in fig. 3.2, the first layer is very thin (<1m) and has a resistivity value of 250 - 400 Ohm-m. This layer overlies a second layer whose resistivity value varies between 40 and 52 Ohm-m with a thickness ranging between 4 and 18m. The third layer, with a resistivity of 73 - 96 Ohm - m, has a thickness ranging between 12 and 46m. This layer overlies the fourth layer which has a much higher resistivity value (2000 - 4000 Ohm - m) than any of the three layers overlying it.

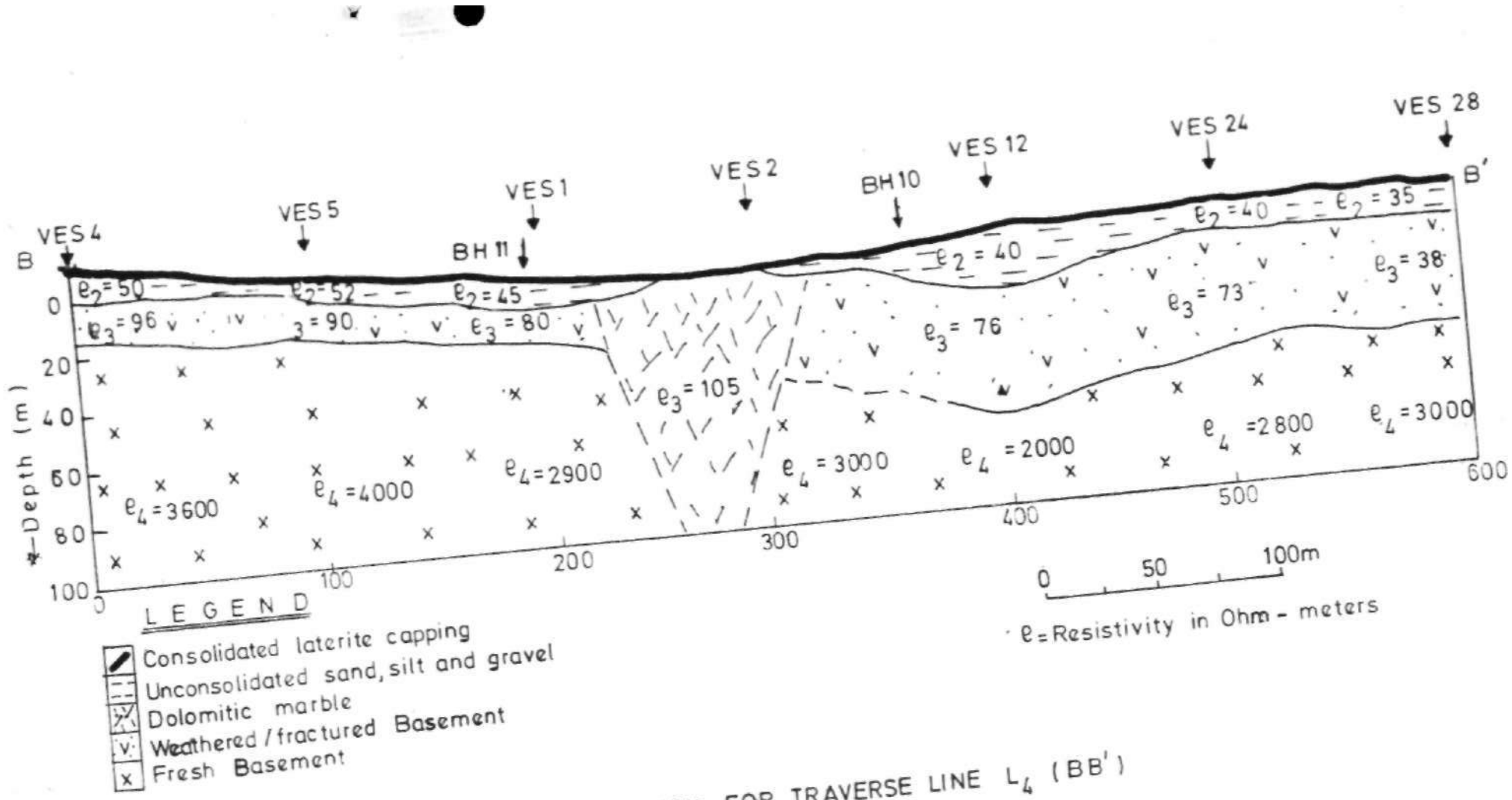


FIG. 3·2 : GEOELECTRIC AND GEOLOGIC SECTION FOR TRAVERSE LINE L_4 (BB')

At VES 2, the second layer (2.5m thick) overlies a third layer with a resistivity value of 105 Ohm - m and a thickness of 41m. This layer is in turn, underlain by the last layer which has a very high resistivity value (3000 Ohm - m) and an infinite thickness.

3.3.3 Geoelectric Section of Traverse Line L2 (CC')

The geoelectric section obtained from the interpretation of the VES points on L2 is shown in fig. 3.3. Four geoelectric layers could be distinguished below VES 27. The four layersconsist of an upper, relatively thin layer (<1m) with a resistivity value of about 500 Ohm - m. This layer overlies a second layer, about 12m thick, with a resistivity value of about 40 Ohm - m. This second layer overlies a relatively thicker layer (about 32m) with a resistivity value of about 80 Ohm - m. The fourth layer has an infinite thickness and a relatively high resistivity value of about 3200 Ohm - m.

The interpreted section suggests that, at VES 14 and 25, the first two layers described above are underlain by a geoelectric unit that has some discordant relationship with the third and fourth layers (figs 3.1, 3.2 and 3.3). This geoelectric unit has a resistivity value of 105 Ohm - m and is about 42.9m thick beneath VES 14 and about 39.5m thick beneath VES 26.

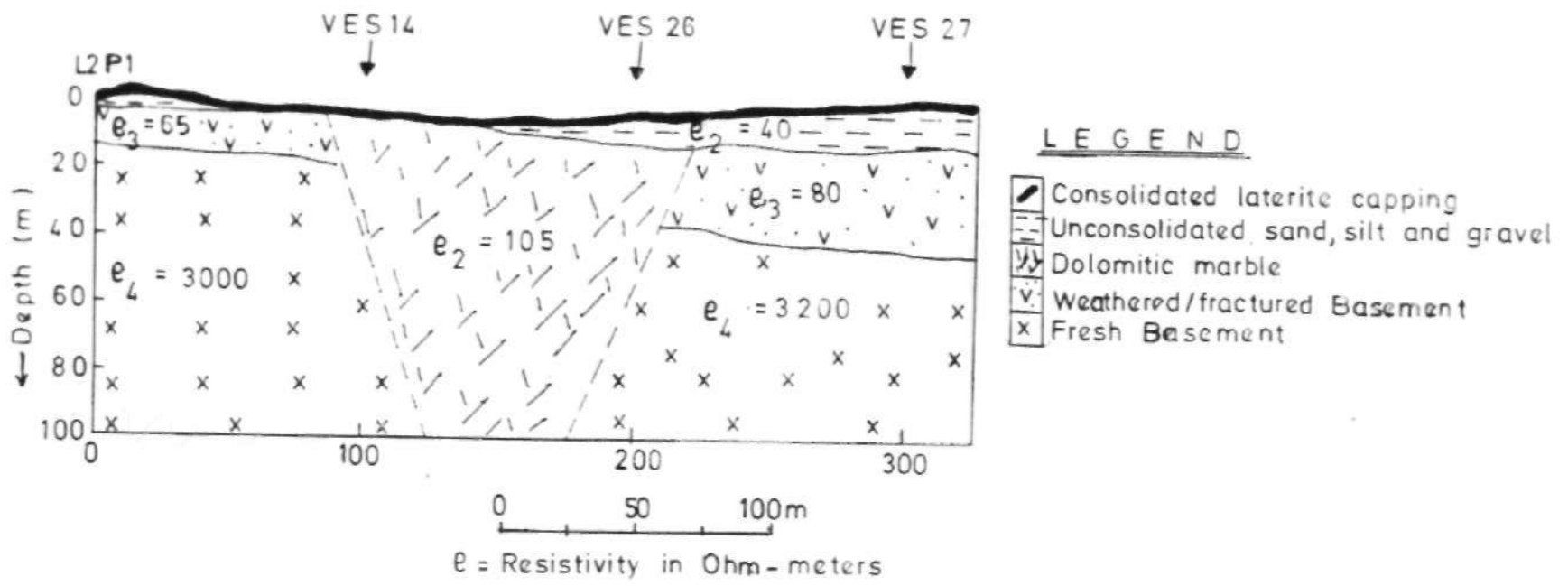


FIG. 3.3 : GEOELECTRIC AND GEOLOGIC SECTION ACROSS LINE L_2 (CC')

3.3.4 Geoelectric Section for Profile DD'

A geoelectric section cutting diagonally through L_7 P_{-1} and L_0 P_4 is shown in fig. 3.4. It was obtained from results of the interpretation of the VES points lying on or close to section DD' (fig. 2.5). As in most of the profiles discussed above, four geoelectric units were identified on this profile. The first unit is a relatively thin layer (<1m) with a resistivity value varying between 200 and 1000 Ohm-m. The second layer has a resistivity value of 35 - 50 Ohm-m while its thickness varies from 0 around VES 23 to 16.2m at VES 33. The third layer with a resistivity value ranging from 105 to 135 Ohm-m has a variable thickness of between 39.5 and 102m. This third unit is underlain by the highly resistive layer (2000 - 3200 Ohm-m) of infinite thickness.

3.3.5 Geoelectric Section for Profile P_3 (EE')

Fig.3.5 shows the geoelectric section obtained from interpretation of the VES points on profile P_3. As in the previous cases, the figure suggests that four geoelectric units generally occur beneath this profile. They consist of a very thin upper layer with a resistivity value ranging between 200 and 1000 Ohm-m. This layer overlies a lower resistive unit with a resistivity value of 40 - 50 Ohm-m and a thickness varying between 2.4 and 9m. On either side of VES 26 about 50m away from it, the second layer is underlain by a third layer with a resistivity value between 70 and 80 ohm-m and thickness between 10.5 and 38m.

AHMADU BELLO UNIVERSITY
ZARIA NIGERIA

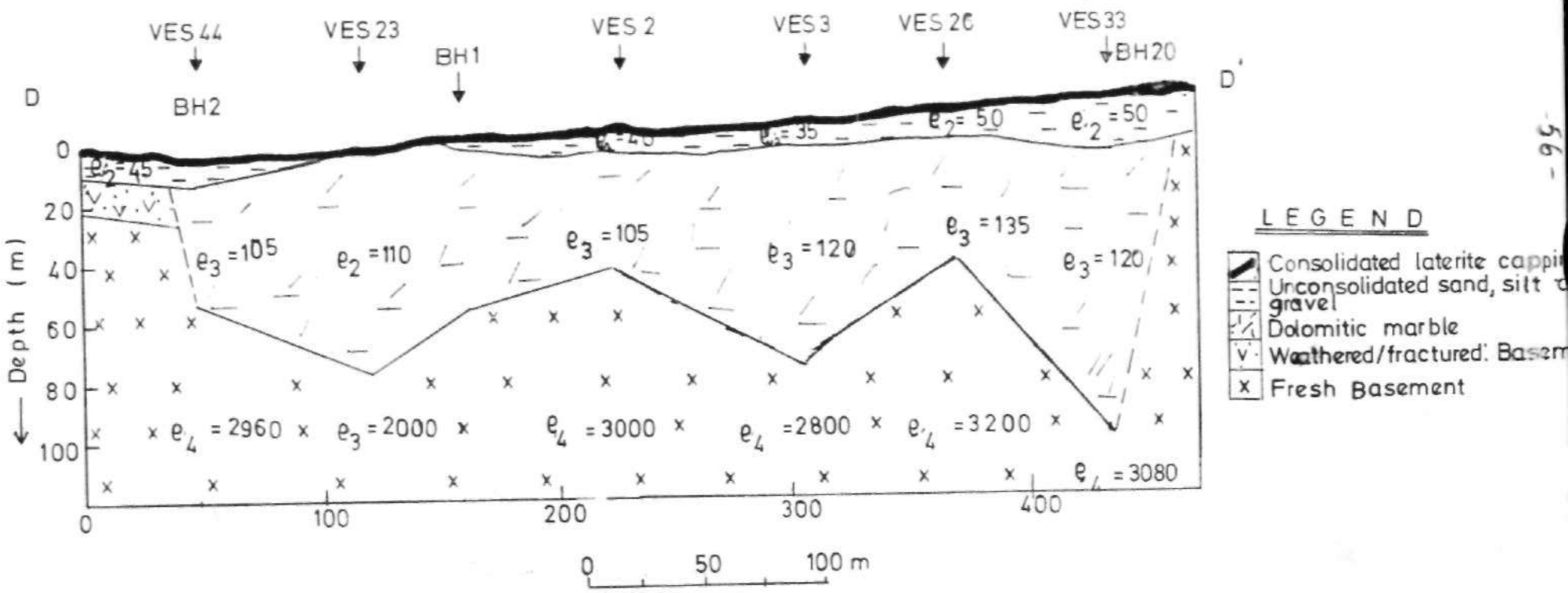


FIG. 3.4 : GEOELECTRIC AND GEOLOGIC SECTION FOR PROFILE DD'

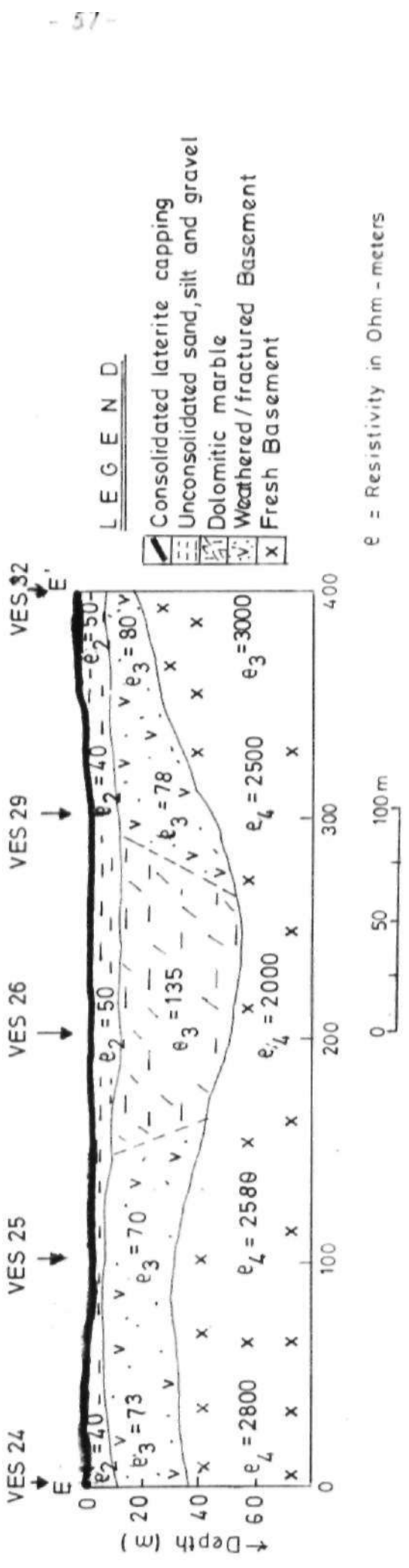


FIG-3.5 :GEOELECTRIC AND GEOLOGIC SECTION ACROSS PROFILE P_3 (EE')

At VES 26, the second layer is underlain by a unit with a resistivity of 135 Ohm - m and a thickness of 39.5 Ohm - m. The fourth layer of infinite depth has a high resistivity ranging from 2000 to 3000 Ohm - m.

3.3.6 **Geologic Sections from Borehole data**

Information on the geology of an area is very important for any meaningful interpretation of geophysical data acquired from the area. Borehole information from some boreholes drilled by SRMEA within the project area were, accordingly, taken into consideration in deriving the geologic units represented by the geoelectric layers discussed above.

A geologic section produced from data from Borehole BH.2 is shown in fig. 3.6a. The figure shows that the following three lithological units exist in the borehole:

i) A laterilic top soil which essentially consists of brownish sand, silt and gravel. Its thickness is 9.85m.

ii) A whitish granoblastic fine to coarse grained rock, composed chiefly of dolomite. This rock unit which shows a streaky alteration of light and dark patches is part of the marble deposit. Its thickness is 42.5m.

iii) The third layer is a light coloured igneous rock. It is coarse grained and consists essentially of feldspars, quartz, biotite, horneblende etc. This third layer is the fresh crystalline basement which constitutes the bedrock in the area.

10a

LEGEND



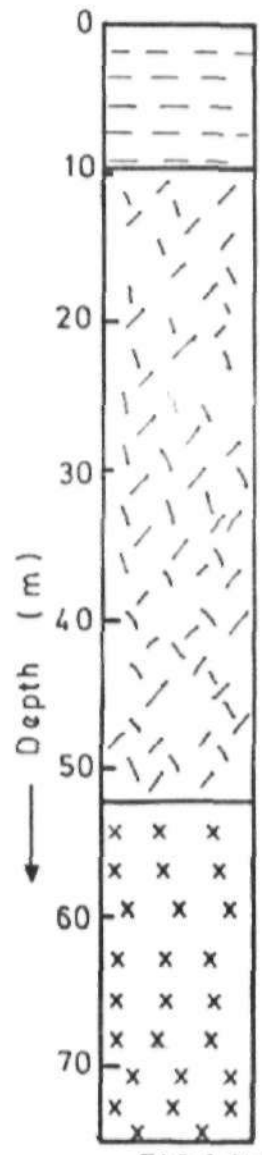


FIG-3.6a.
GEOLOGIC SECTION FROM BH-2

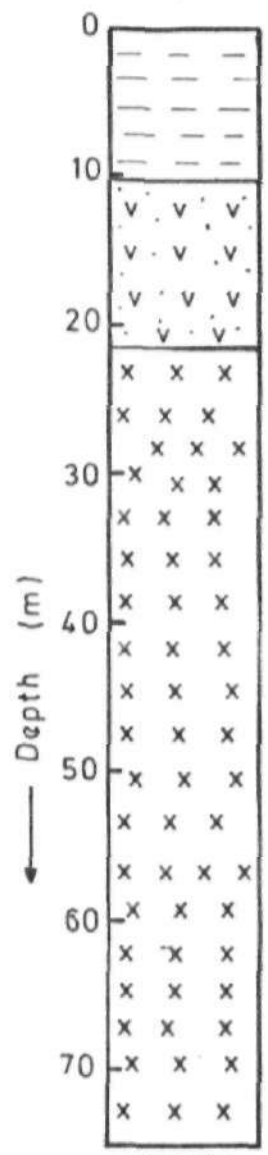


FIG-3.6 b
GEOLOGIC SECTION FROM BH-11

Borehole log for BH.11 (fig. 3.6b) also confirms the presence of the three lithological units discussed above for BH.2. However, the thickness of the second layer is much smaller than that for BH.2. The layer is about 42.55 in BH.2 while it is only about 11m in BH.11. Also, while the second layer is dolomite marble in BH.2, it is weathered basement in BH.11.

3.3.7 Correlating the Geoelectrical and Geologic Sections

The geoelectric section of an area may differ from its' geologic section because the boundaries between geoelectric layers are determined by resistivity contrasts as against a combination of factors used in establishing geological boundaries between beds-Keller and Frischknecht (1970). Boundaries of geoelectric sections may coincide with boundaries in geologic sections, particularly when there is a pronounced change in texture at such a boundary. A single geologic unit may consist of several rocks with quite different texture, and so, correspond to several geoelectric units. Conversely, rocks of different geologic ages may be uniform electrically, and may therefore be classified as a single unit in geoelectric section. To minimise this problem, some of the VES points were, therefore, located beside existing boreholes in the project area.

Such VES stations are 1, 44 and 33 which were located beside Boreholes BH.11, BH.2 and BH.20 respectively. The geoelectric and geologic sections for the first two stations are shown in figs. 3.7a and 3.7b respectively.

Fig. 3.7a and 3.7b show that the geoelectric and geologic boundaries approximately coincide with the thicknesses of the corresponding layers differing by about 2.5%. The only exception being that the first relatively thin geoelectric layer was not distinguished in the geologic section. On the basis of the observed good correlation between the geoelectric and geologic boundaries at these boreholes, the geoelectric sections were then directly converted to geologic sections for the remaining VES stations. Doing so is expected not to introduce errors higher than 3% in the thickness of the various layers.

As earlier discussed in the text, four geoelectric layers were generally identified within the project area. Based on the above correlation of the geoelectric and the geologic sections, the four layers have been assigned lithological units as follows.

The first layer of resistivity value between 250 and 2000 Ohm - m and a thickness of less than 1m which is not identified in the borehole log is thought to be consolidated lateritic soils (duricrust);

LEGEND

Lateritic top soil consolidated sand and silt

Dolomitic marble

Weathered/Fractured basement

Fresh basement (Granitic gneiss)

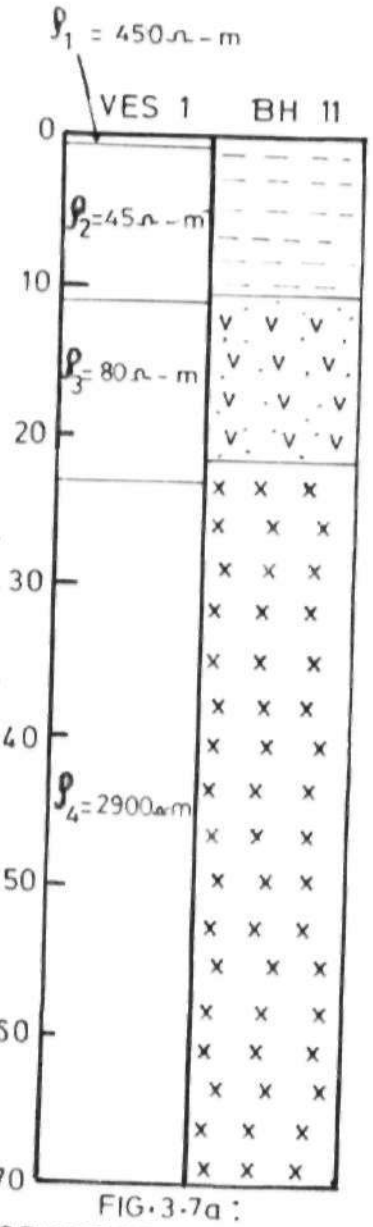


FIG. 3.7a :
GEOELECTRIC AND GEOLOGIC SECTION BENEATH $L_4 P_0$

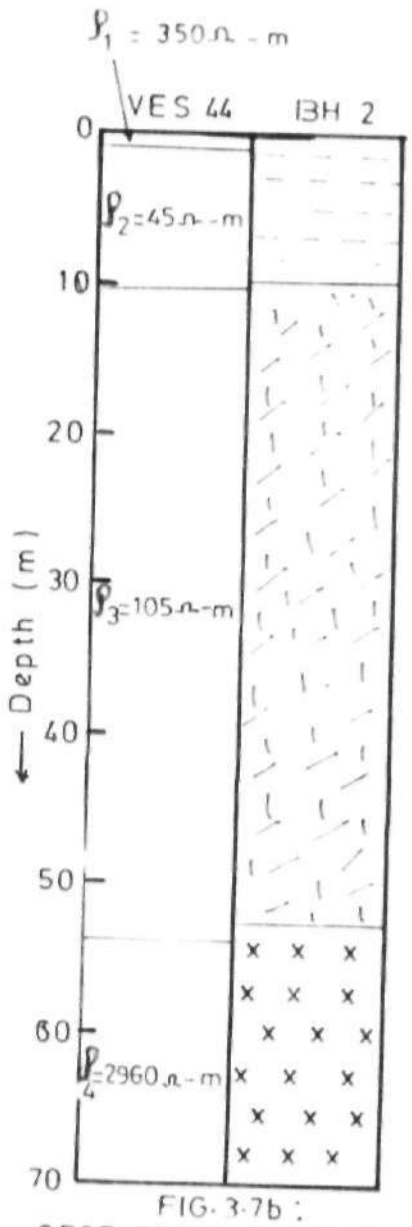


FIG. 3.7b :
GEOELECTRIC AND GEOLOGIC SECTION BENEATH $L_7 P_{-1}$

The second layer which is generally associated with relatively low resistivity values (25 - 60 Ohm - m) and whose thickness varies between 2 and 20m, is thought to be the layer of unconsolidated sand, silt and gravel identified in the borehole log. As can be seen from the borehole section, these first two geoelectric layers constitute the overburden within the project area.

The third geoelectric layer with resistivity values ranging between 65 and 96 Ohm - m and a thickness varying between 10 and 46m corresponds to the weathered and fractured basement. This third layer is replaced in some areas by the "anomalous layer" with resistivity values ranging between 105 and 135 Ohm - m and a thickness varying between 39.5 and 102m. As can be seen in fig. 3.7b, this "anomalous layer" is the whitish coarse grained dolomitic marble.

The fourth geoelectric layer which is associated with very high resistivity values (2000 - 4000 Ohm - m) and of infinite thickness, corresponds to the fresh basement which forms the bedrock of the entire project area.

CHAPTER 4

DISCUSSIONS

The results obtained in the last chapter are discussed in this chapter with respect to specific issues of interest related to the aims and objectives of this study. The issues concerned are discussed below:

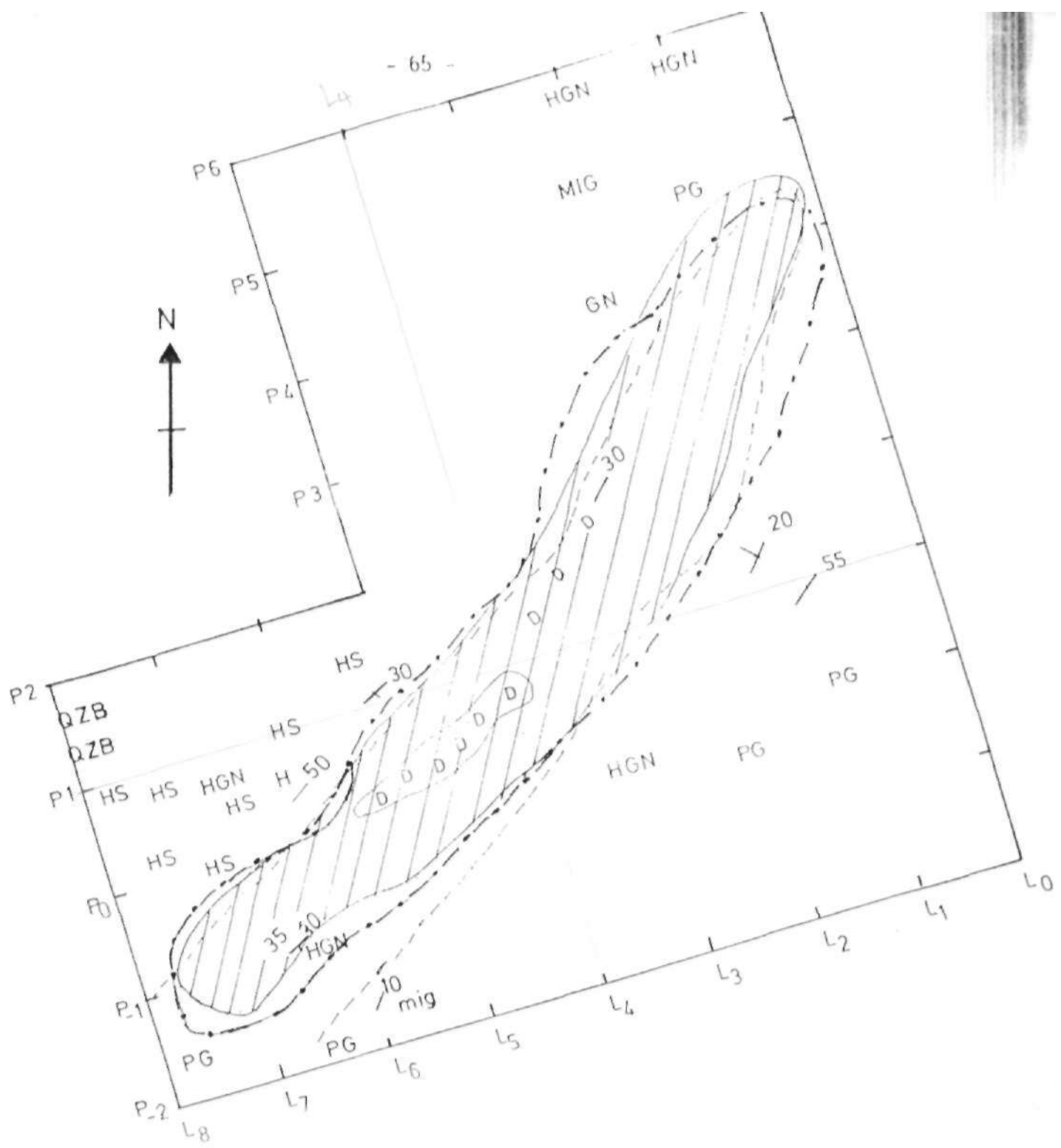
4.1 Outline of the Marble Deposit

The results of the resistivity profiling and VLF surveys revealed that the deposit extends laterally for about 950m in the NNE - SSW direction with an average width of about 120m.

There is a striking agreement between the outline inferred from the iso - resistivity contour map (fig. 2.8) and those inferred from VLF (EM) data (figs. 2.12 and 2.13). A superposition of the outlines of the marble deposit as obtained from the resistivity profiling and VLF (EM) surveys, on the geological map of the project area is shown in fig. 4.1.
The close match between these independently obtained outlines of the marble deposit tends to suggest that the outline of the deposit has been reasonably delineated within the limits of measurement errors.

4.2 Preliminary Estimate of the Quantity of the Marble Deposit

Mining is a very expensive venture which requires a very huge initial capital investment.



LEGEND

—·—·— Outline of the deposit from RP Survey

– – – – – Outline of the deposit from VLF Survey

Outline of the deposit from geological Observations and borehole data

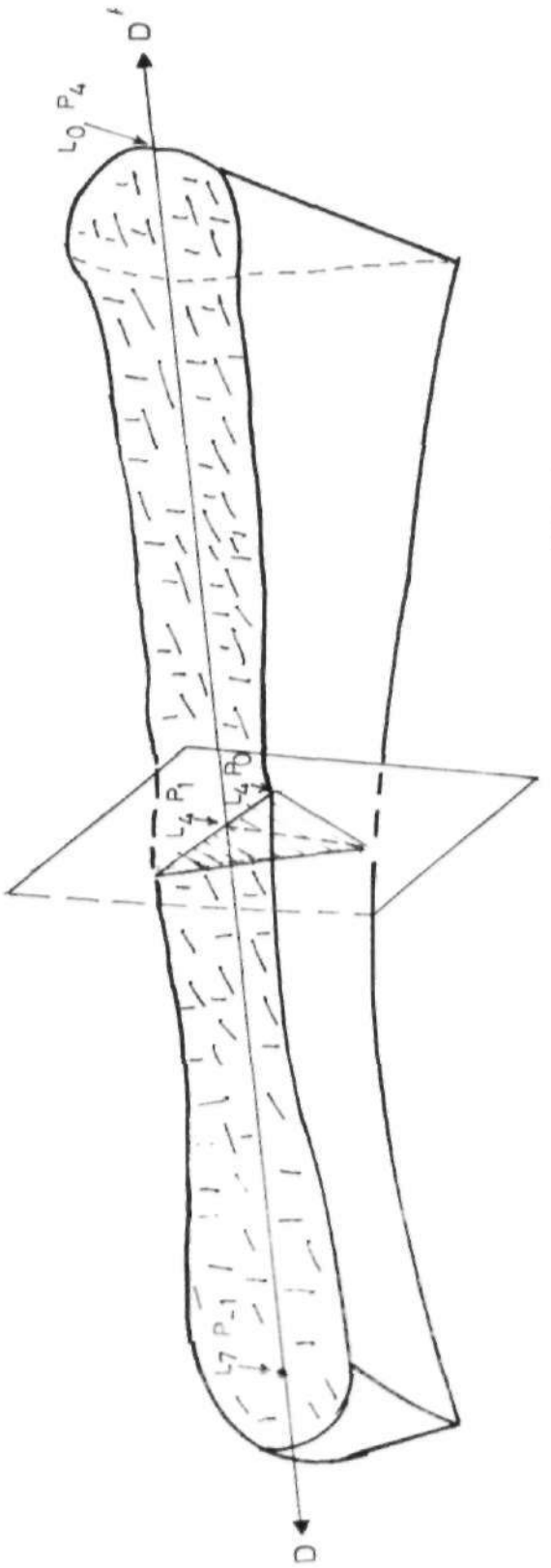
PG — Pegmatite
QZB — Quartzite boulders/pebbes
HS — Hornblende schist
G — Granite
D — Dolomite outcrop
⁄ — Strike and dip direct

FIG.4.1:A GEOLOGIC MAP OF THE PROJECT SITE SHOWING THE DELINEATED MARBLE DEPOSIT

Consequently, it is very essential to ascertain whether the marble deposit in Burum is in sufficiently large quantity as to be of mining interest to the Steel Raw Materials Exploration Agency (SRMEA). Therefore, it was considered necessary to estimate the quantity of the marble deposit based on the geophysical information obtained in this work.

For mathematical convenience, the outline of the deposit as deduced from fig. 4.1 can be approximated by a rectangle about 950m long and about 120m wide. The geoelectric sections in figs 3.1 to 3.5 suggest that the cross section of the marble deposit is most likely an inverted triangle, giving the body the shape of an inverted prism (fig. 4.2). Therefore the thickest portion of the deposit occurs beneath the basal central axis. Fig. 3.4 suggests that the thickness along the axis of the deposit is non-uniform. This thickness varies from 39.5m at VES 26 to 102m at VES 33. Using this shape, the volume of the marble deposit was computed to be 3.47×10^6 M^3. With the density of marble being 2.8×10^3 Kg M^{-3}, the minimum ore reserve within the project site was tentatively calculated to be 9.74×10^6 tonnes. Fig. 4.3 shows a 3 - dimensional distribution of the reserve within the project site.

As can be seen in fig. 4.2, a triangular cross section was assumed in the preliminary estimation of the quantity of the ore reserve above. Other very possible shapes are the dipping parallepiped and a trapezoid.



Not to Scale

FIG. 4.2 : A 3-D SKETCH OF THE MARBLE DEPOSIT

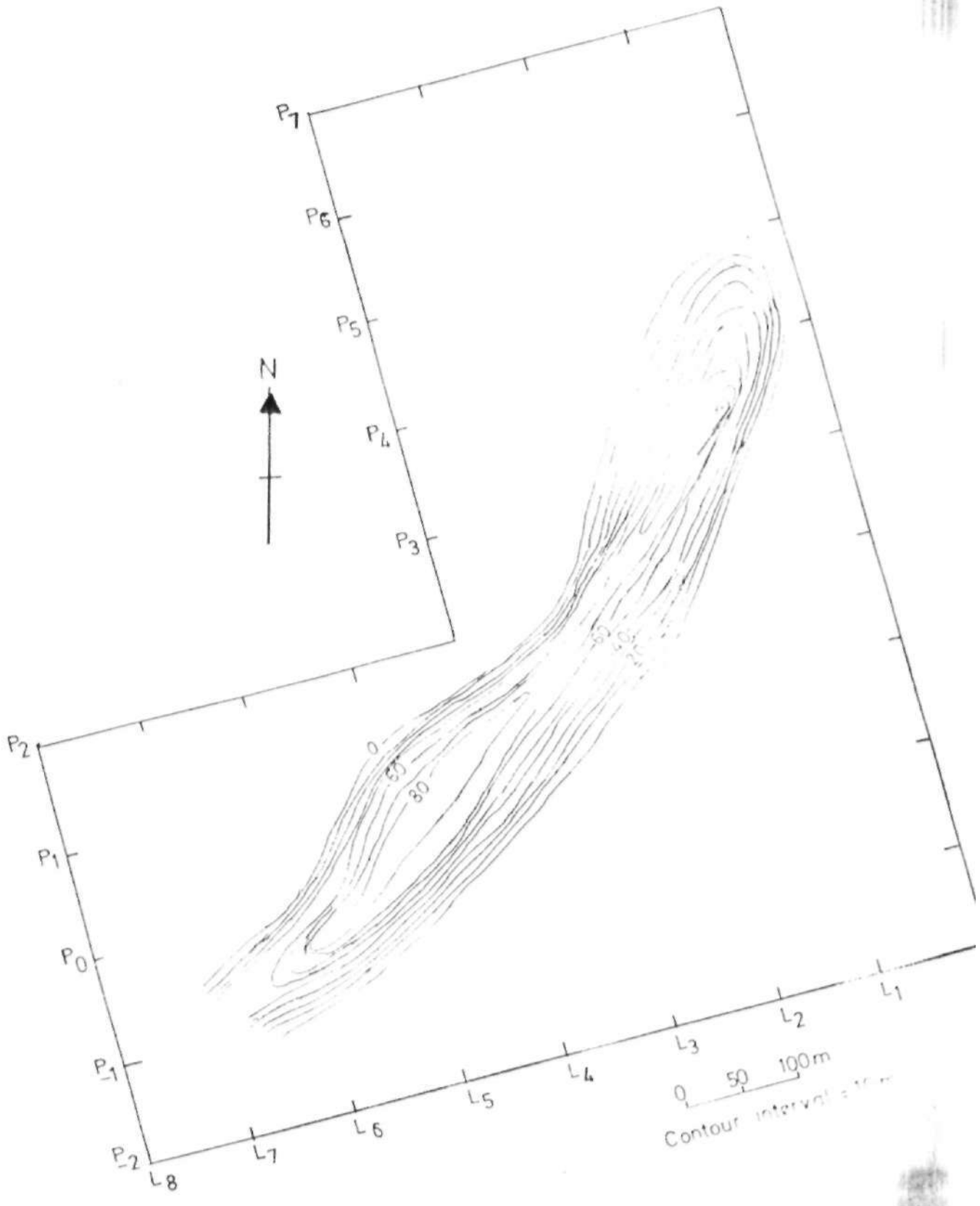


FIG.4.3:A CONTOUR MAP SHOWING THE THICKNESS OF THE MARBLE DEPOSI

A dipping parallepiped will most likely not be valid because both the VES results and the borehole information show that the thickness of the ore diminishes as one moves from the central axis towards either of the two sides. This will not be the case if the ore body were a dipping parallepiped. On the other hand, a trapezoidal shape of the body cannot be ruled out since such a model can still be supported with the results of this investigation. Therefore, if the body has a trapezoidal cross section, then the estimated quantity of the ore reserve will increase by about 30 - 50%. Consequently, the ore reserve earlier estimated above is a very conservative preliminary estimate. Only a detailed drilling exercise can accurately give the true shape and quantity of the reserve.

4.3 The Pre-mining Conditions of the Deposit

A knowledge of the present geotechnical conditions of the deposit is required for appropriate and meaningful advice on possible exploration modes and inherent or associated problems to be envisaged. Such conditions of interest include:

- the thickness of the overburden, the thickness of the marble deposit, concealed geological structures, variation in degree of weathering of the bedrock and the strength of the rocks within the project area.

In order to know the variation of the overburden thickness in the area, an overburden thickness map (fig. 4.4) was produced for the project area. This map is useful for determining whether or not the ore should be mined by open-cast, or using underground techniques. This is so because an estimate of the amount of earth material that would be excavated to reach the marble in an open cast operation can be estimated from the map.

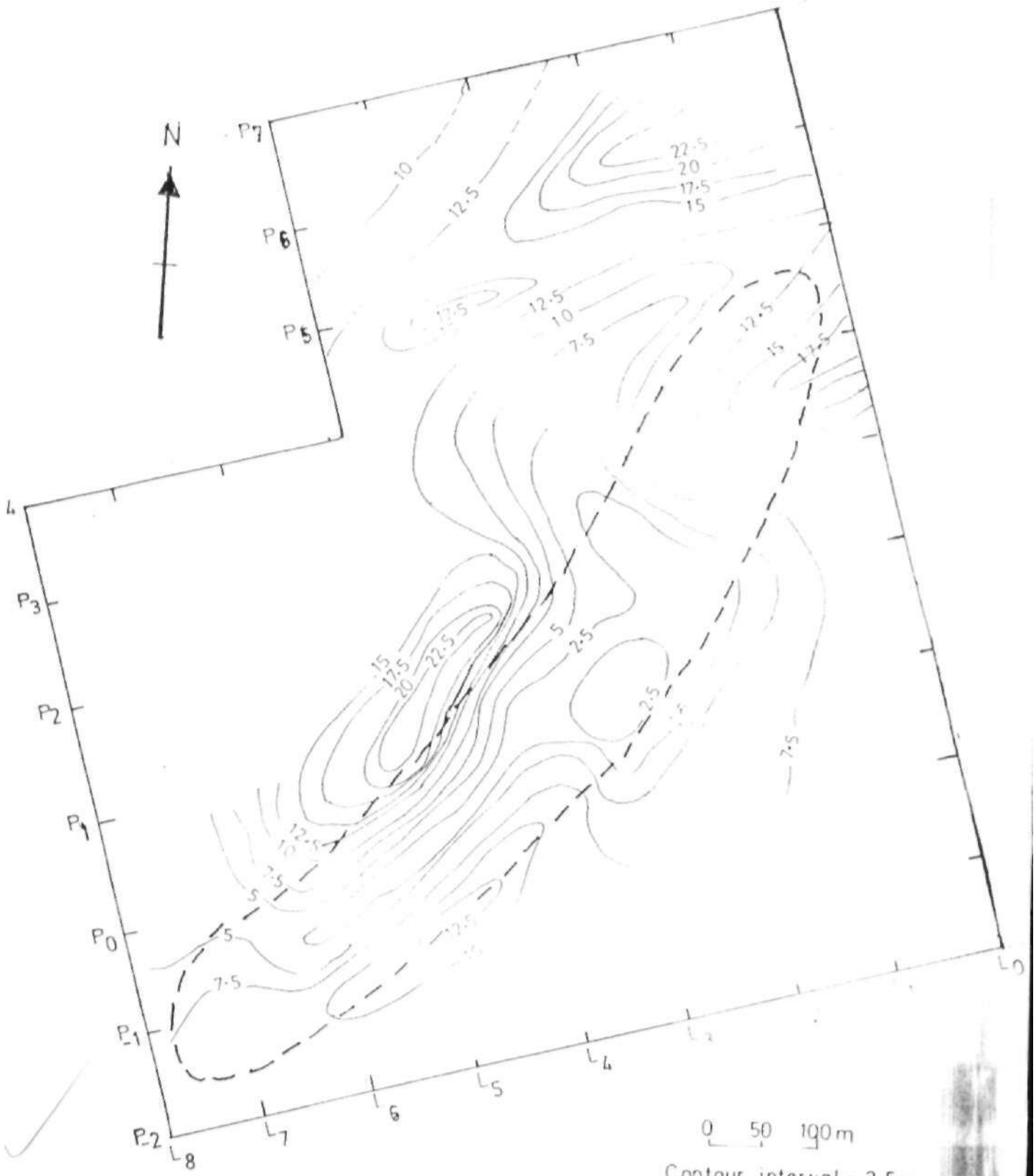


FIG.44:CONTOUR MAP OF TOTAL OVERBURDEN THICKNESS

The map shows that the thickness of the overburden overlying the deposit varies from 0 to 25m with an average of about 12m. From these values, the total volume of overburden overlying the marble deposit is estimated to be about 1.37×10^6 M^3. As can be seen from the map, the overburden is thickest in the areas north of the deposit.

Considering the structural conditions of the area, the region between P_2 and P_4 (fig. 2.8) is generally associated with relatively low apparent resistivity values (18-60 Ohm - m). The VES results also reveal that the overburden and basement resistivity values in this zone are relatively lower than for any other zone of the study area. These low resistivity values most likely suggest that the rocks in this zone are comparatively weaker than those in the rest of the study area. This may possibly be due to a higher degree of weathering and/or fracturing or even faulting of the basement rocks in the area. Mining in this region should be carried out with great caution because some caverns have been confirmed from borehole data, to exist in this zone (Awak and Williams, 1988).

Conversely, the iso-resistivity map (fig. 2.8) shows that the region bounding the deposit to the south is associated with relatively high resistivity values. According to Fagbe (1984), the resistivity of a given rock is related, among other things, to the elastic moduli of the rock. This implies that the strength of a rock is directly related to its' resistivity.

Consequently, the basement rocks in this region, because of their higher resistivity values, are expected to be stronger than those in other regions of the study area.

Hence, they are expected to withstand better, the high pressures and vibrations associated with heavy mining and drilling equipments. This region is, therefore, considered the most appropriate for installing the heavy plants to be used for the mining operations.

4.4 Present Hydrogeological Conditions

A fore - knowledge of the hydrogeological condition of the project site is required in order to know and plan strategies to evade possible hazards which might result from sudden encounter with large volumes of trapped water during mining operations. The present hydrogeological conditions of the site were inferred from the resistivity profiling and VES data.

As mentioned earlier, the relatively low resistivity values in the region between P_2 and P_4 (fig. 2.8) suggests that the area is most likely a comparatively weaker region, with possibly, a higher degree of weathering and fracturing of the basement rocks. If this is so, the region will most likely, also have a higher saturation than other regions of the study area. Also, the VES results suggest that the weathered/fractured basement is most likely thicker in that region than in other regions of the study area. The above conditions are favourable factors for good accummulation and flow of groundwater, especially in a basement terrian. Consequently, the possibility of groundwater interfering with mining/drilling operations within this region should be envisaged and necessary precautions taken to avoid possible losses of lives and/or equipments.

In case there is a need to supply groundwater for the mining operations, the chances of getting productive wells within this region is higher than in any other part of the project area. This is because the aquiferous layer (the weathered/fractured basement) is most likely thickest in the region.

CHAPTER 5

CONCLUSIONS AND RECOMMENDATIONS

5.1 Conclusions

The geophysical investigation discussed in this work has attempted to unravel the outline and shape of the Burum Marble deposit. It has also provided an idea of the behaviour of the basement topography, the distribution and thickness of the overburden, the nature and respective thicknesses of the lithologic units within the project area. The lateral variation in the values of apparent resistivity within the area, at a horizon whose depth is between 15 and 20m from the surface, was also revealed.

Using results from the resistivity profiling and VLF (EM) surveys, the outline of the marble deposit was reasonably delineated (See fig. 4.1). The outline suggests that the deposit trends in the NNE - SSW direction with an average width of 120m and a length of 950m, extending diagonally from $L_{7.8}\ P_{-1.2}$ to $L_{0.2}\ P_{4.2}$ (fig. 4.1).

Results from the vertical Electrical Soundings (VES) and borehole logs in the area suggest that the body possibly has a triangular cross section (figs. 3.1, 3.2, 3.3) and is thickest along its central axis. Its thickness tends to diminish as one moves from its middle (L_4P_1) towards the side boundaries (say L_4P_0) as shown in fig. 4.2.

Geoelectric section DD' (fig. 3.4) further suggests that the axial core thickness is not uniform but undulates between 43.5m at VES 44 and 102m at VES 33, with an average of about 61m. From these geophysical and borehole evidences, an inverted triangular prism with a rectangular top model has been proposed for the deposit.

With this approximation the quantity of the in-situ ore reserve of the Burum dolomitic marble deposit has been preliminarily estimated at about 9.74×10^6 metric tonnes. A map showing the variation in thickness of the marble deposit within the area (fig. 4.3) was also produced for the deposit.

Generally, the geoelectric sections suggest the existence of four units (layers) in the area. The borehole sections in the area show the existence of three such layers whose boundaries approximately coincide with the boundaries of the geoelectric layers, excluding the first geoelectric layer which was not distinguished in the geologic log. The four geoelectric layers were correlated with the geologic layers as follows:

i) The surface layer with a resistivity value between 250 and 2000 Ohm - m and a thickness of less than 1m is essentially a consolidated lateritic layer (duricrust).

ii) The second layer with resistivity value ranging between 25 and 60 Ohm - m and a thickness of between 2 and 20m is an unconsolidated layer of sand, silt and gravel shown in the borehole log (fig. 3.7a).

iii) The third layer with a resistivity value between 65 and 96 Ohm - m and a thickness between 10 and 46m is most likely the weathered/fractured basement.

iv) The third layer above is replaced in some regions of the study area by the marble deposit. In such areas, the resistivity of the marble layer varies between 105 and 150 Ohm - m while its thickness varies between 39.5 and 102m.

v) The fourth layer which underlies the whole project area has a resistivity value of 2000 - 4000 Ohm - m with an infinite thickness. This layer is most likely the fresh basement.

The VES results suggest that the total thickness of the overburden (layers (i) and (ii) above) varies between 0 and 24m within the area. The overburden thickness was generally less than 15m within the area occupied by the deposit but is relatively greater in the region north of the deposit where its maximum depth may be up to 24m (at $L_{4.5}$ $P_{1.5}$).

The investigations further suggest that the northern half of the project area, which is generally associated with relatively low apparent resistivity values (especially between P_2 and P_4) in fig. 2.8, may be a comparatively weak zone. The resistivity results further suggest that the layer of weathered and fractured basement in this region is most likely relatively thicker than in the southern part of the project area (fig. 3.2). Consequently, the basement rocks in the southern half of the project area are expected to be stronger than those in the northern part. Hence, the southern part of the project area will most likely withstand high pressures and vibrations than the northern part. Hence the heavy machineries that will be used in the mining activities should be located in the southern part of the project area.

Finally, because the thickness of the weathered/fractured layer, which constitutes the aquiferous layer within the area, is most likely thicker in the northern part of the project area, the area most likely has the highest ground water potentials. Borehole data at BH.20 located at L_1 $P_{3.5}$ have confirmed this inferrence (Williams, 1988). Hence, future water development for the mining activities should be sited in this region.

5.2 Recommendations and Suggestions for future Work

This investigation is expected to reduce, considerably, the overall cost of exploration of the Burum marble deposit. The results should help in controlling and limiting the siting and drilling of exploratory boreholes. The predicted ore reserve is a rough estimate based on geophysical results which have some obvious limitations as discussed in the text. It is therefore recommended that this estimate be improved upon using more information from boreholes that should be strategically and meticulously located within the area, based on the results of this work.

There is a possibility that the marble deposit extends north-eastwards beyond L_o (fig. 4.1). Further investigation is, therefore, recommended to ascertain this possibility. For this future work, profiles P_3 to P_6 should be extended eastwards beyond traverse line L_o.

In case of groundwater requirement, stations L_4 P_4 and L_4 P_3 have great potentials of yielding productive wells. The weathered/fractured basements, which is expected to constitute the aquifer is relatively thick at these points. They are, consequently, recommended for siting of water boreholes should the need arise.

REFERENCES

Aggarwal, N. (1983): Application of Geophysical Methods to delineate Kaolin Depositsand Survey for groundwater potentialities at Minjibir, Kano State. Unpublished M.Sc. Thesis, A.B.U. Zaria.

Ajibade, A.C. and Wright J.B. (1988):"Structural relationships in the Schist belts of North Western Nigeria" - The Precambrian Geology of Nigeria.
Geological Survey of Nigeria (1988) pp. 103 - 109.

Alade, O.N. (1981): Direct Current Resistivity and Self-Potential investigations at Shonga (Kwara State), Nigeria. Unpublished M.Sc. Thesis, A.B.U. Zaria.

Atlas Copco ABEM, (1981) Geophysical Instruments Limited.
ABEM Terameter SAS - 300 Instrument Manual.

Bates, R.L. (1969): Geology of the Industrial Rocks and Minerals.
Dover Publications, Inc., New York.

Bhattacharya, P and Patra, H. (1968): Direct Current Geoelectric Sounding.
Methods in Geochemistry and Geophysics.
Elsevier Publishing Co., New York.

Dada O. (1988): "The Schist Belt of the Nigerian Precambrian and its potential for Raw Materials Development for Steel Plants in Nigeria". - The Precambrian Geology of Nigeria.
Geological Survey of Nigeria (1988). pp. 211 - 218.

Deeson A.F.L. (1973): The Collectors Encyclopedia of Rocks and Minerals.
David and Charles: Newton Abbot, Devon.

Dobrin, M.B. (1976): Introduction to Geophysical Prospecting.
McGraw - Hill Book Co., Inc., New York.

Fagbe, O. (1984): A Resistivity Depth Sounding Survey applied to Hydrogeologic and Engineering Geologic problems. Unpublished M.Sc. Thesis, University of London.

Fraser, D.C. (1969): "Contouring of VLF - EM data" Geophysics Vol. 34, pp. 958 - 967.

Geonics Limited (1979): VLF - EM 16 Operating Manuals, 2, Thornoliffe, Park Drive, Toronto.

George, A. (1976): Analytical Interpretation of High Frequency E.M. Prospecting Data (VLF System). Unpublished M.Sc. Thesis, ITC Delft, Netherlands.

Ginzburg, A. (1974): "Resistivity Surveying", Journal of Geophysical Surveys, Vol. I, No. 3, pp. 325 - 355.

Grant, F.S. and West, G.F. (1965): Interpretation Theory in Applied Geophysics McGraw Hill Book Company, New York.

Habberjam, G.M. (1975): Apparent Resistivity, Anisotropy and Strike measurements Geophysical Prospecting, Vol. 23, No. 2 pp 211 - 247.

Hassan, M. (1987): Geoelectrical Investigations of the Western Half of the Kubanni River Basin, Zaria, Nigeria Unpublished M.Sc. Thesis, A.B.U. Zaria.

Jain S.C. (1980): "Electrical Properties of Rocks and Principles of Electrical prospecting". Methods and Techniques for Exploration Geophysics. NGRI Publication, Hyderabad, India.

Keller, G.V. and Frischknetch F.C. (1966) Electrical Methods in Geophysical Prospecting. Pergamon Press, New York.

Koefoed, O. (1969): "An Analysis of Equivalence in Resistivity Sounding", Geophysical Prospecting, Vol. XVII, No. 8.

Maeda, K. (1975): Apparent Resistivity over Dipping Beds.
Geophysics, Vol. 20, pp. 123 - 139.

Mooney, H.M. (1973): Handbook of Engineering Geophysics.
Bison Instruments Inc., Minnesota.

Ofomata G.E.K. et al (1973): Atlas of the Federal Republic of Nigeria.
Federal Surveys, Lagos, Nigeria.

Orellana, E and Mooney, H.M. (1966): Master Tables and Curves for vertical electrical sounding over layered structures, Madrid, Intersiecia Publishers.

Oyawoye, M.O. (1964): Geology of the Nigerian Basement Complex,
Journ. of Min. and Geol., Vol. I, pp. 87 - 102.

Parasnis, D.S. (1968): "Prospecting for Ore by Electromagnetic Waves"
Geophysical Memorandum 1/68,
Atlas Copco ABEM, Sweden.

Parasnis, D.S. (1971): "Physical Property Guide for Rocks and Minerals".
Geophysical Memorandum 4/71,
Atlas Copco ABEM, Sweden.

Parasnis, D.S. (1975): Mining Geophysics,
Elsevier Publisher Company, New York.

Parasnis, D.S. (1979): Principles of Applied Geophysics,
Chapman and Hall, London.

RaO, A.A. (1980): Resistivity Profiling and Data interpretation,
Methods and Techniques for exploration
Geophysics, NGRI publication,
Hyderabad, India.

Read, H.H. and Watson J. (1973): Introduction of Geology. vol. I.
Macmillan Press Limited London and Bassingstoke.

Telford, W.M. Geldart, L.P., Sherif, R.E. and Keys,
D.A. (1976): Applied Geophysics,
Cambridge University Press.

Trustwell, J.F. and Cope, R.N. (1963): The geology of parts of Niger and Zaria Provinces, Northern Nigeria. Geological Survey of Nigeria Bulletin 29.

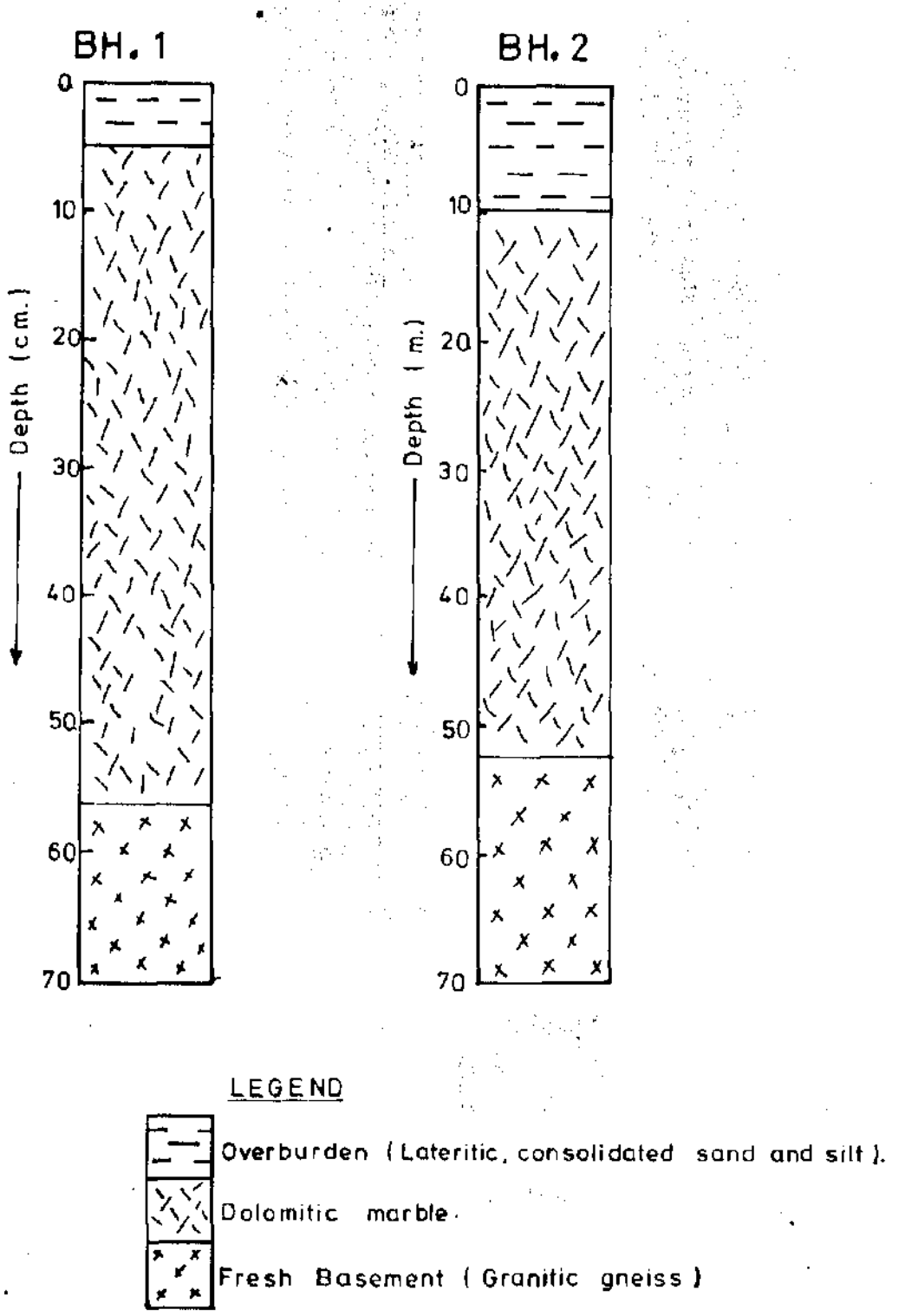
Turner, F.J. (1963): The Daura Igneous complex, Northern Nigeria. A Link between the Younger Granites districts of Nigeria and S. Niger. Journal of the Geological Society pp. 71 - 78.

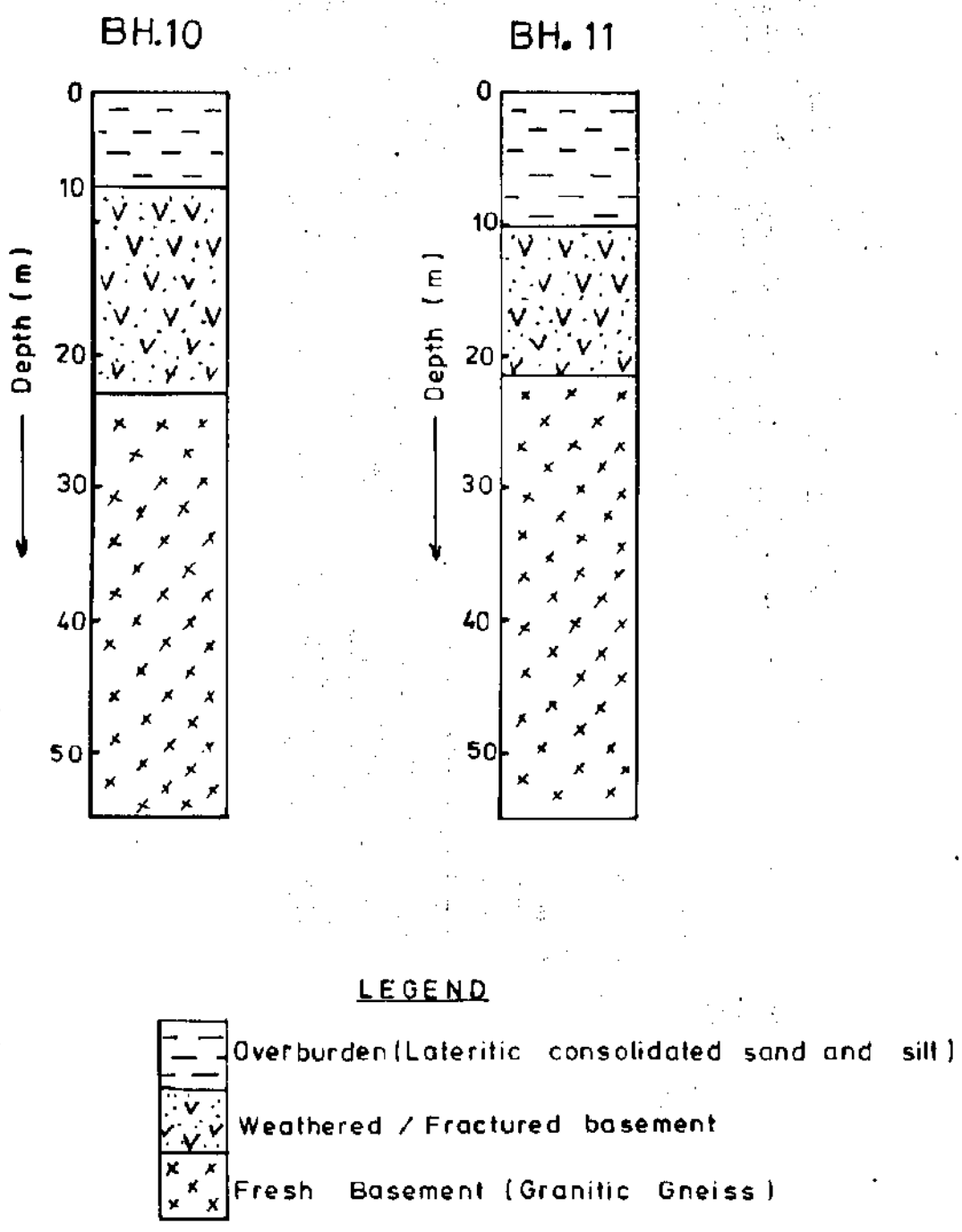
Vingoe P. (1972): "Electrical Resistivity Surveying". Geophysical Memorandum 5/72. Atlas Copco ABEM, Sweden.

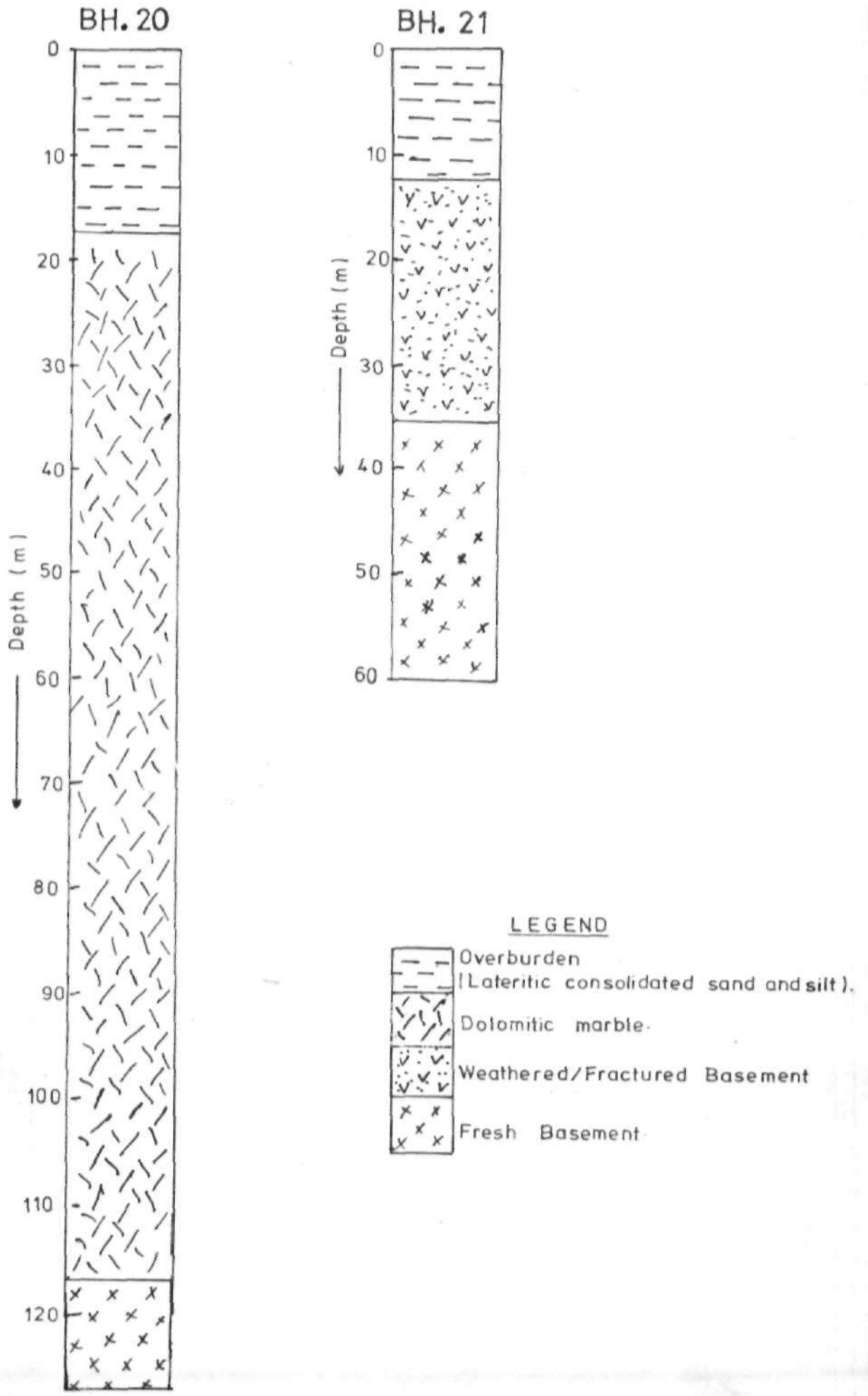
Wright J.B. and McCurry, P. (1970): The geology of the Zaria sheet 102 S.W. Zaria and its Region. Edited by M.J. Mortimore. Department of Geography occasional Paper No. 4. A.B.U. Zaria.

APPENDIX I

GEOLOGICAL SECTIONS FROM BOREHOLE DATA

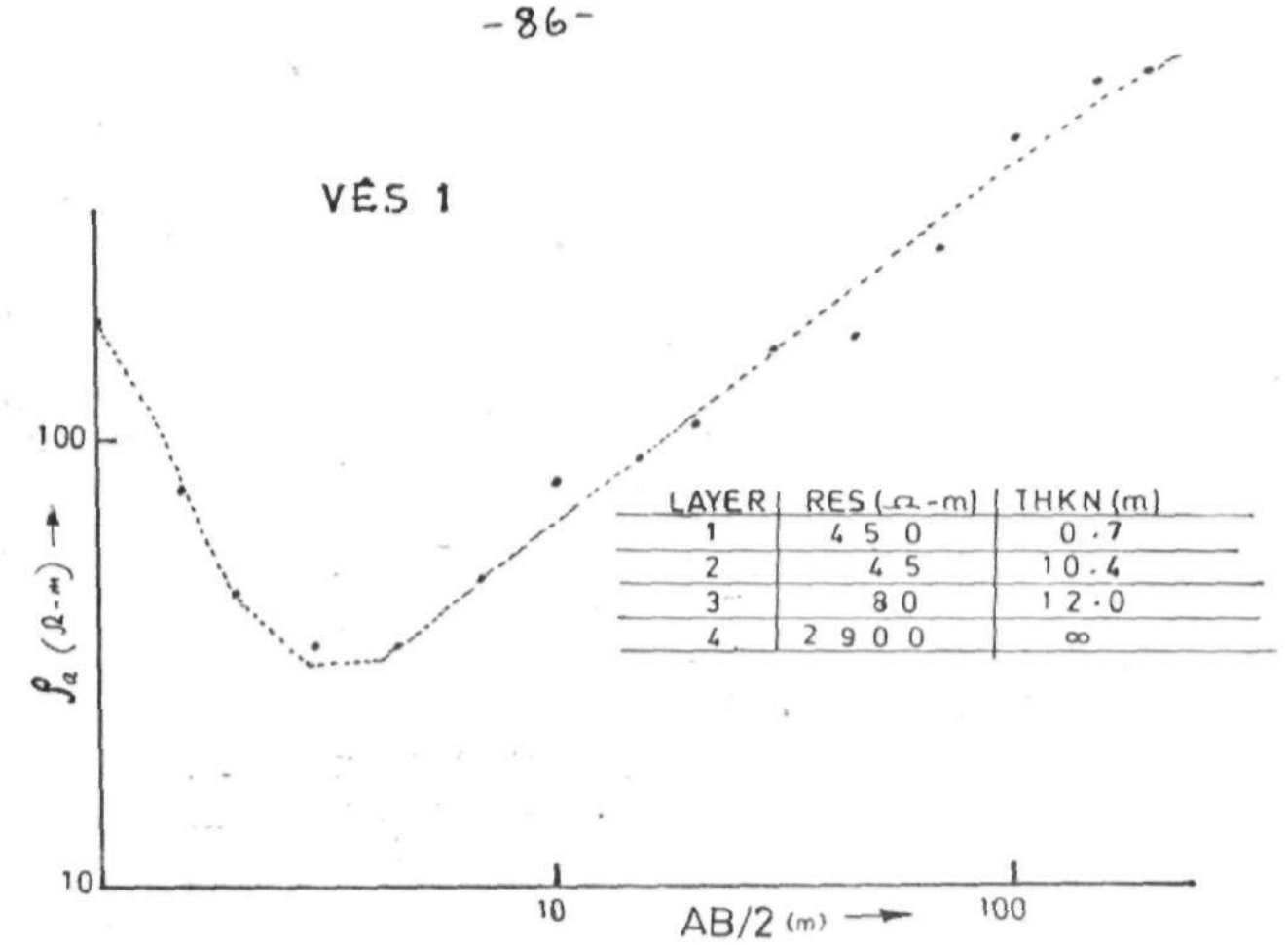

BH. 1
BH. 2
Depth (cm.)
Depth (m.)
0
10
20
30
40
50
60
70
LEGEND
Overburden (Lateritic, consolidated sand and silt).
Dolomitic marble.
Fresh Basement (Granitic gneiss)

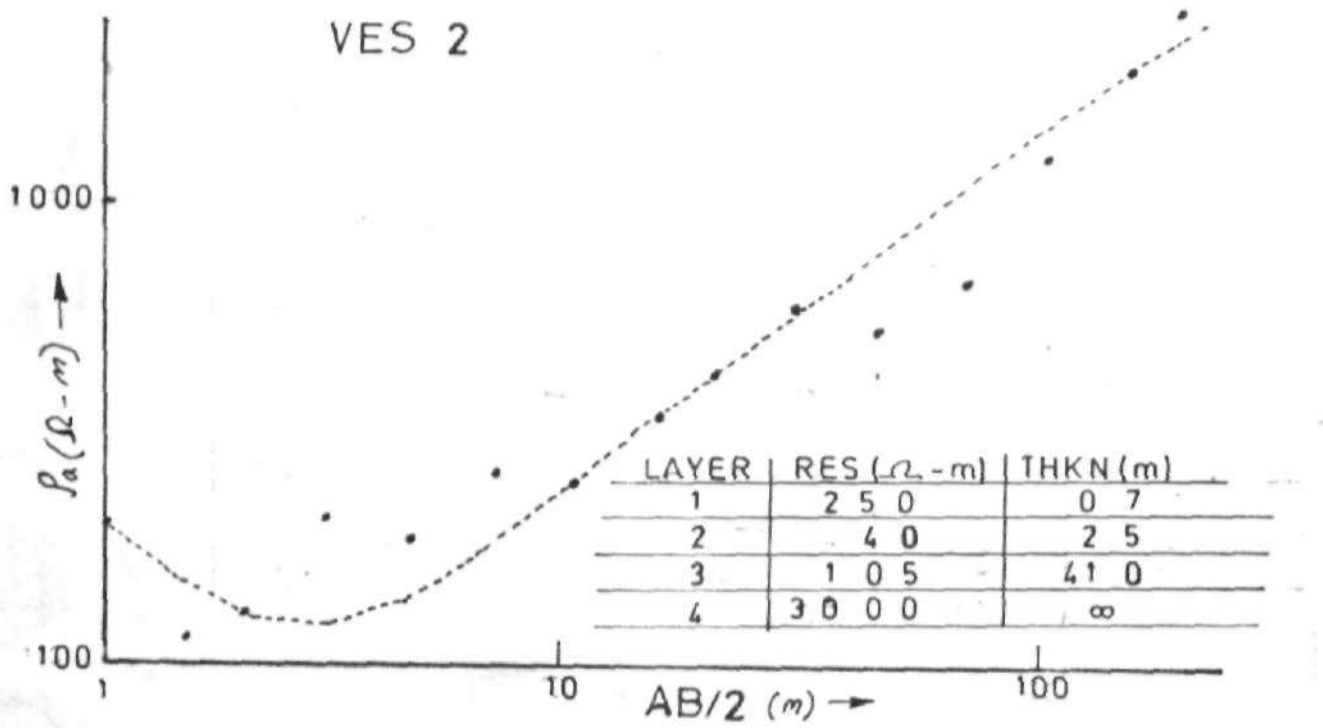

BH.10
BH. 11
Depth (m)
0
10
20
30
40
50
LEGEND
Overburden (Lateritic consolidated sand and silt)
Weathered / Fractured basement
Fresh Basement (Granitic Gneiss)

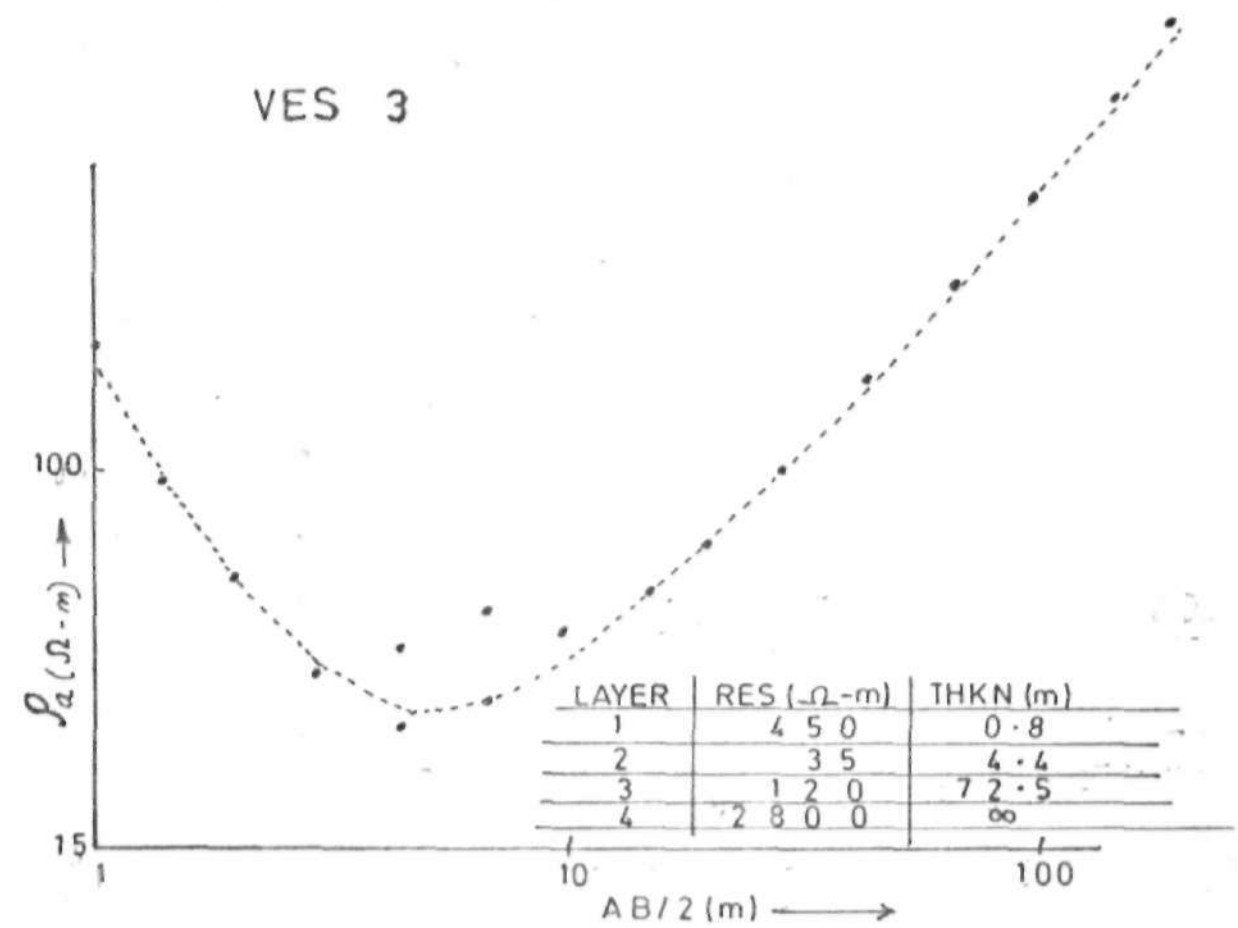

BH. 20
BH. 21
Depth (m)
0
10
20
30
40
50
60
70
80
90
100
110
120
LEGEND
Overburden
(Lateritic consolidated sand and silt).
Dolomitic marble.
Weathered/Fractured Basement
Fresh Basement

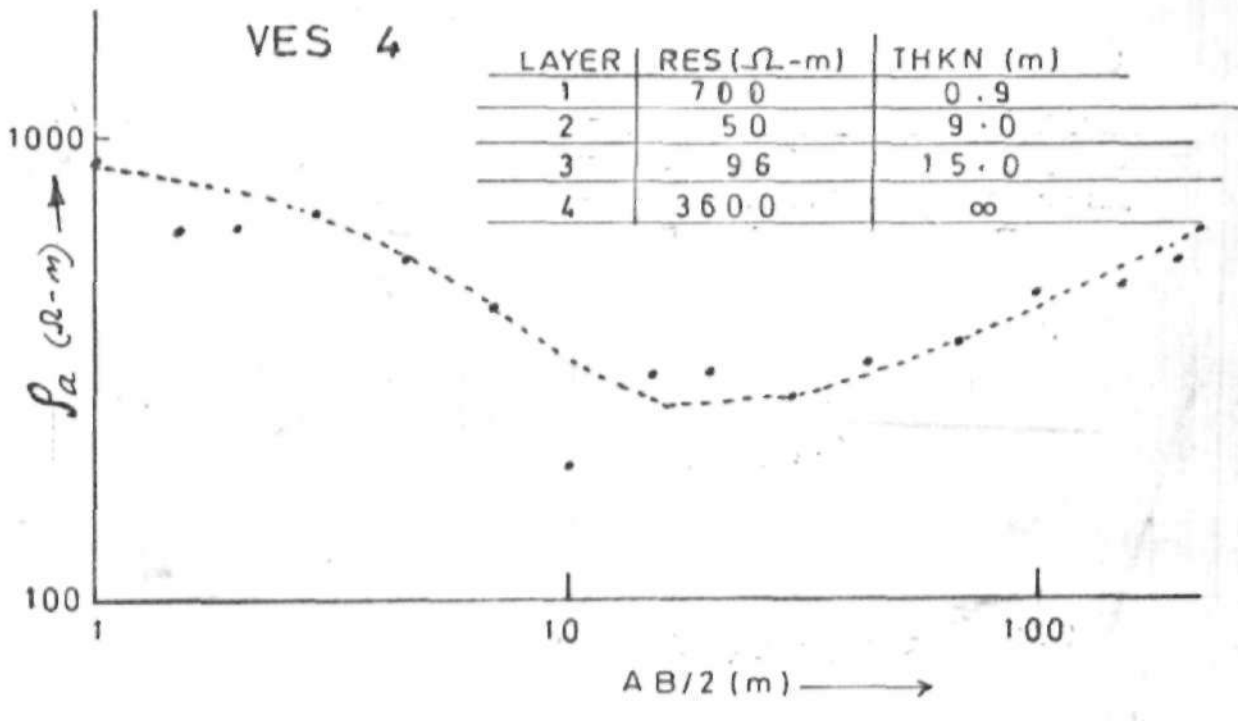
APPENDIX II

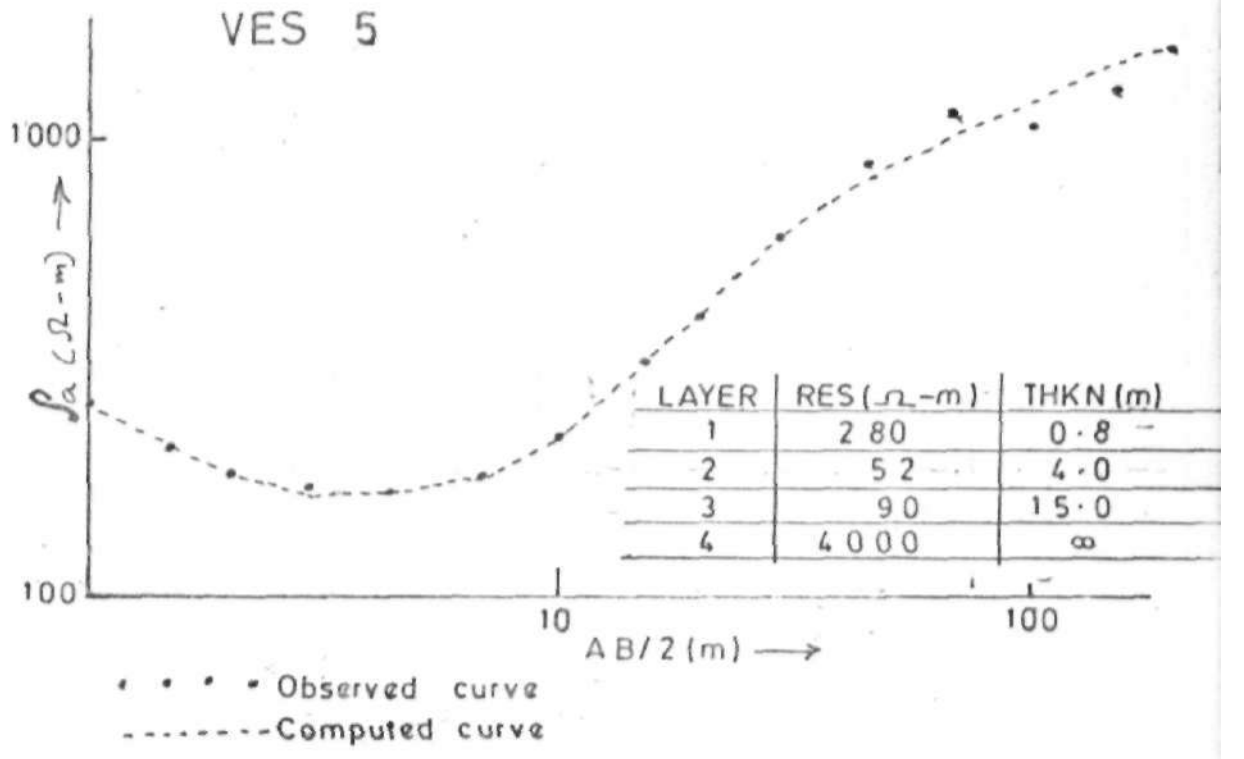
INTERPRETED VES FIELD CURVES

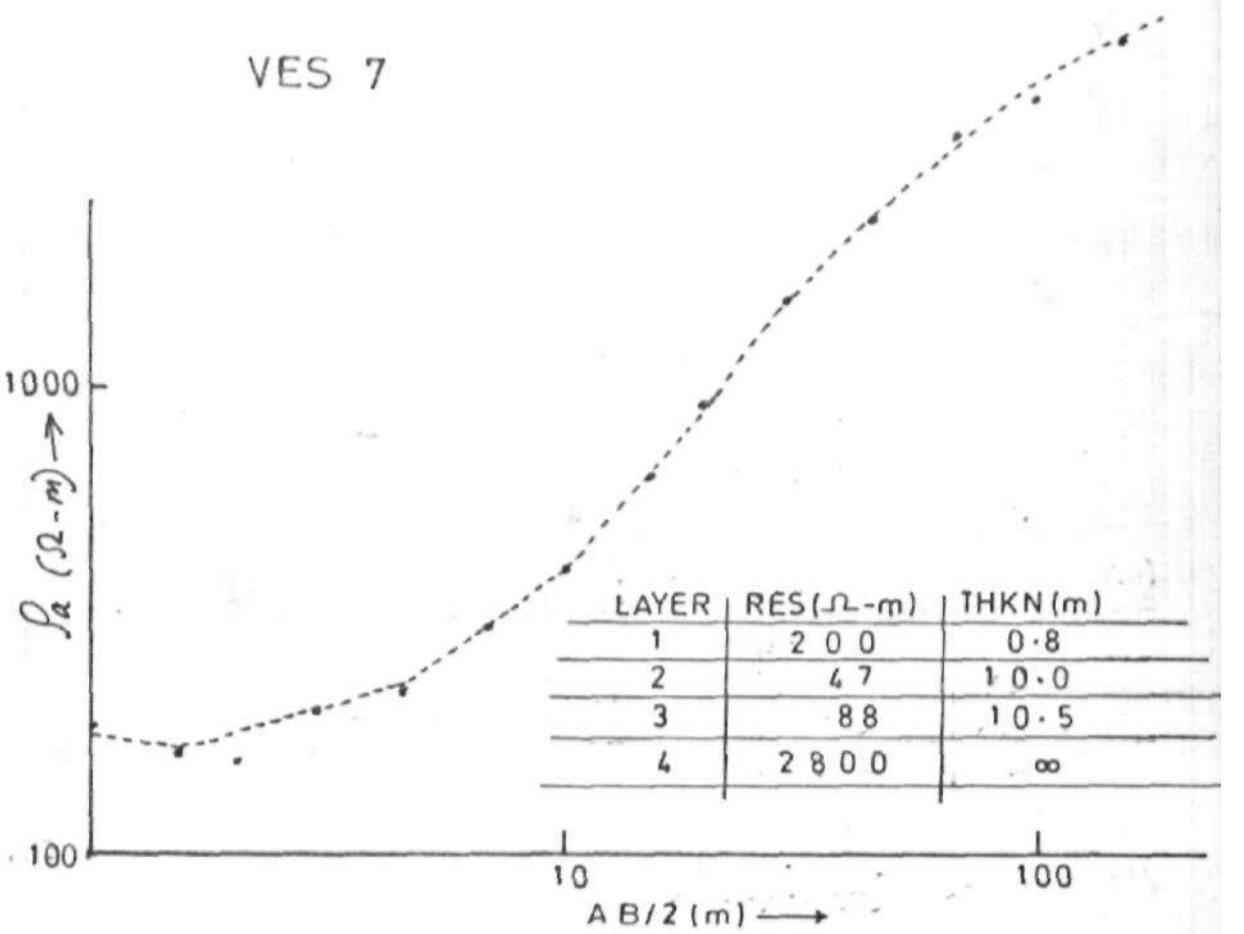

VES 1
100
10
ρ_a (Ω-m) →
10
AB/2 (m) →
100
LAYER | RES (Ω-m) | THKN (m)
1 | 450 | 0.7
2 | 45 | 10.4
3 | 80 | 12.0
4 | 2900 | ∞
- - - - Observed curve
– – – – Computed curve

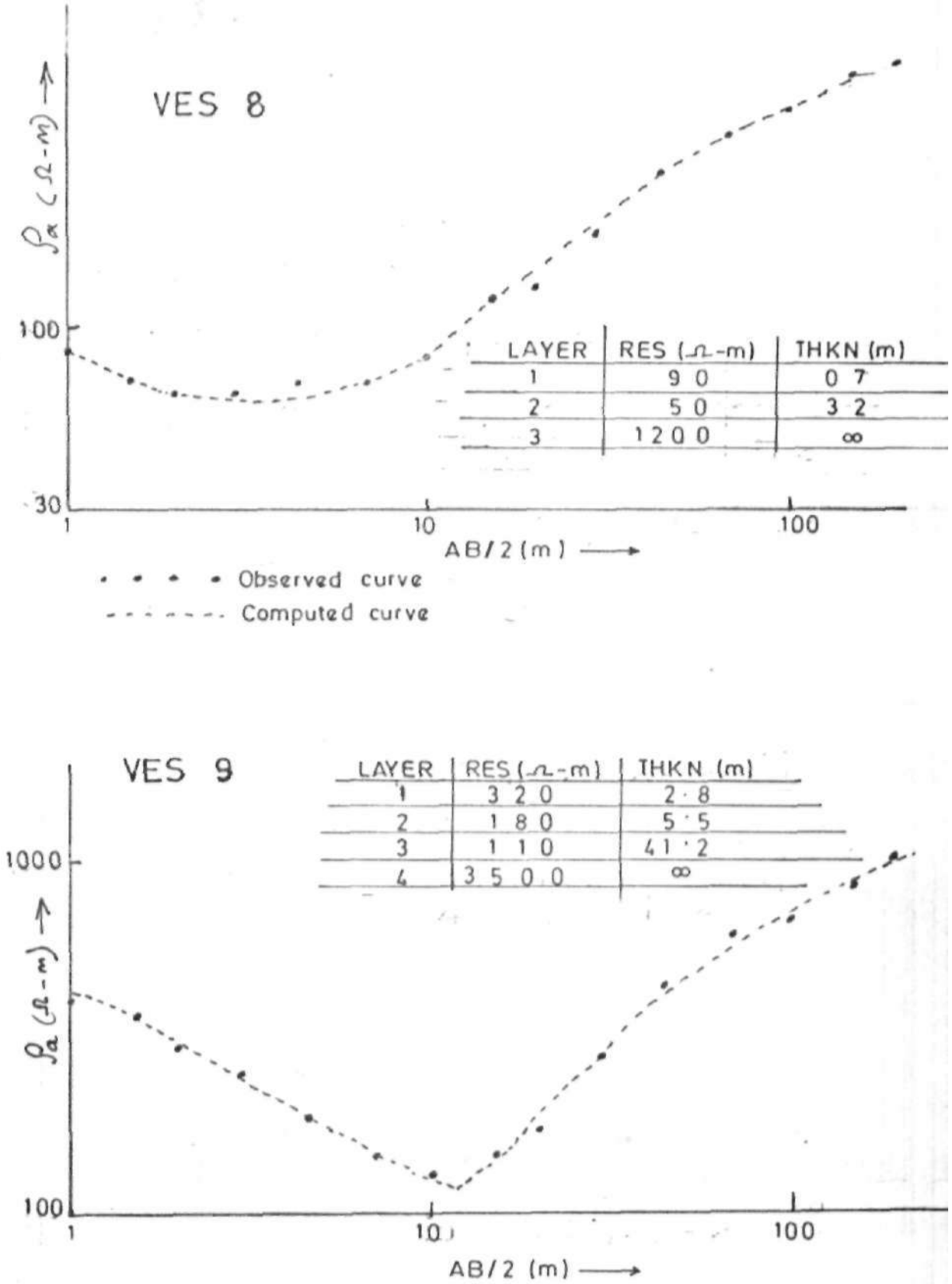

VES 2
1000
100
ρ_a (Ω-m) →
1
10
AB/2 (m) →
100
LAYER | RES (Ω-m) | THKN (m)
1 | 250 | 07
2 | 40 | 25
3 | 105 | 410
4 | 3000 | ∞

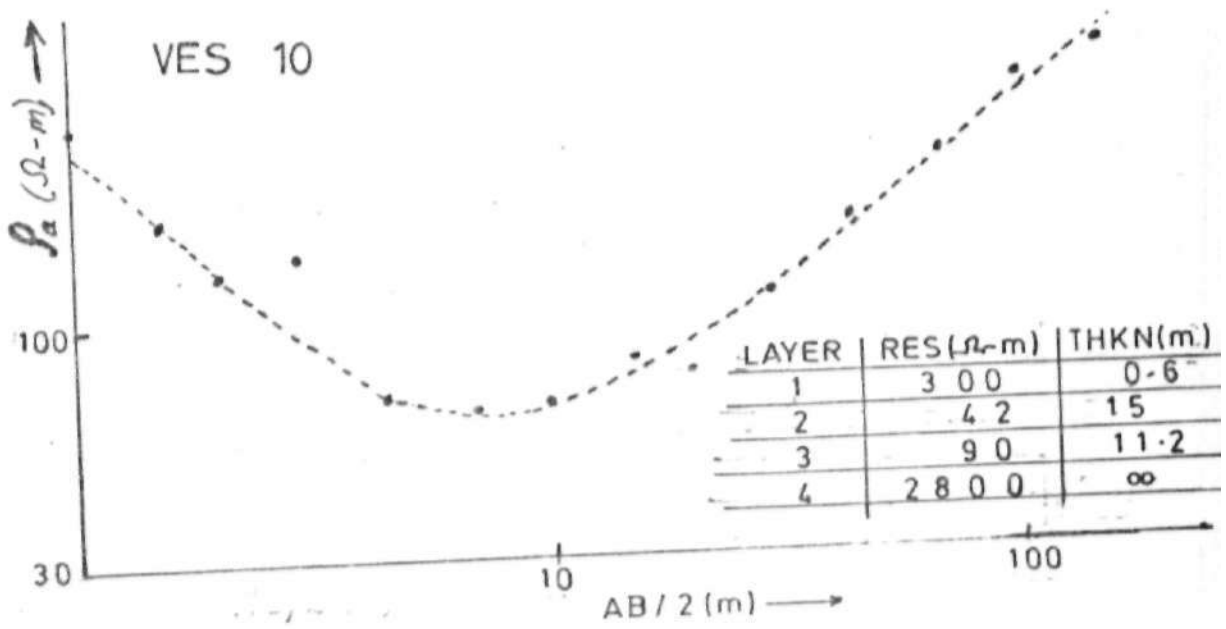

VES 3
100
15
ρ_a (Ω-m) ⟶
1
10
100
AB/2 (m) ⟶
LAYER | RES (Ω-m) | THKN (m)
1 | 450 | 0·8
2 | 35 | 4·4
3 | 120 | 72·5
4 | 2800 | ∞
• • • • Observed curve
------- Computed curve

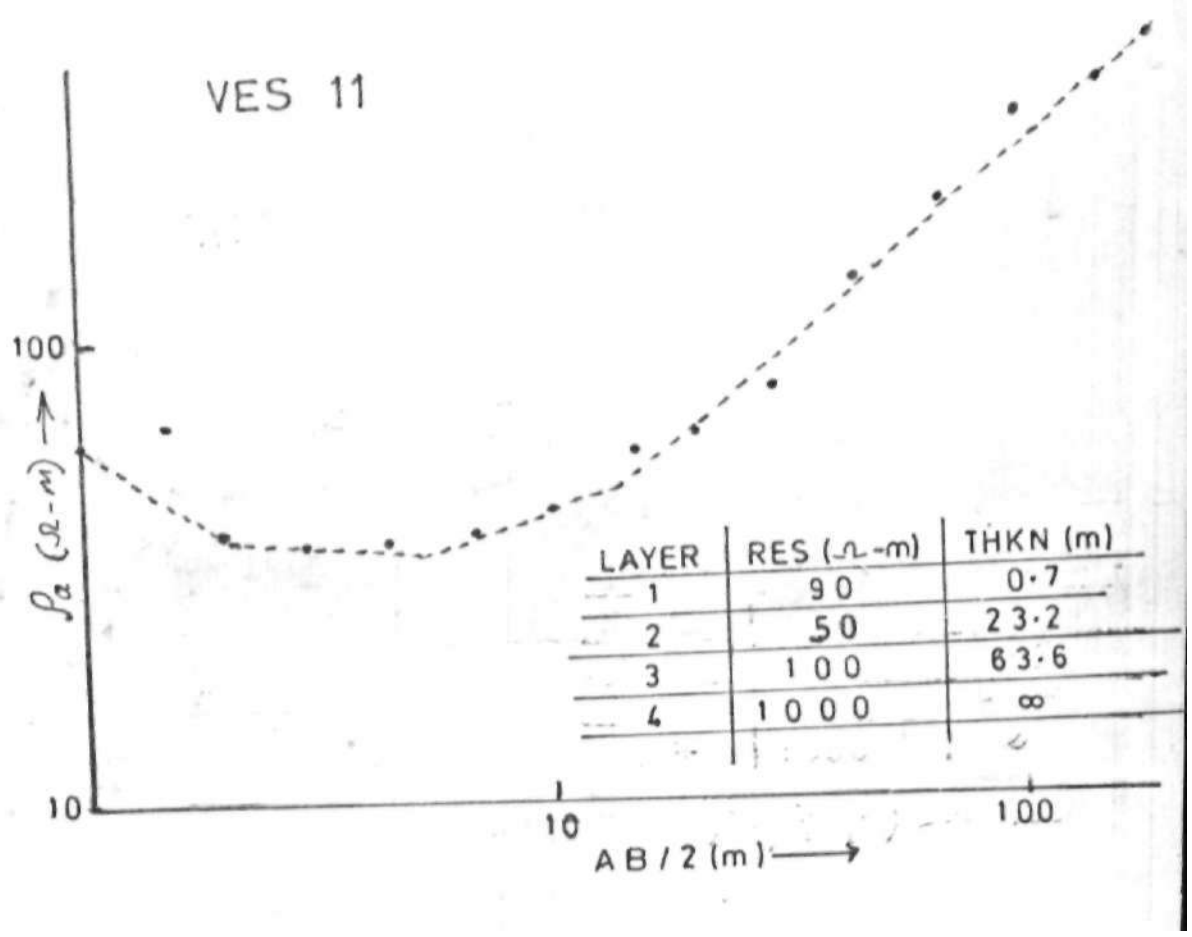

VES 4
1000
100
ρ_a (Ω-m) ⟶
1
10
100
AB/2 (m) ⟶
LAYER | RES (Ω-m) | THKN (m)
1 | 700 | 0.9
2 | 50 | 9·0
3 | 96 | 15·0
4 | 3600 | ∞

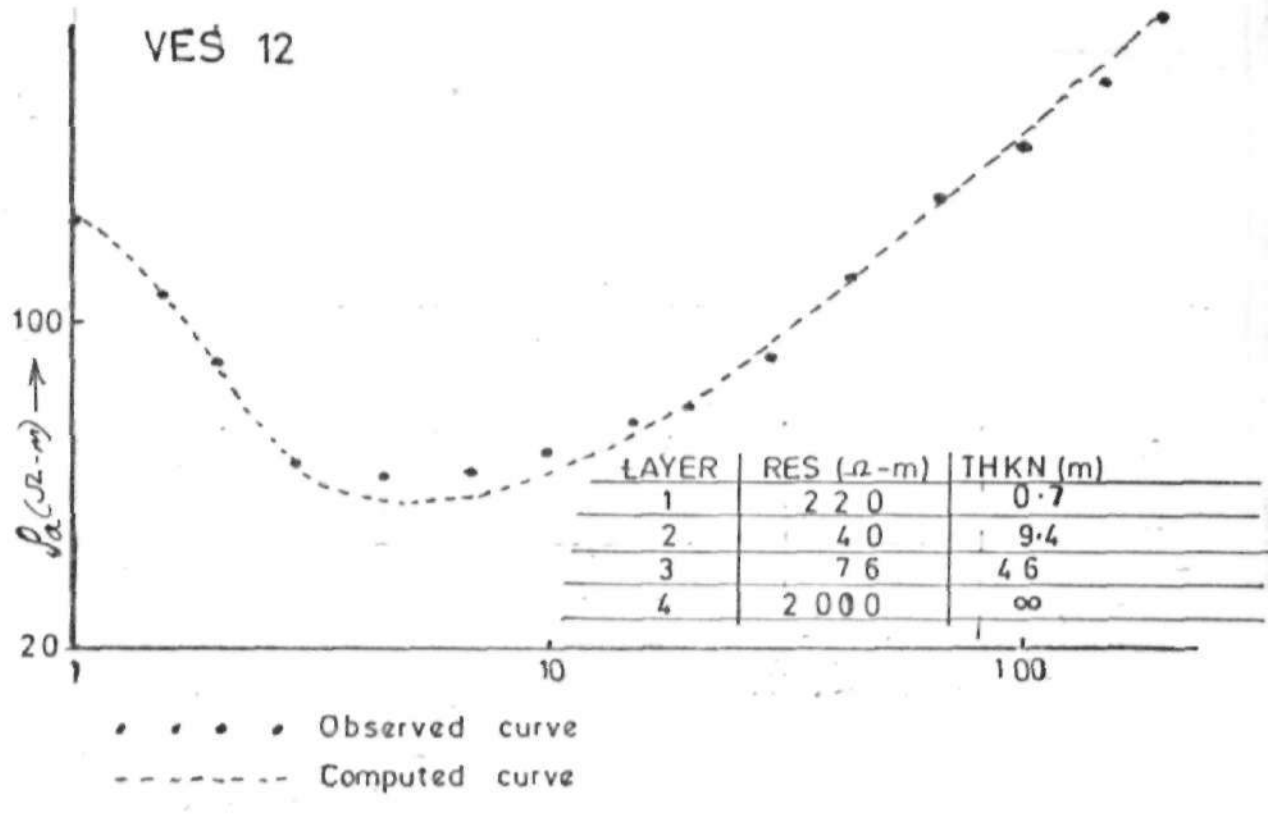

VES 5
1000
100
ρ_a (Ω-m) →
10
100
AB/2 (m) →
• • • • Observed curve
--------Computed curve
LAYER | RES(Ω-m) | THKN(m)
1 | 280 | 0·8
2 | 52 | 4·0
3 | 90 | 15·0
4 | 4000 | ∞

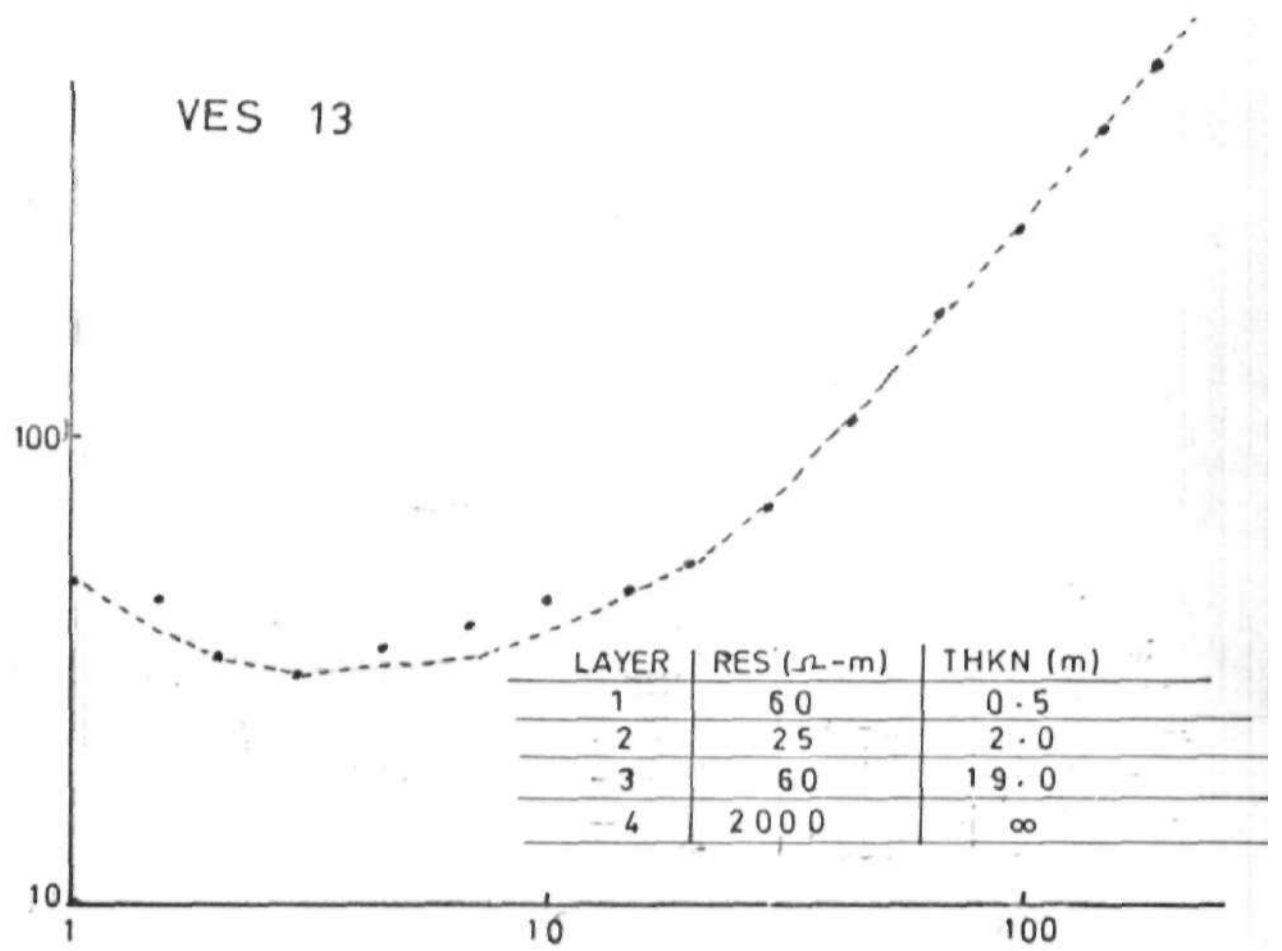

VES 7
1000
100
ρ_a (Ω-m) →
10
100
AB/2 (m) →
LAYER | RES(Ω-m) | THKN(m)
1 | 200 | 0·8
2 | 47 | 10·0
3 | 88 | 10·5
4 | 2800 | ∞

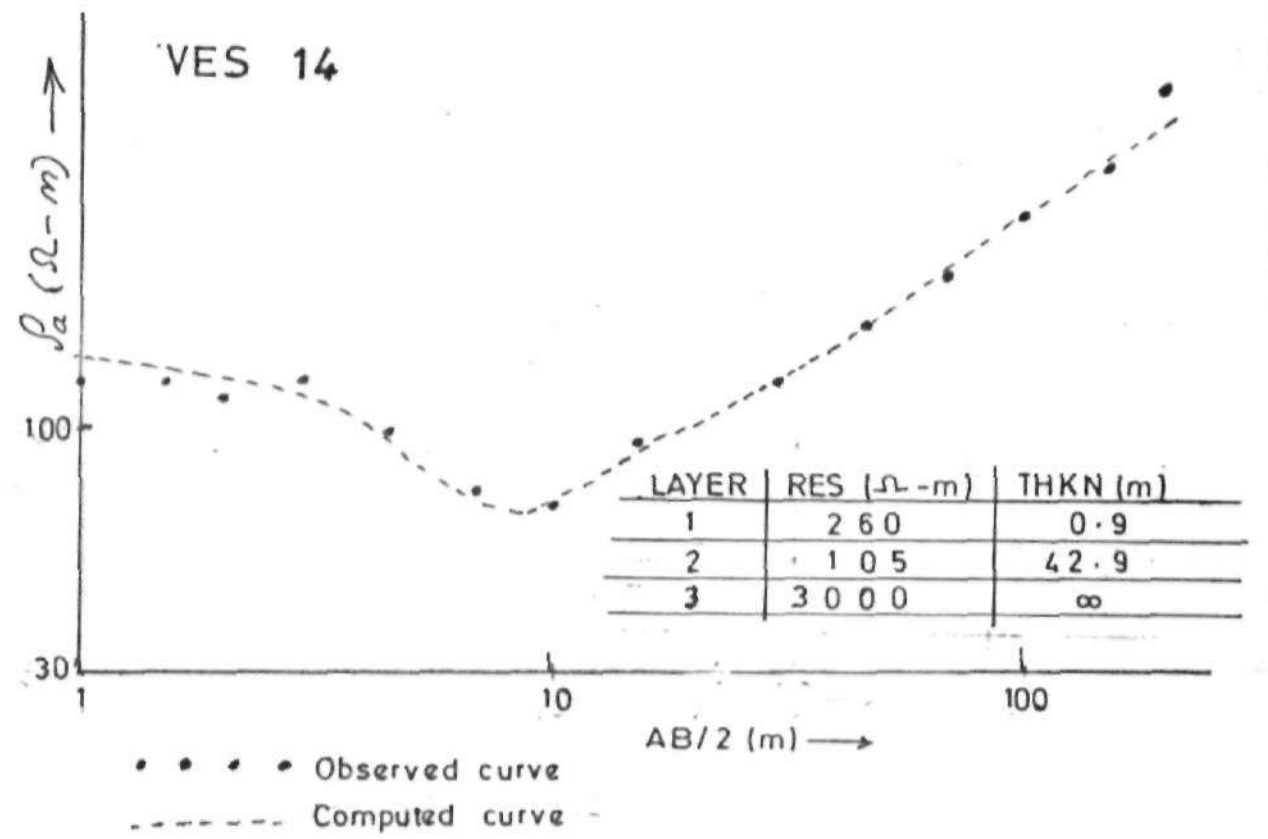

VES 8
ρ_a (Ω-m)
100
30
1
10
100
AB/2 (m)
Observed curve
Computed curve
LAYER | RES (Ω-m) | THKN (m)
1 | 90 | 07
2 | 50 | 32
3 | 1200 | ∞
VES 9
1000
100
ρ_a (Ω-m)
1
10
100
AB/2 (m)
LAYER | RES (Ω-m) | THKN (m)
1 | 320 | 2·8
2 | 180 | 5·5
3 | 110 | 41·2
4 | 3500 | ∞


VES 10
ρ_a (Ω-m)
100
30
10
100
AB / 2 (m)
LAYER | RES(Ω-m) | THKN(m)
1 | 300 | 0·6
2 | 42 | 15
3 | 90 | 11·2
4 | 2800 | ∞
Observed curve
Computed curve

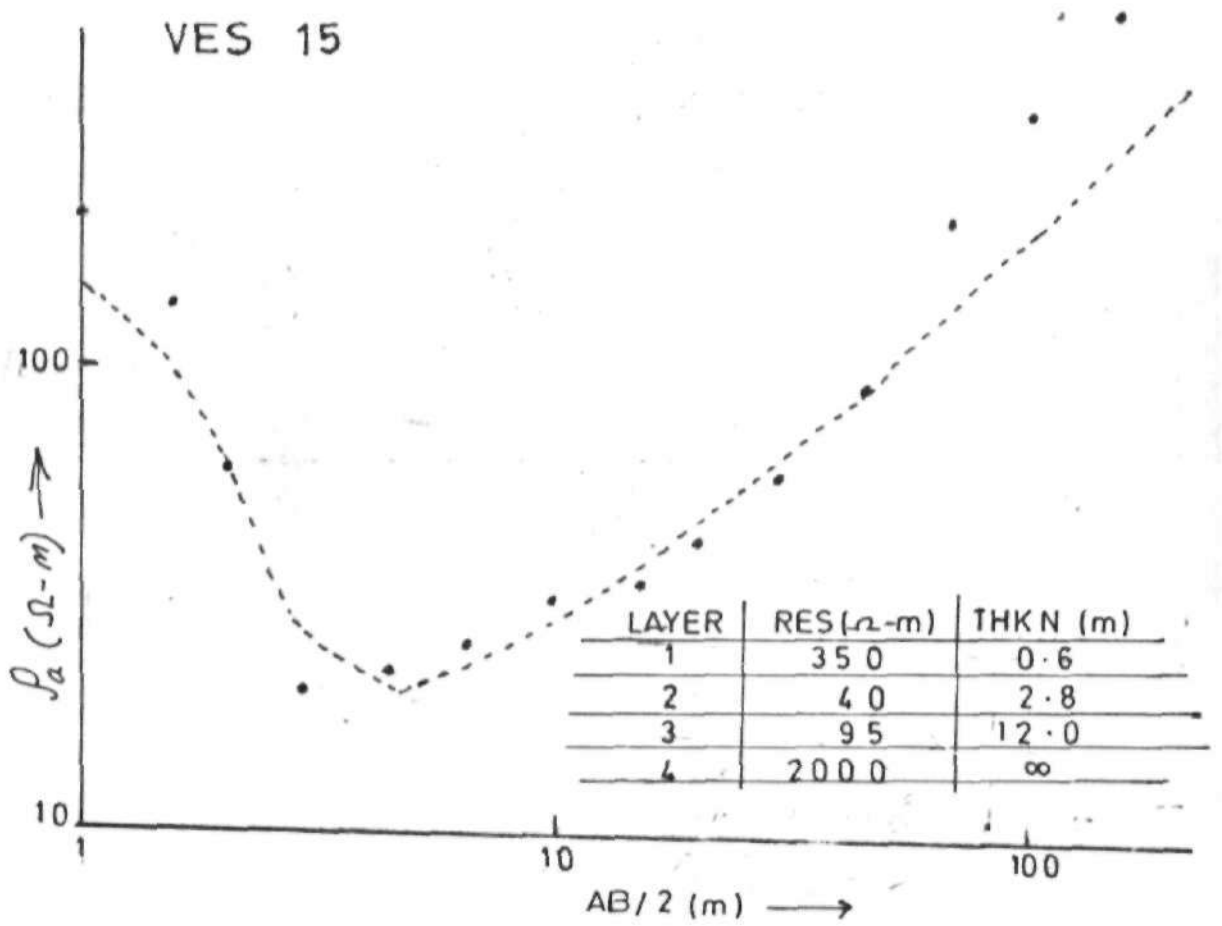

VES 11
ρ_a (Ω-m)
100
10
10
100
AB / 2 (m)
LAYER | RES (Ω-m) | THKN (m)
1 | 90 | 0·7
2 | 50 | 23·2
3 | 100 | 63·6
4 | 1000 | ∞


VES 12
100
20
1
10
100
ρa (Ω-m) →
LAYER | RES (Ω-m) | THKN (m)
1 | 220 | 0·7
2 | 40 | 9·4
3 | 76 | 46
4 | 2000 | ∞
Observed curve
Computed curve

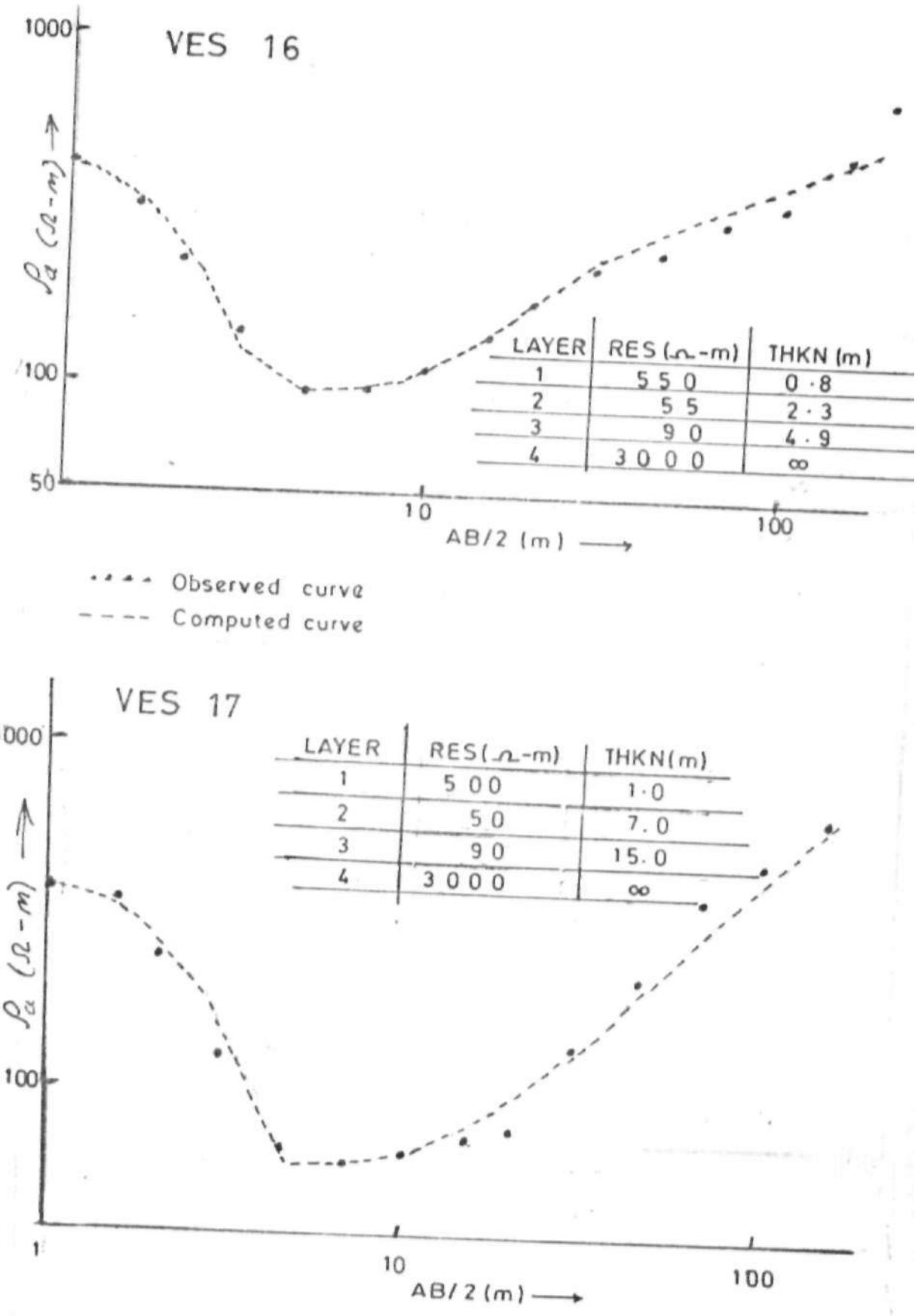

VES 13
100
10
1
10
100
LAYER | RES (Ω-m) | THKN (m)
1 | 60 | 0·5
2 | 25 | 2·0
3 | 60 | 19·0
4 | 2000 | ∞

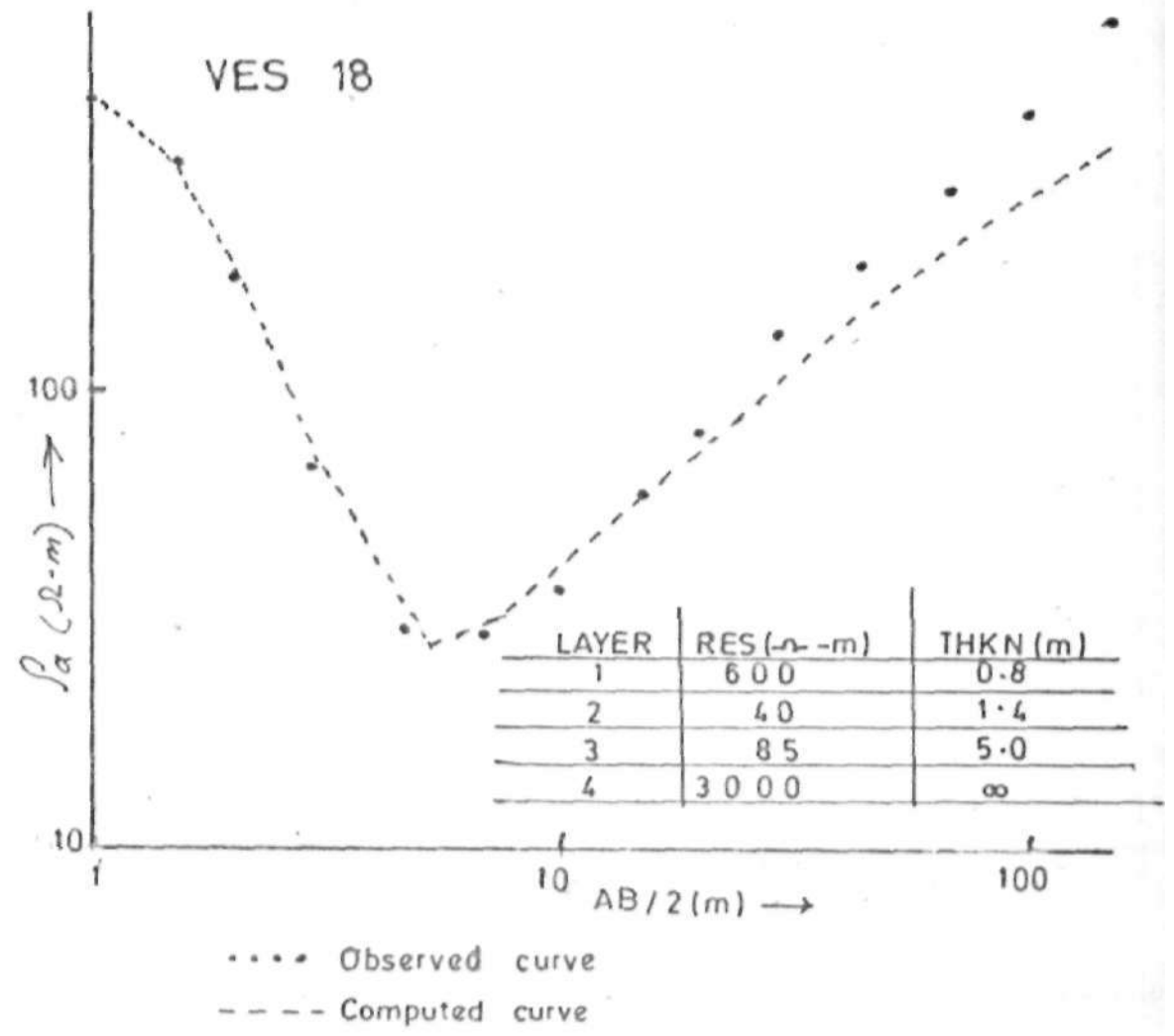


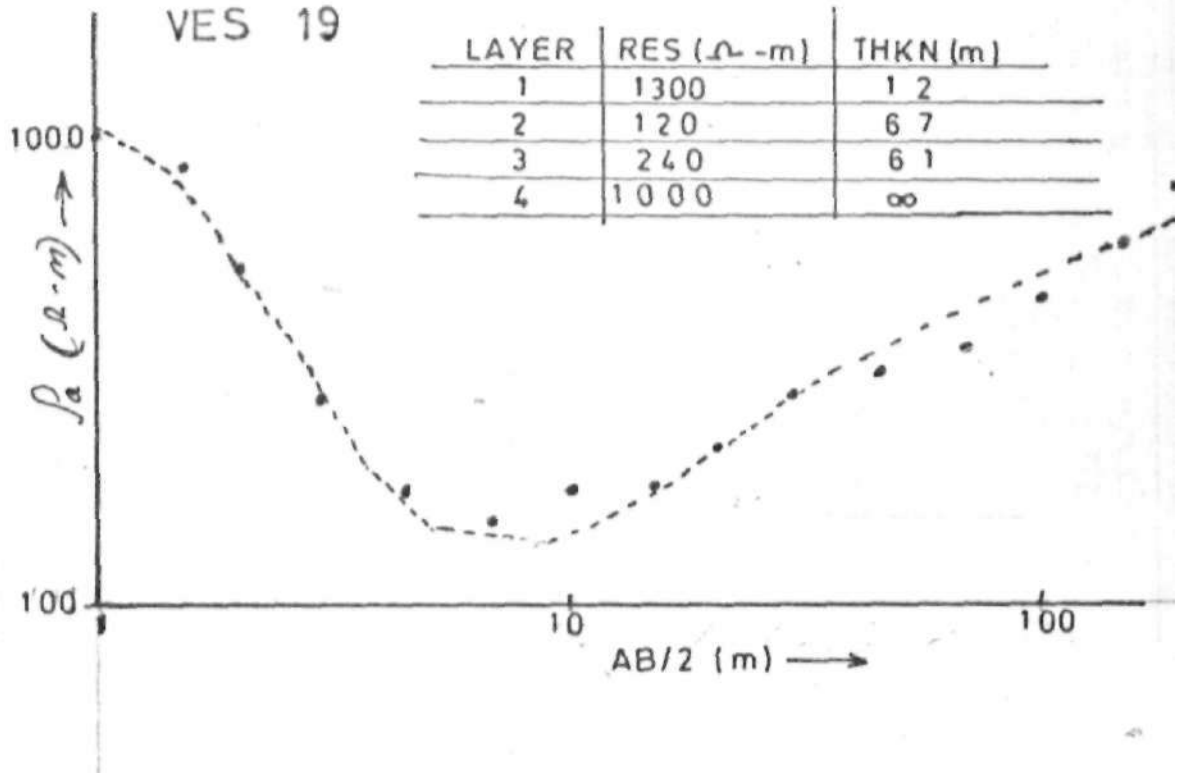
LAYER	RES (Ω-m)	THKN (m)
1	260	0·9
2	105	42·9
3	3000	∞

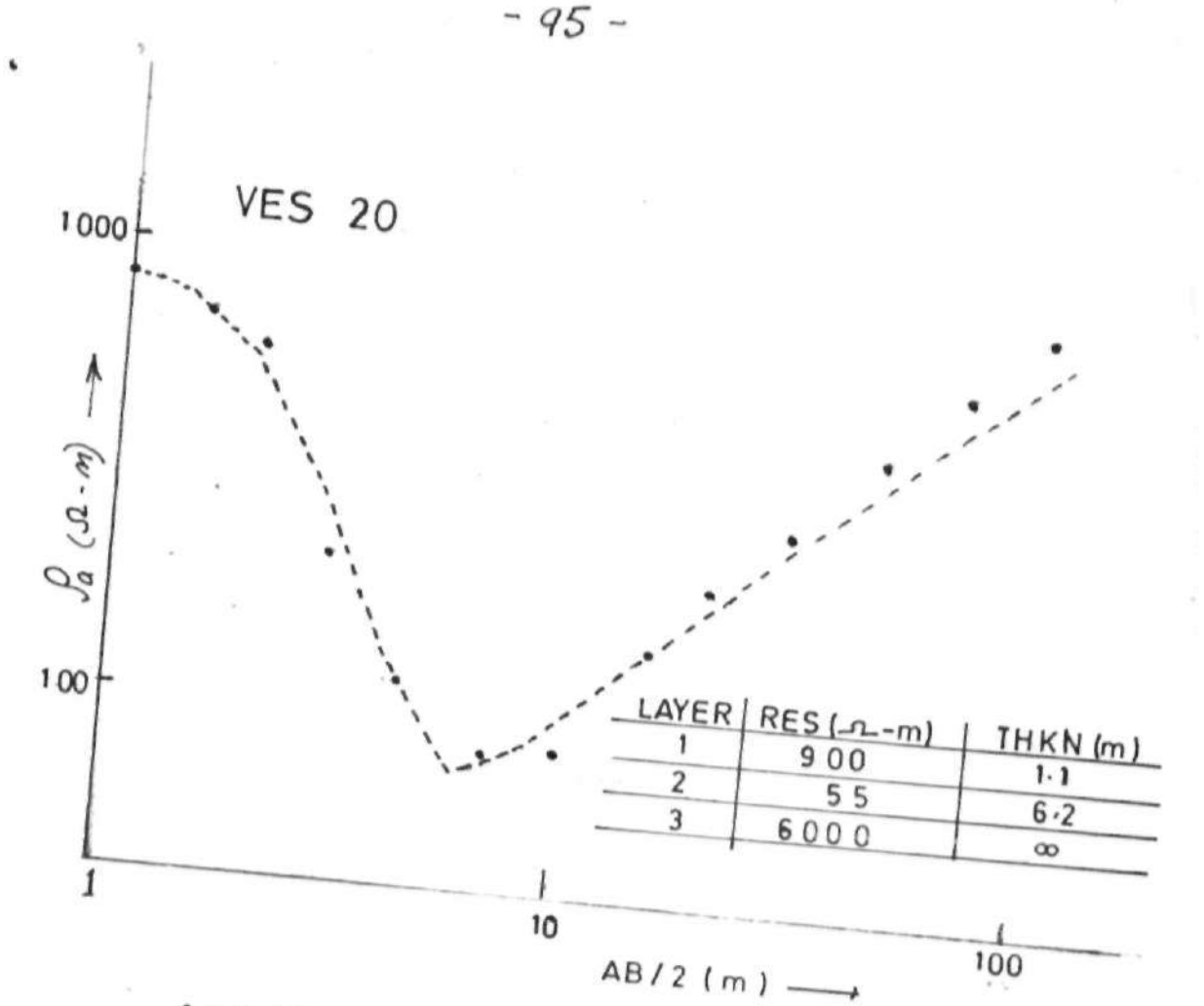


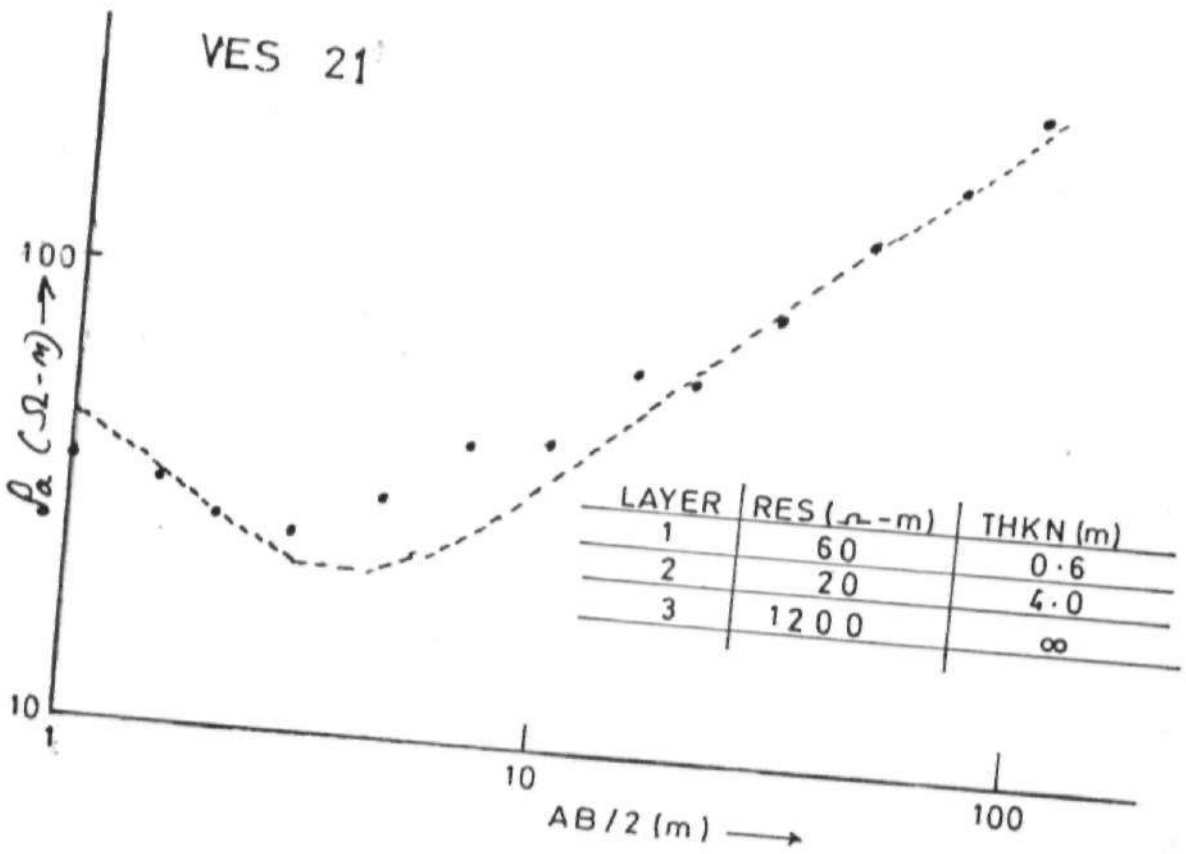
LAYER	RES (Ω-m)	THKN (m)
1	350	0·6
2	40	2·8
3	95	12·0
4	2000	∞


VES 16
1000
100
50
ρ_a (Ω-m) →
10
100
AB/2 (m) →
LAYER | RES (Ω-m) | THKN (m)
1 | 550 | 0·8
2 | 55 | 2·3
3 | 90 | 4·9
4 | 3000 | ∞
Observed curve
Computed curve
VES 17
1000
100
ρ_a (Ω-m)
1
10
100
AB/2 (m) →
LAYER | RES(Ω-m) | THKN(m)
1 | 500 | 1·0
2 | 50 | 7.0
3 | 90 | 15.0
4 | 3000 | ∞


VES 18
100
10
1
10
100
AB/2(m) ⟶
LAYER | RES(Ω-m) | THKN(m)
1 | 600 | 0.8
2 | 40 | 1·4
3 | 85 | 5·0
4 | 3000 | ∞
···· Observed curve
– – – – Computed curve

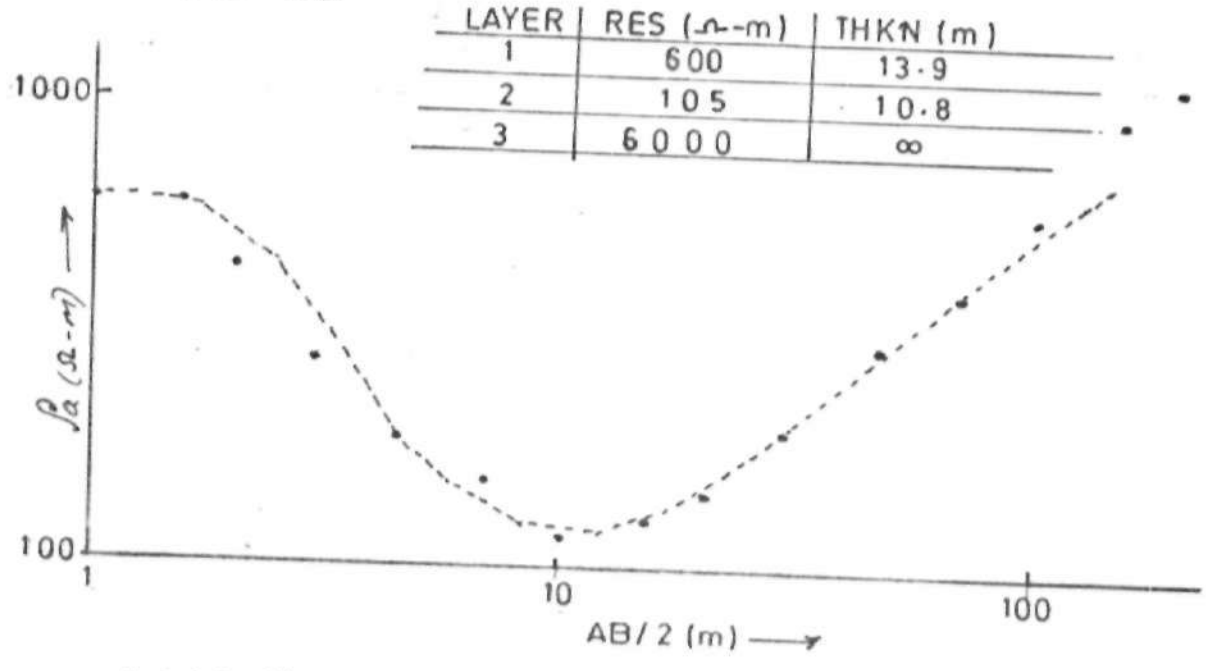

VES 19
1000
100
1
10
100
AB/2 (m) ⟶
LAYER | RES (Ω-m) | THKN (m)
1 | 1300 | 1 2
2 | 120 | 6 7
3 | 240 | 6 1
4 | 1000 | ∞


VES 20
1000
100
ρ_a (Ω-m) ⟶
1
10
100
AB/2 (m) ⟶
LAYER | RES (Ω-m) | THKN (m)
1 | 900 | 1·1
2 | 55 | 6·2
3 | 6000 | ∞
Observed curve
Computed curve

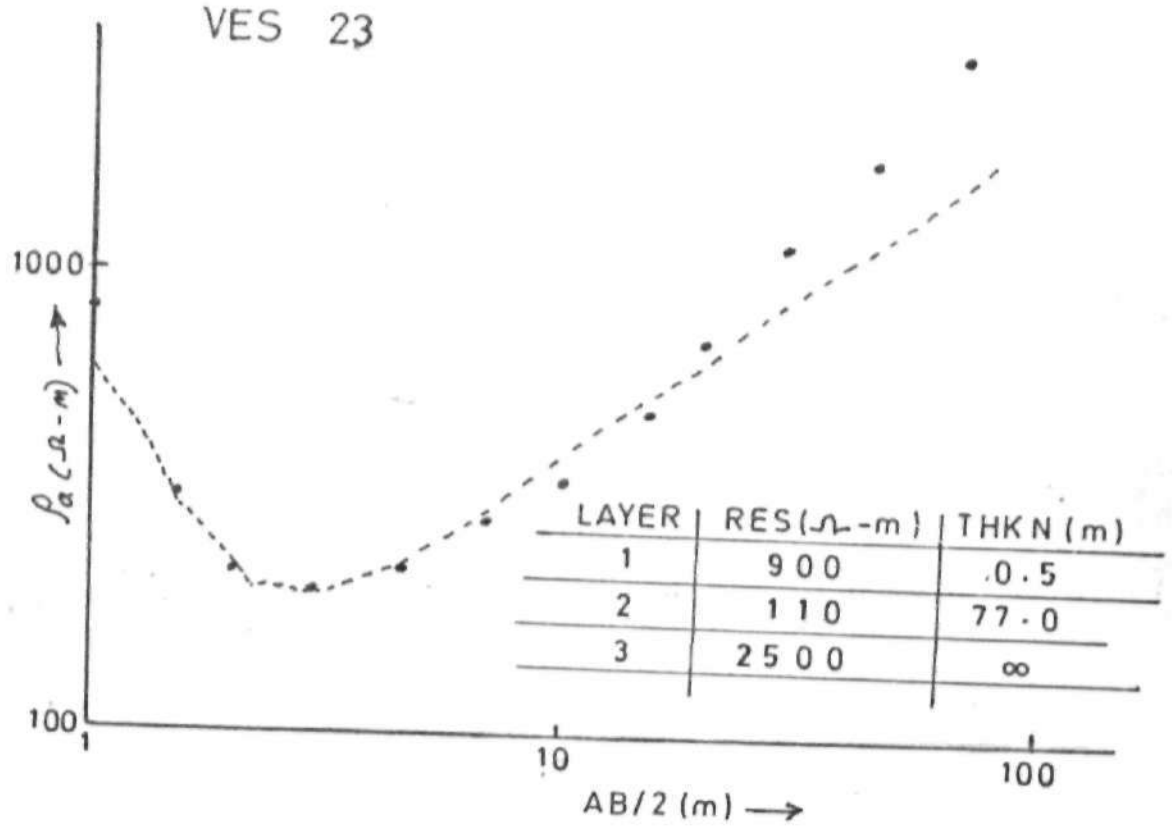

VES 21
100
10
ρ_a (Ω-m) ⟶
1
10
100
AB/2 (m) ⟶
LAYER | RES (Ω-m) | THKN (m)
1 | 60 | 0·6
2 | 20 | 4·0
3 | 1200 | ∞

VES 22

LAYER	RES (Ω-m)	THKN (m)
1	600	13·9
2	105	10·8
3	6000	∞

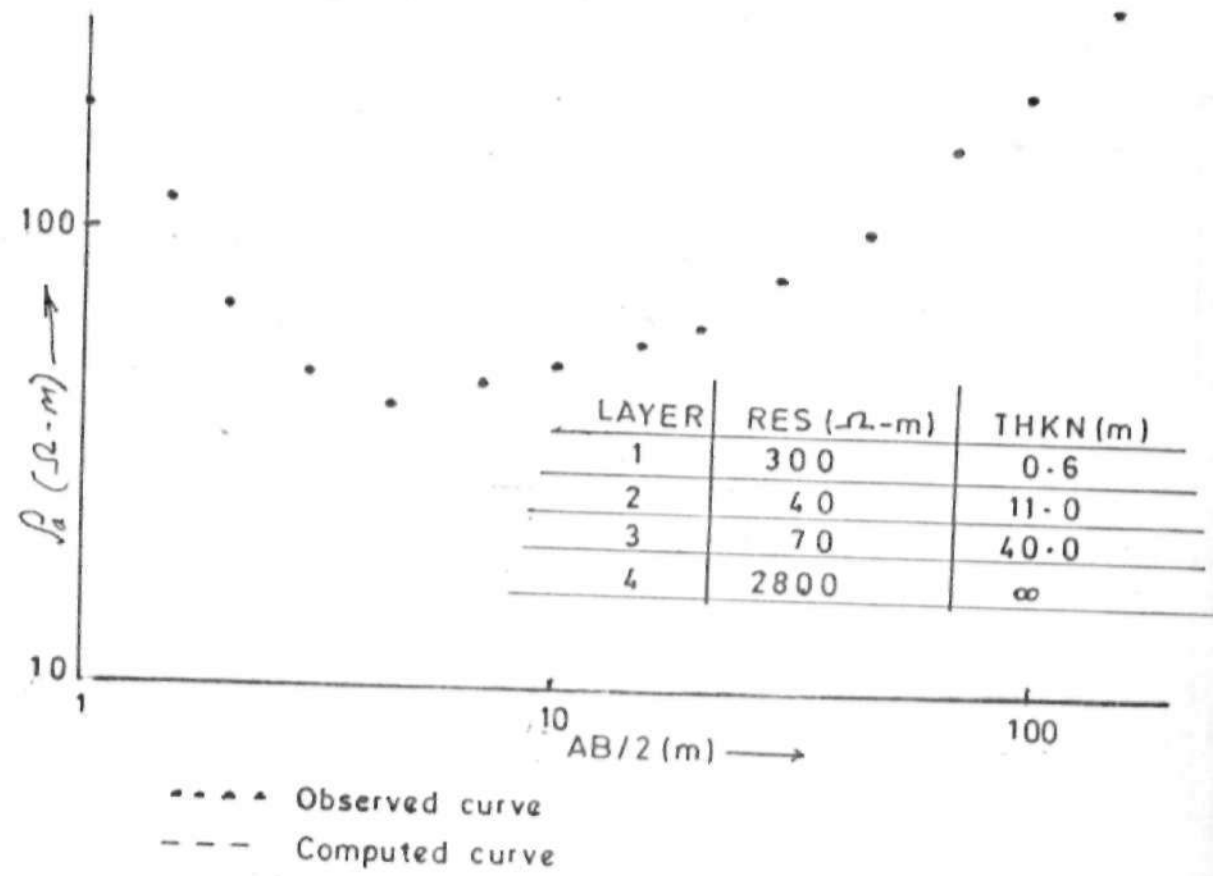


VES 23



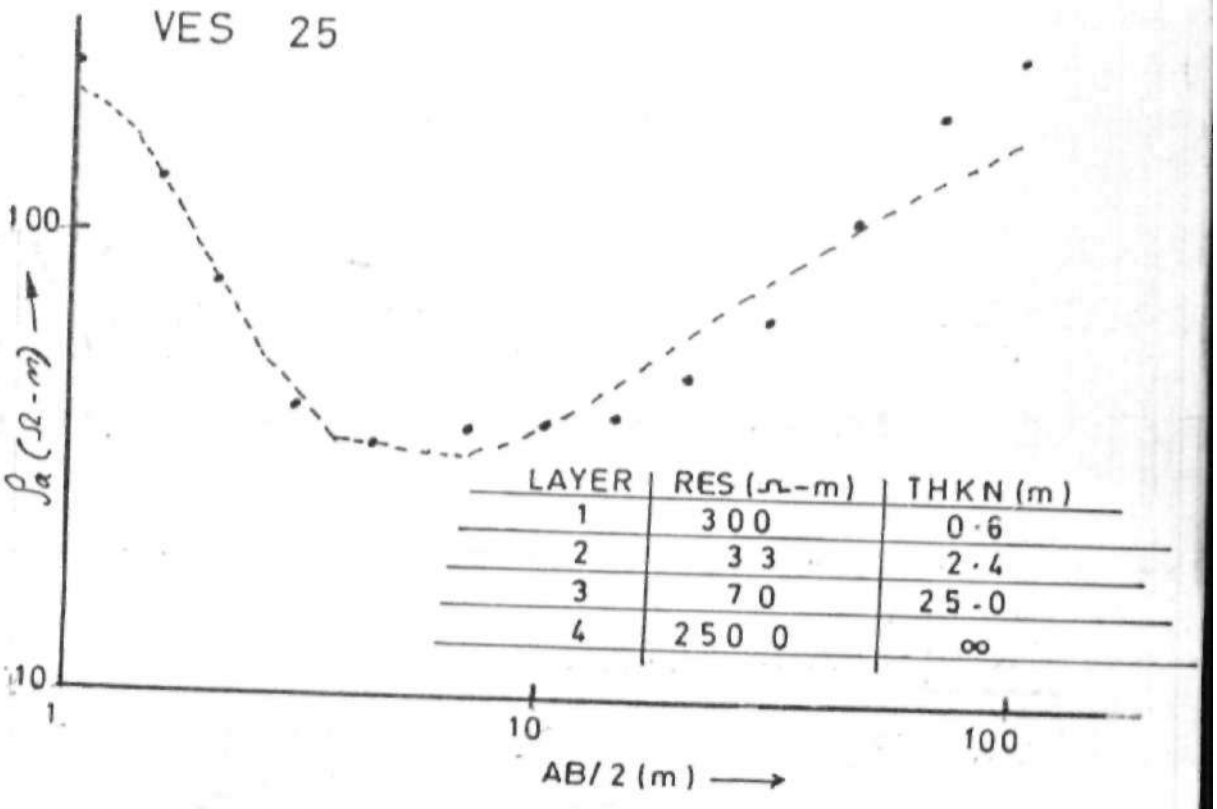
LAYER	RES (Ω-m)	THKN (m)
1	900	0.5
2	110	77.0
3	2500	∞

VES 24

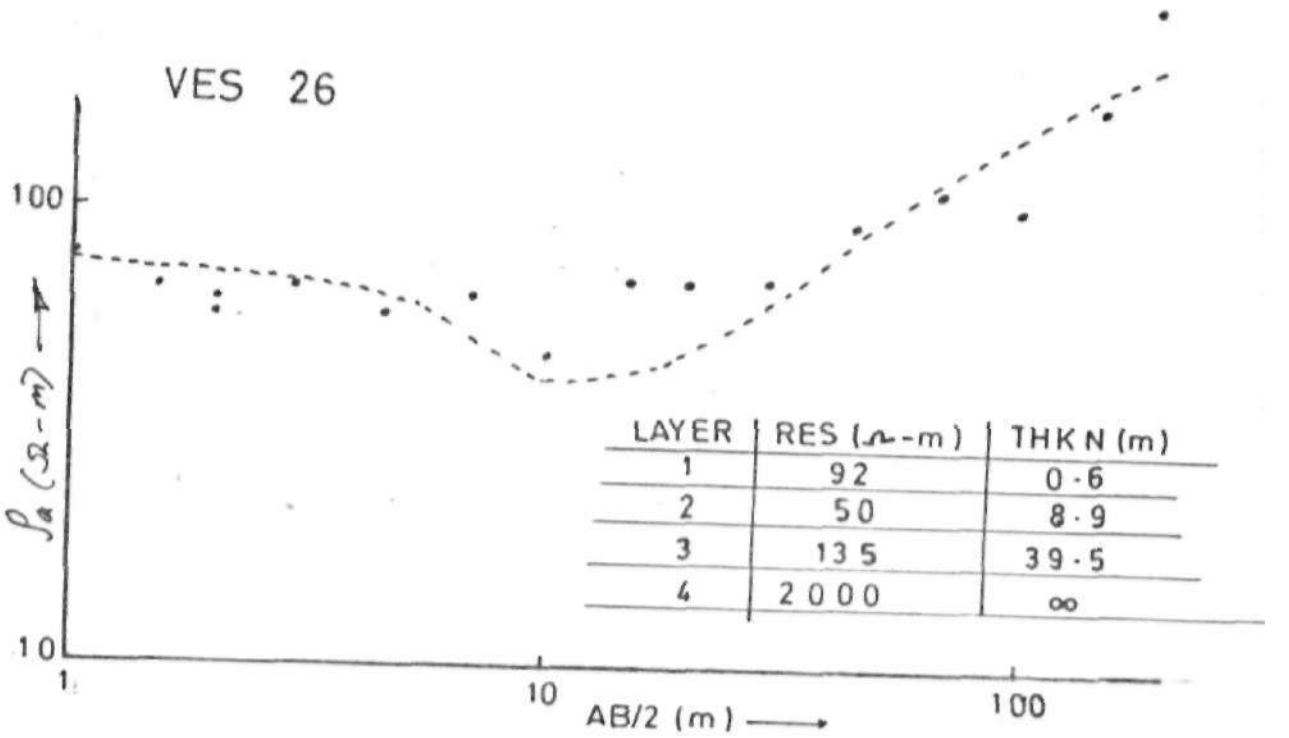


LAYER	RES (Ω-m)	THKN (m)
1	300	0·6
2	40	11·0
3	70	40·0
4	2800	∞

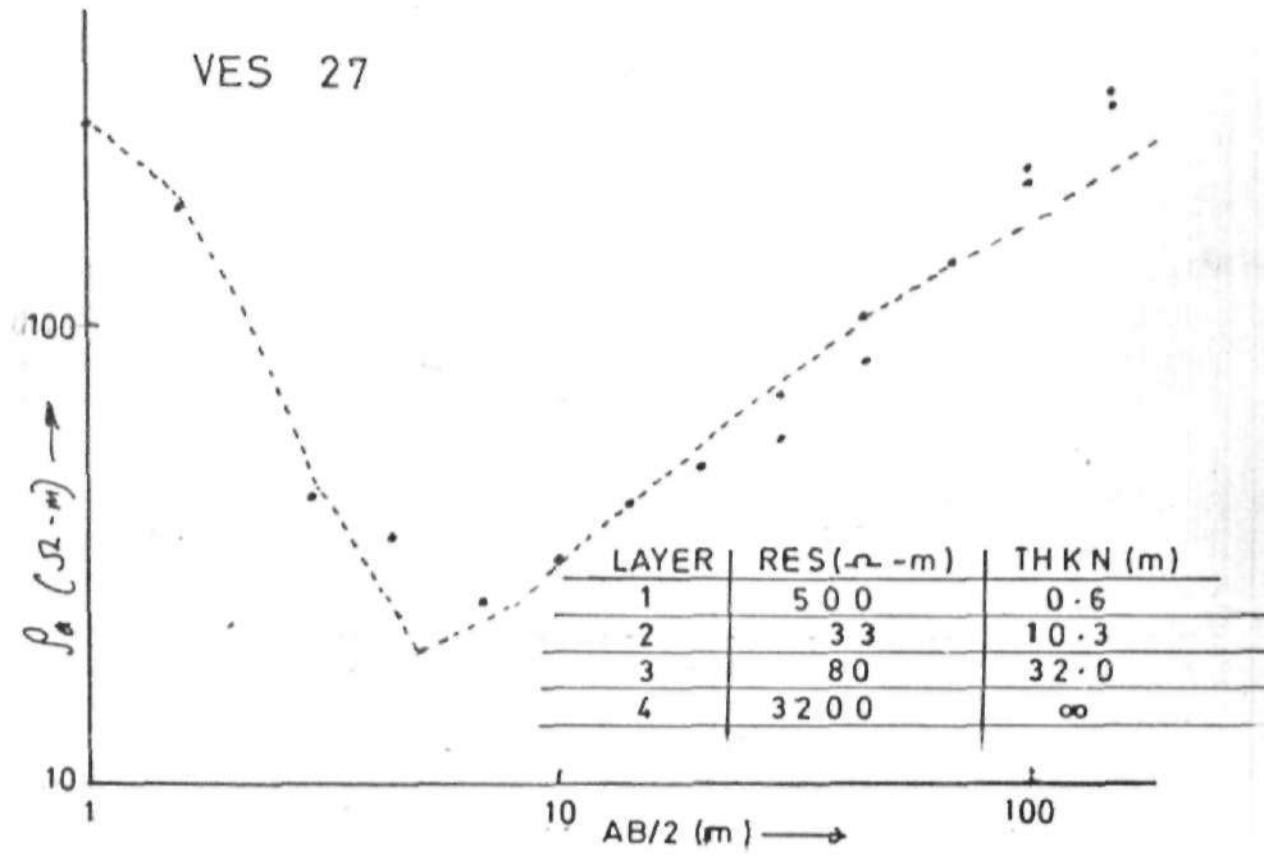
VES 25



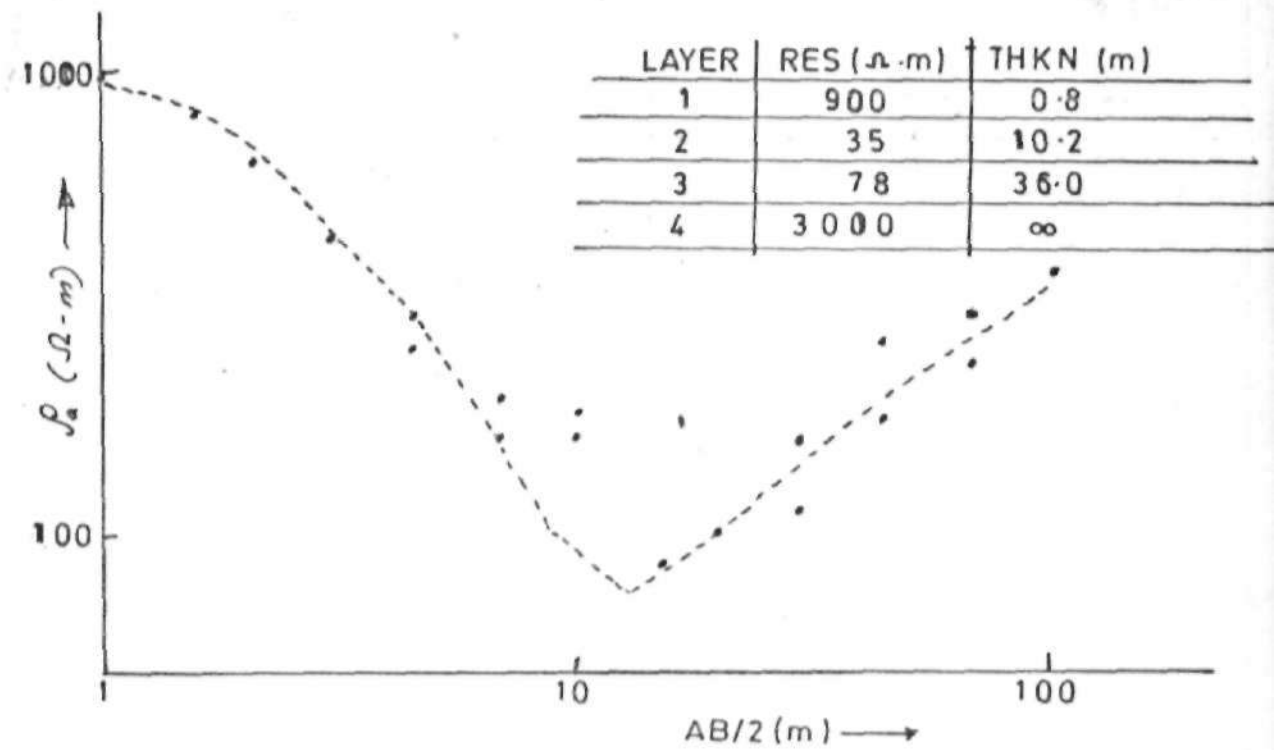
LAYER	RES (Ω-m)	THKN (m)
1	300	0·6
2	33	2·4
3	70	25·0
4	2500	∞



Observed curve
Computed curve



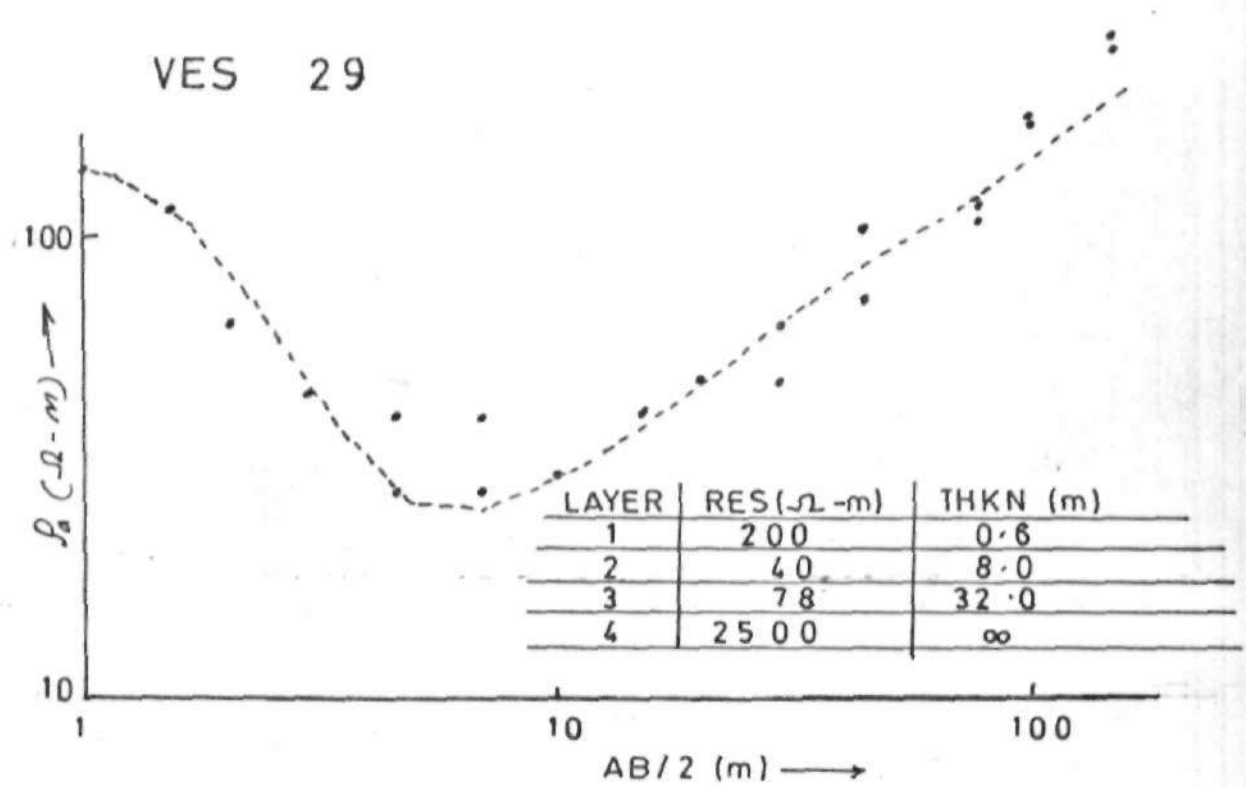
VES 28



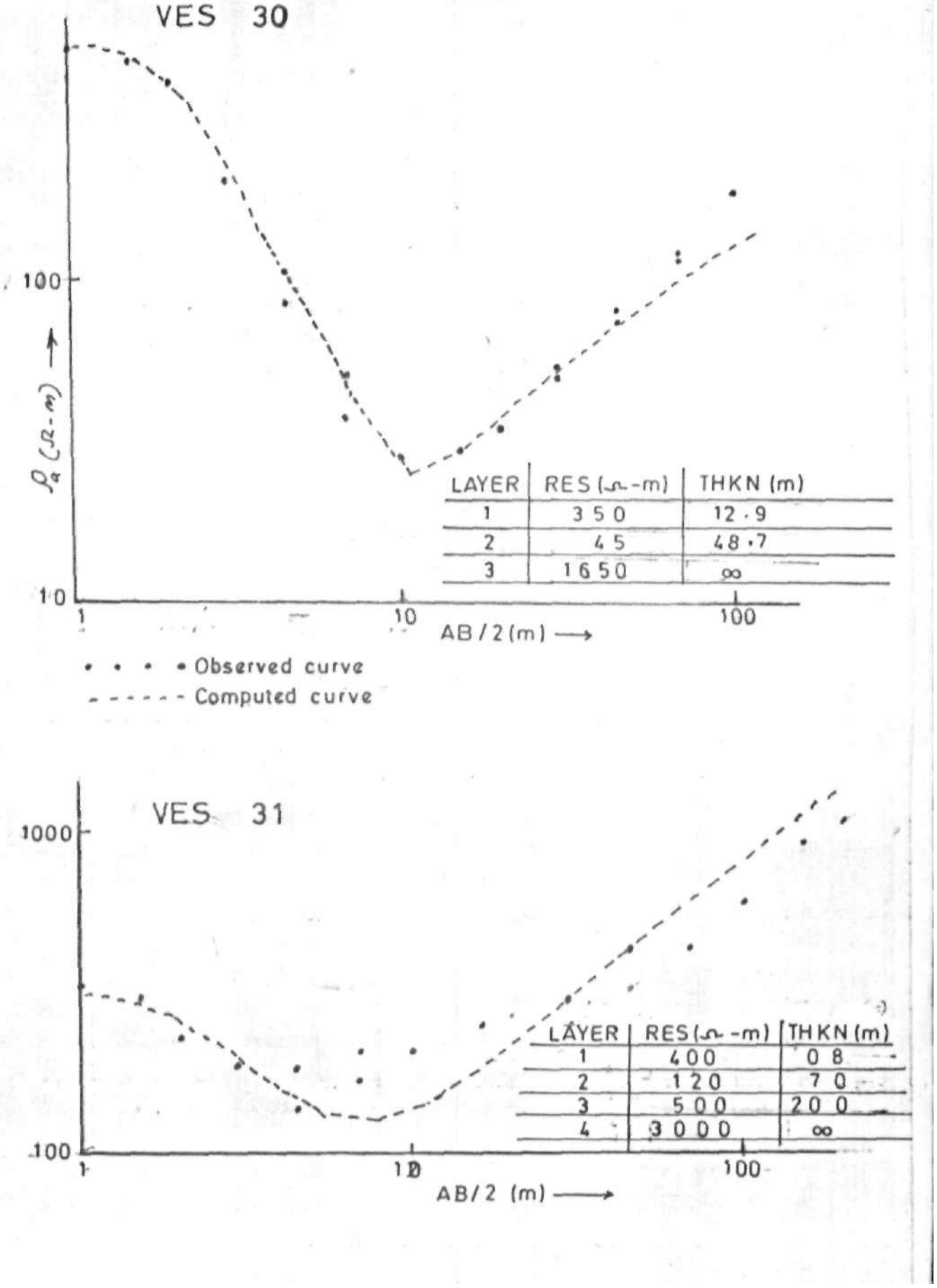
LAYER	RES (Ω·m)	THKN (m)
1	900	0·8
2	35	10·2
3	78	36·0
4	3000	∞

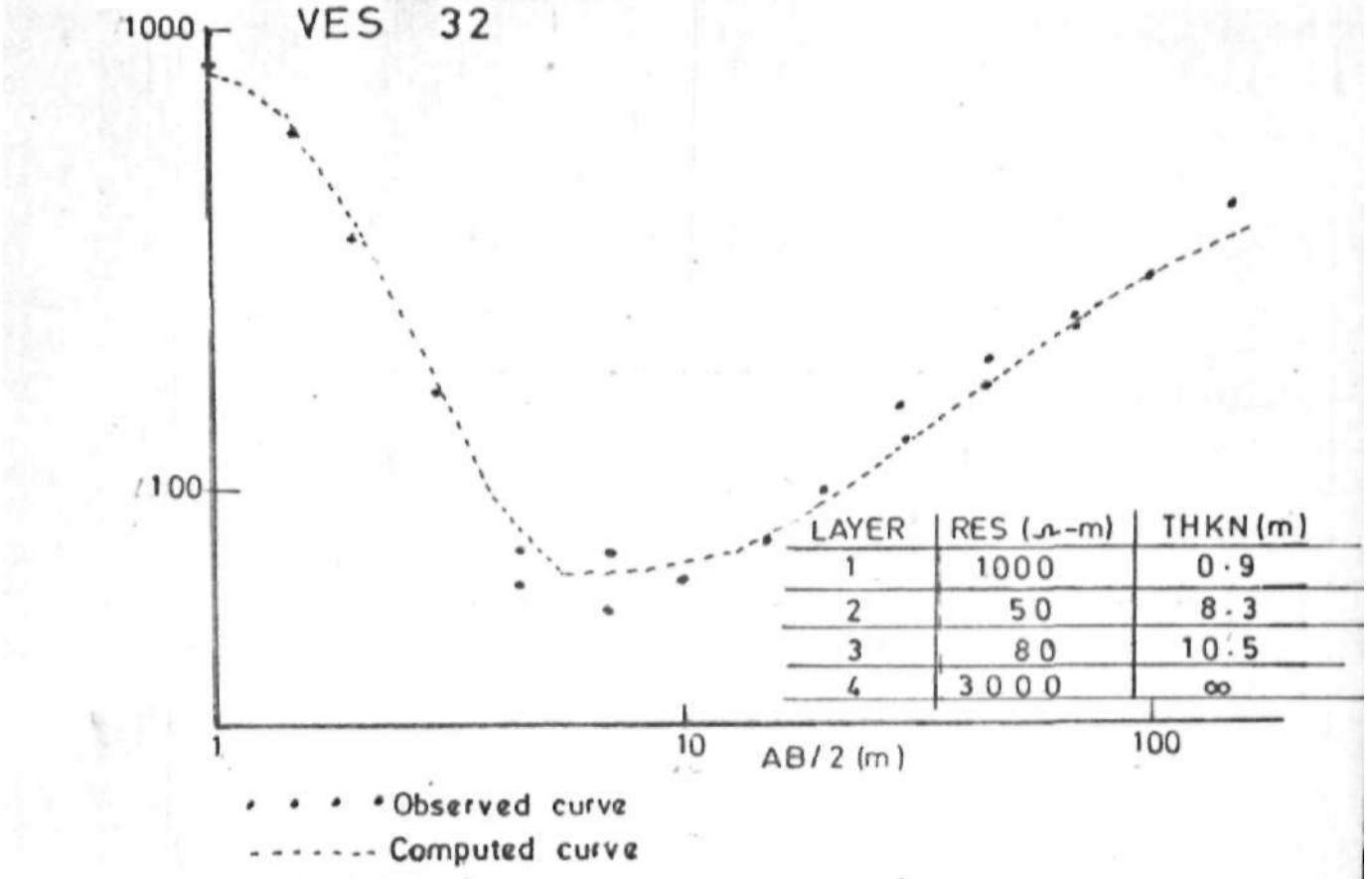
- - - - Observed curve
– – – – Computed curve

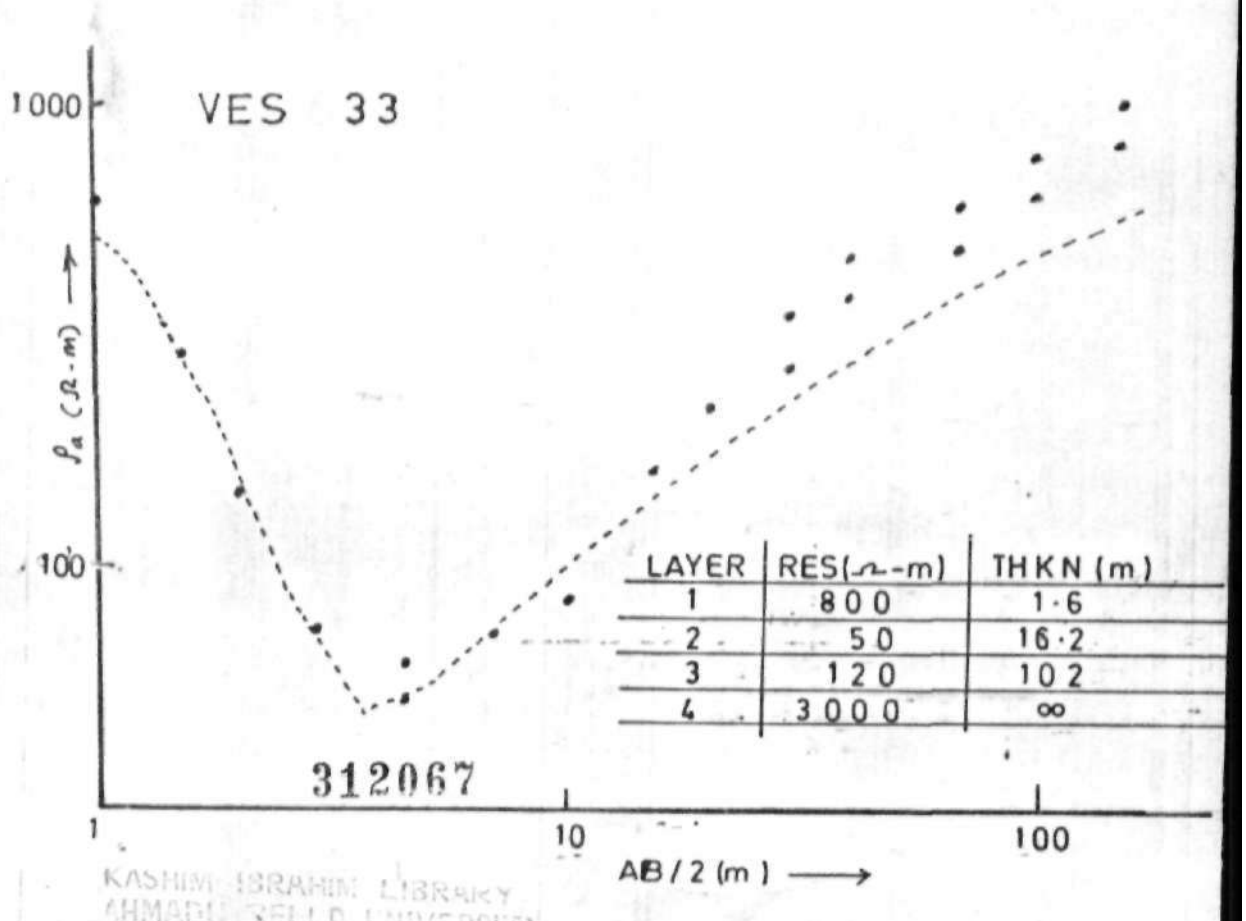
VES 29



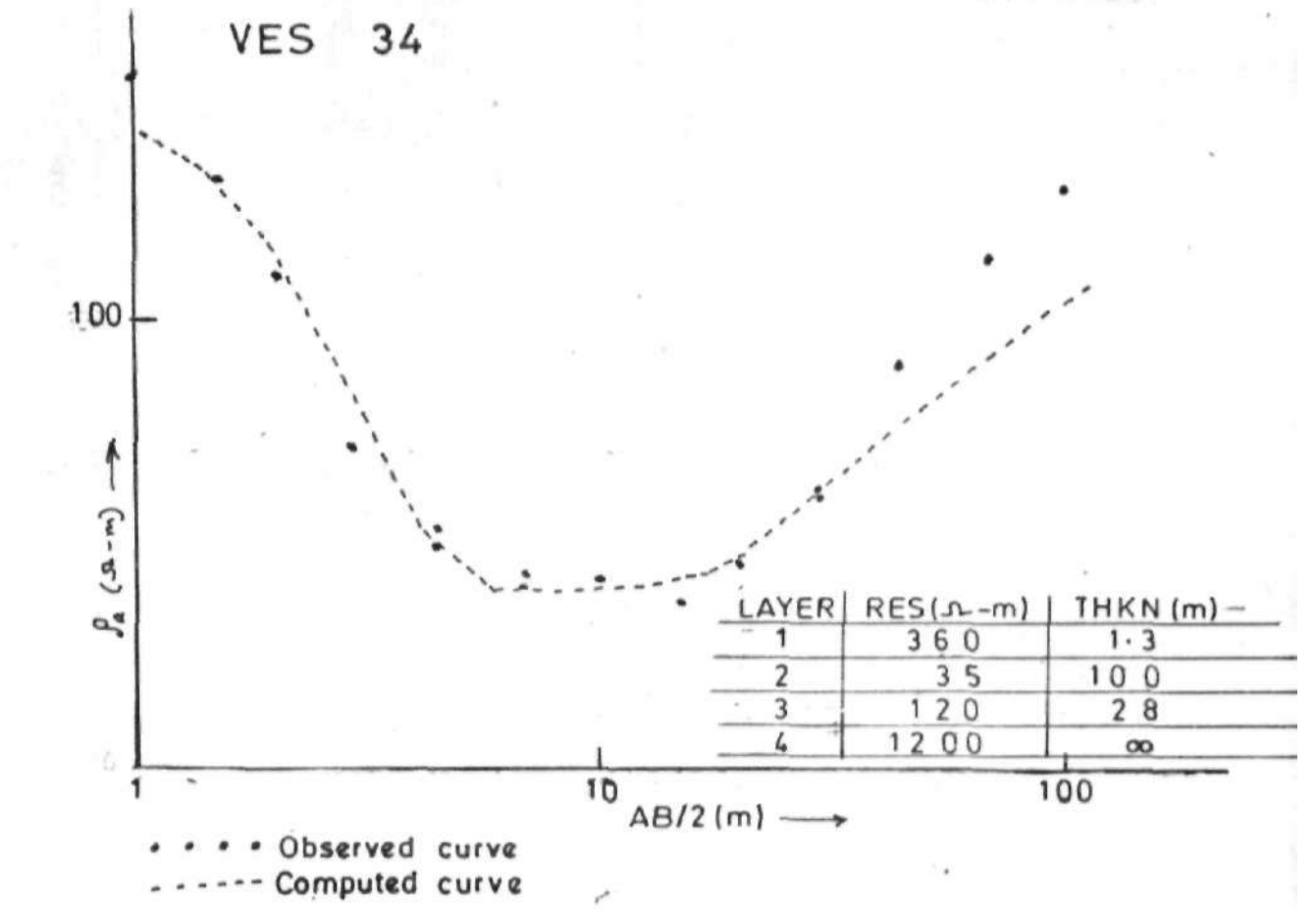
LAYER	RES (Ω-m)	THKN (m)
1	200	0·6
2	40	8·0
3	78	32·0
4	2500	∞

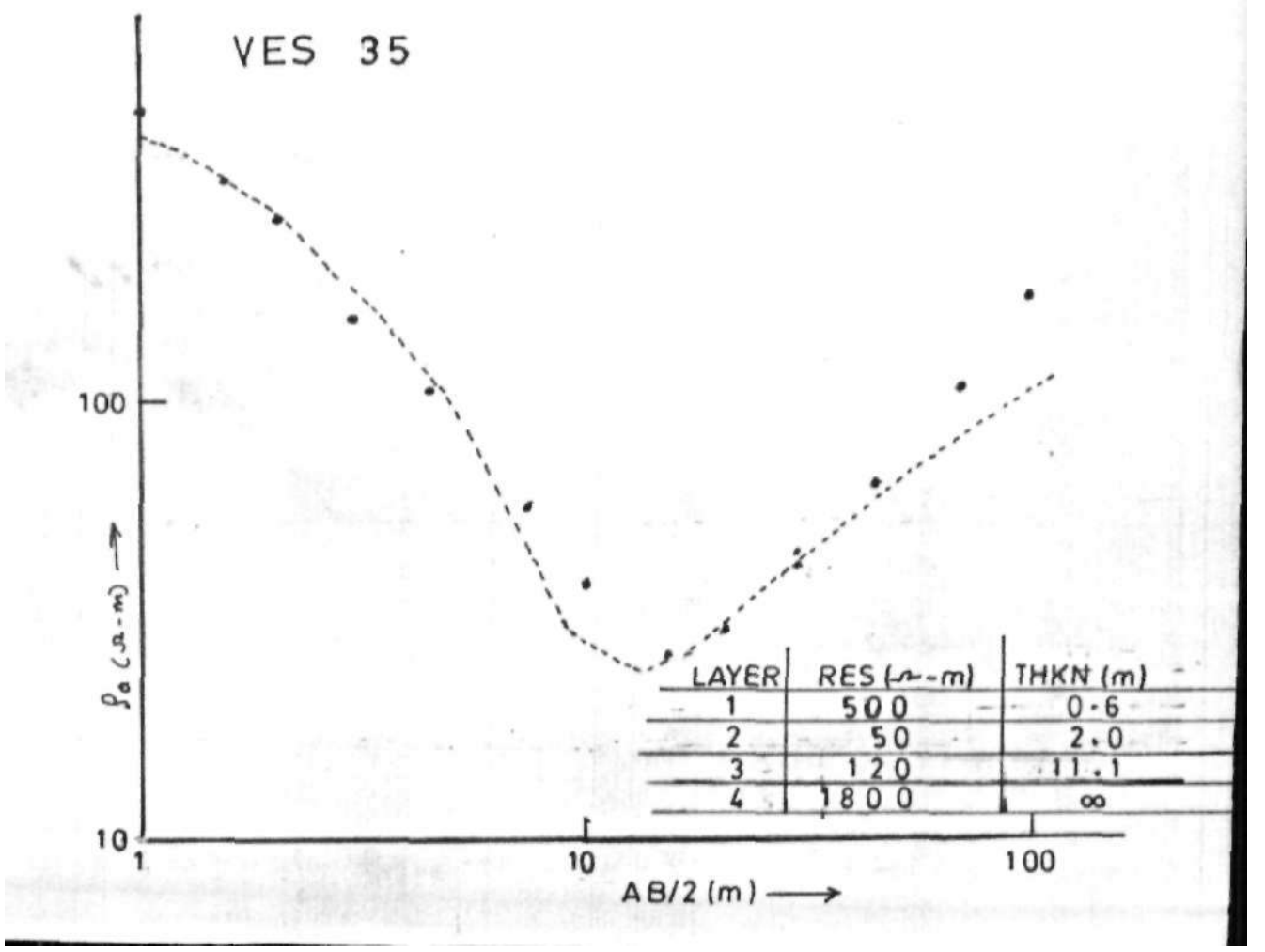

VES 30
100
10
ρ_a (Ω-m) →
1
10
100
AB/2 (m) →
LAYER | RES (Ω-m) | THKN (m)
1 | 350 | 12·9
2 | 45 | 48·7
3 | 1650 | ∞
• • • • Observed curve
- - - - - - Computed curve
VES 31
1000
100
1
10
100
AB/2 (m) →
LAYER | RES (Ω-m) | THKN (m)
1 | 400 | 08
2 | 120 | 70
3 | 500 | 200
4 | 3000 | ∞

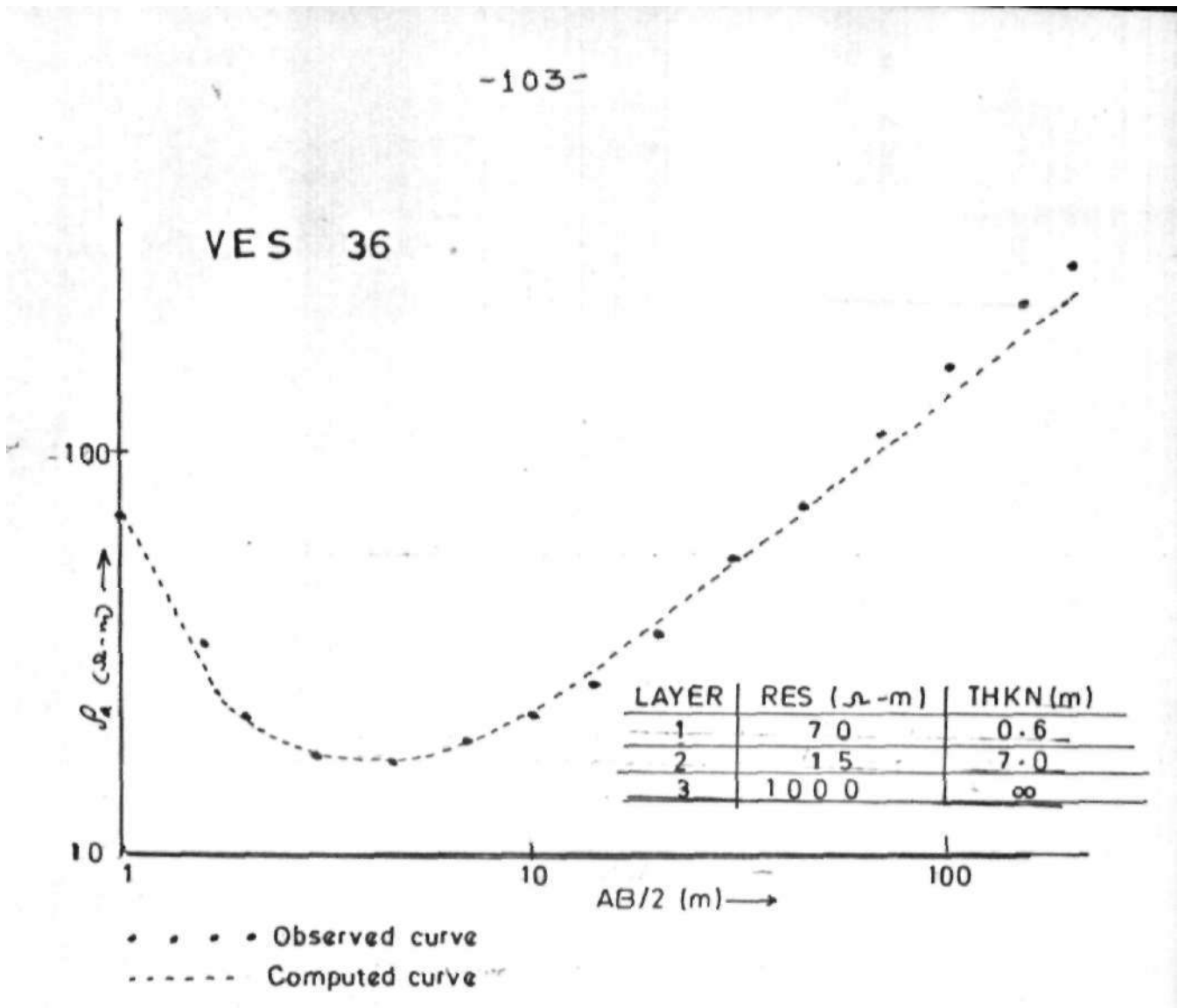


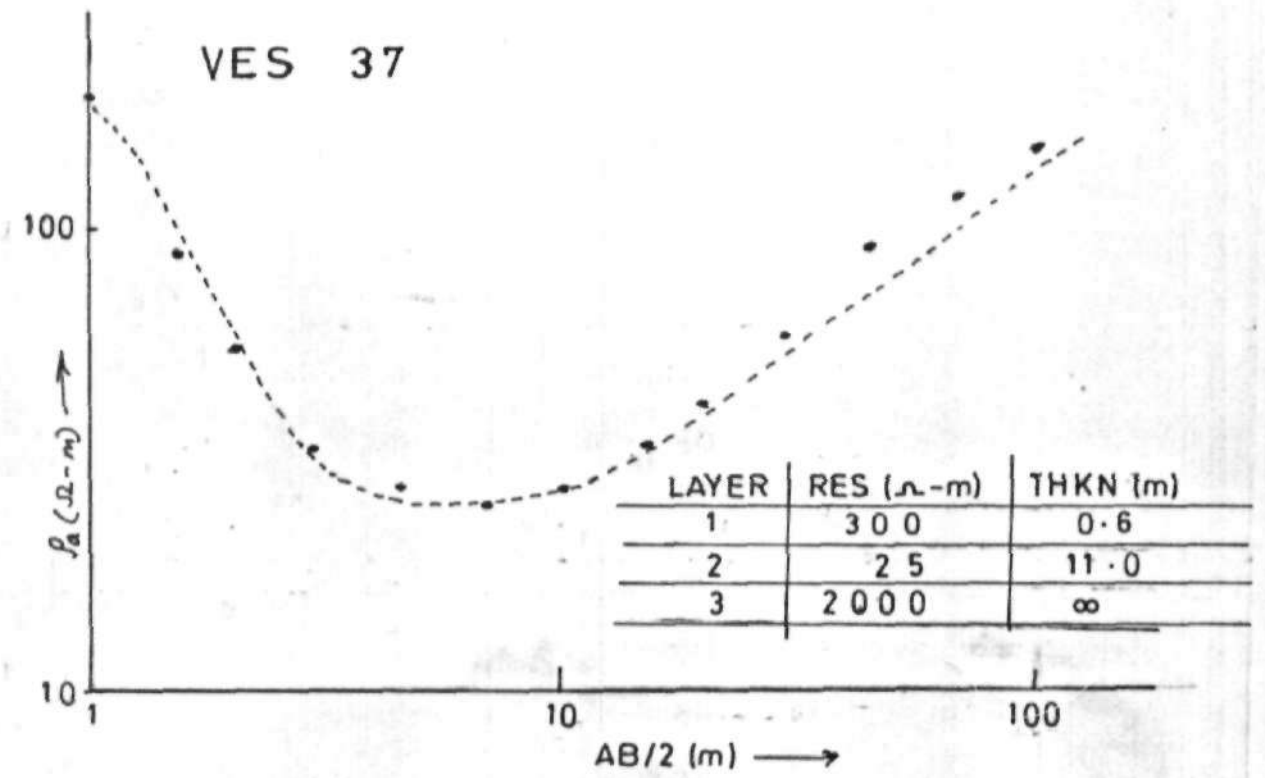


312067
KASHIM IBRAHIM LIBRARY
AHMADU BELLO UNIVERSITY

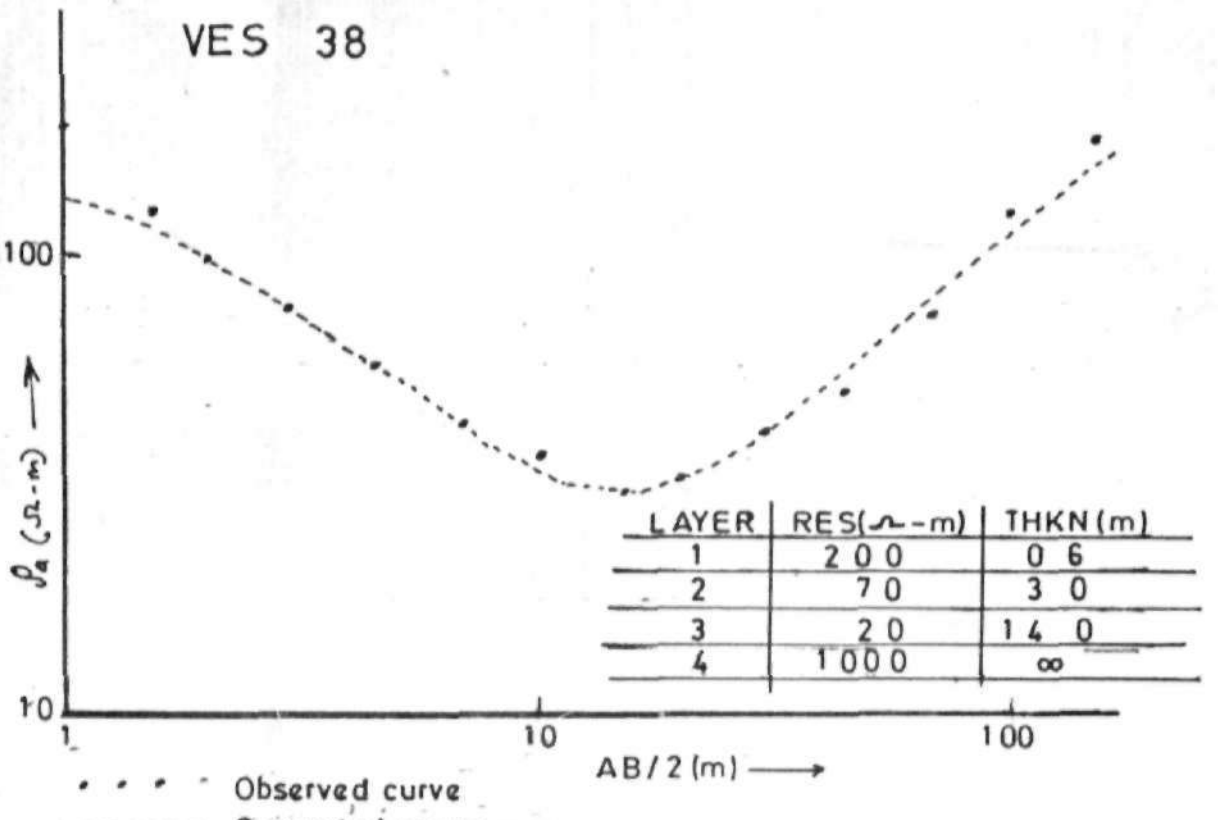

VES 34
100
ρ_a (Ω-m) ⟶
1
10
100
AB/2 (m) ⟶
• • • • Observed curve
- - - - - Computed curve
LAYER | RES(Ω-m) | THKN (m)
1 | 360 | 1·3
2 | 35 | 100
3 | 120 | 28
4 | 1200 | ∞


VES 35
100
10
ρ_a (Ω-m) ⟶
1
10
100
AB/2 (m) ⟶
LAYER | RES (Ω-m) | THKN (m)
1 | 500 | 0·6
2 | 50 | 2·0
3 | 120 | 11·1
4 | 1800 | ∞


VES 36
100
10
ρ_a (Ω-m)
1
10
100
AB/2 (m)
LAYER | RES (Ω-m) | THKN (m)
1 | 70 | 0.6
2 | 15 | 7.0
3 | 1000 | ∞
• • • • Observed curve
- - - - - - Computed curve

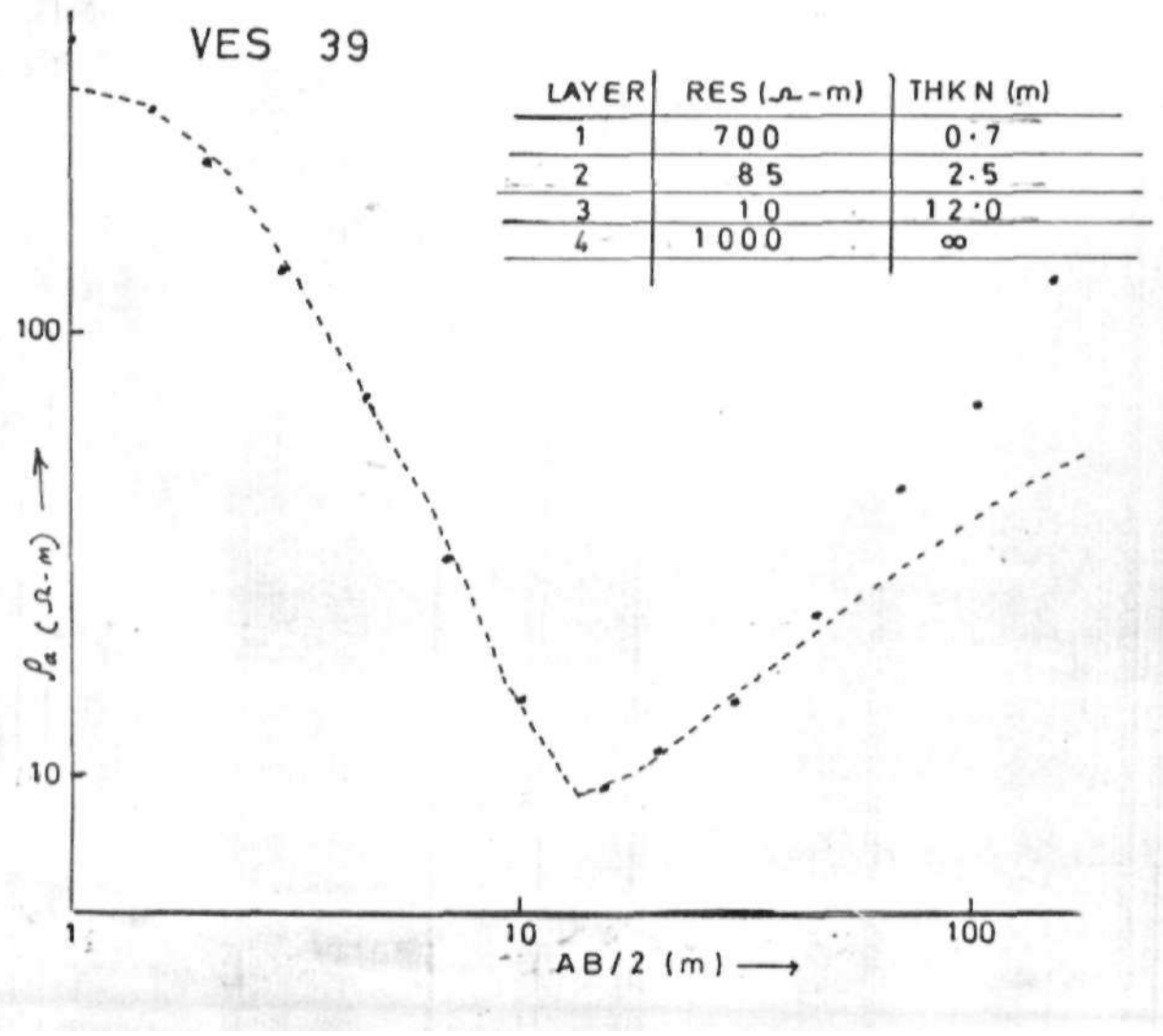

VES 37
100
10
ρ_a (Ω-m)
1
10
100
AB/2 (m)
LAYER | RES (Ω-m) | THKN (m)
1 | 300 | 0.6
2 | 25 | 11.0
3 | 2000 | ∞

VES 38



LAYER	RES(Ω-m)	THKN(m)
1	200	06
2	70	30
3	20	140
4	1000	∞

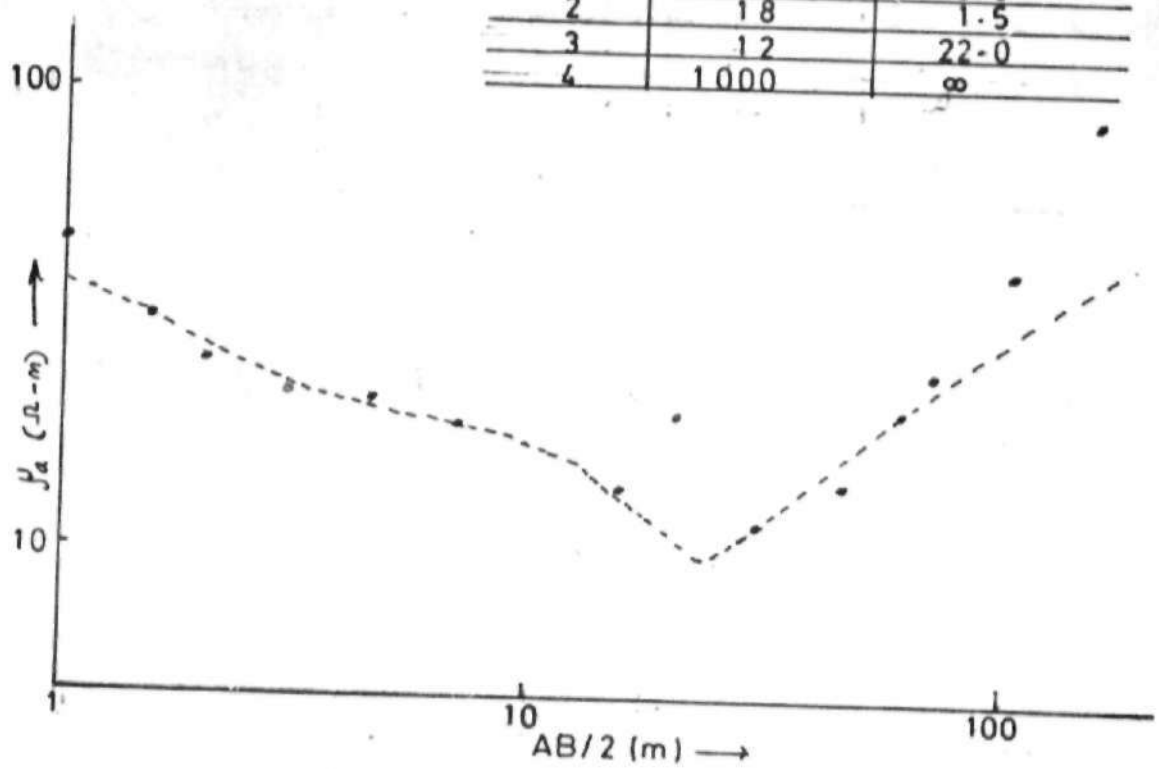
VES 39



LAYER	RES (Ω-m)	THKN (m)
1	700	0·7
2	85	2·5
3	10	12·0
4	1000	∞

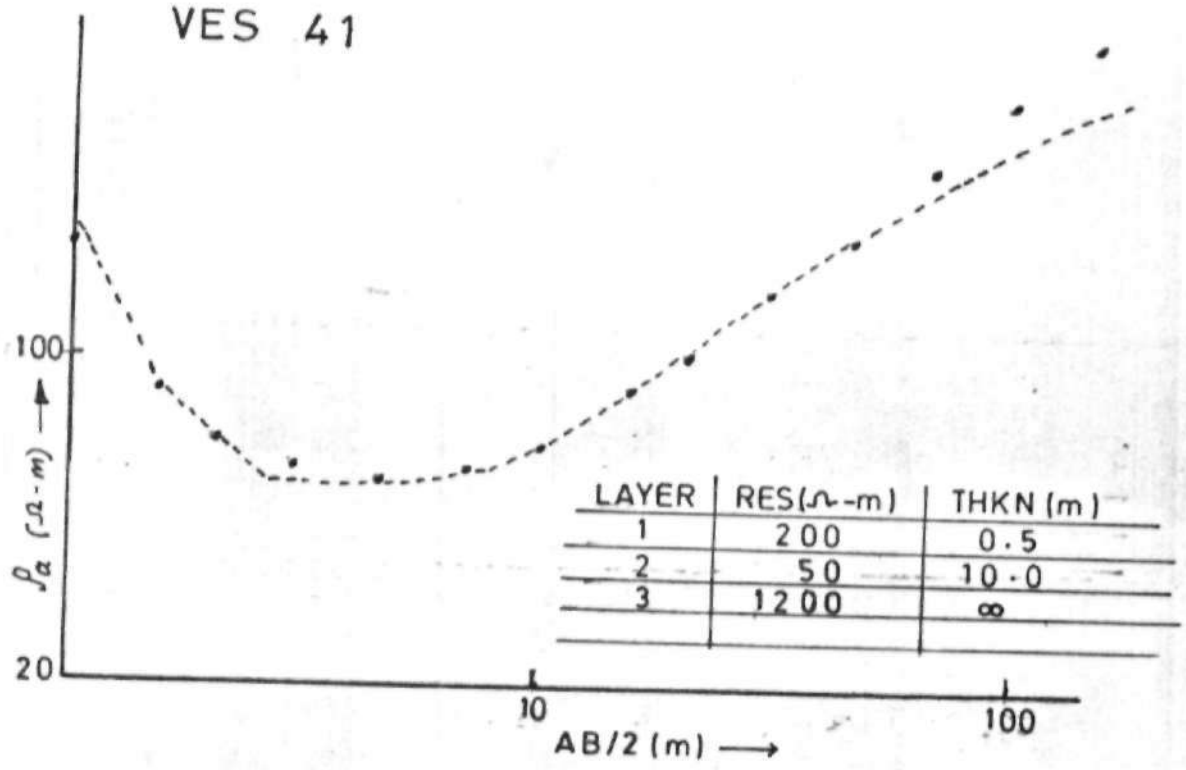
VES 40

LAYER	RES (Ω-m)	THKN (m)
1	40	0·6
2	18	1·5
3	12	22·0
4	1000	∞

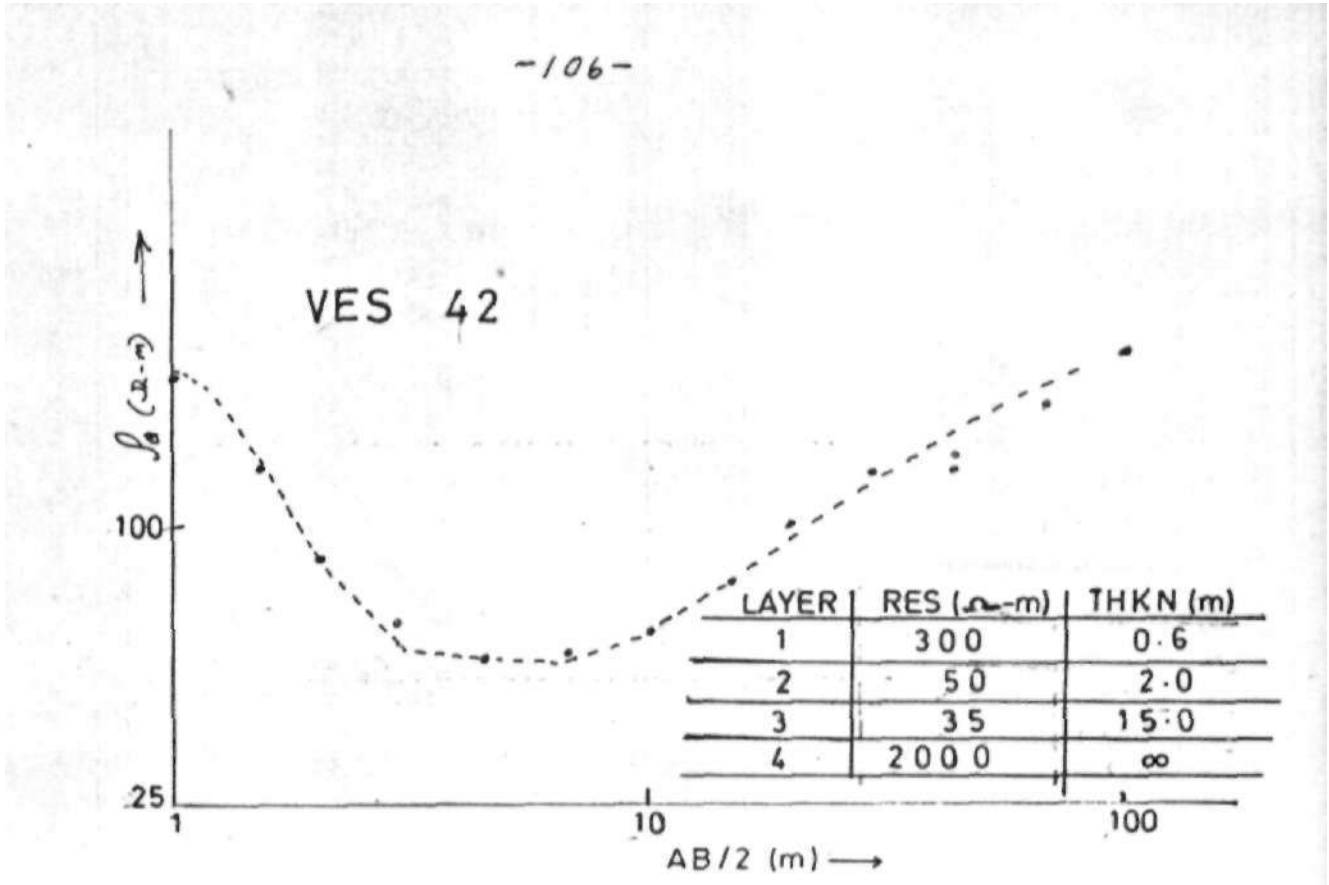


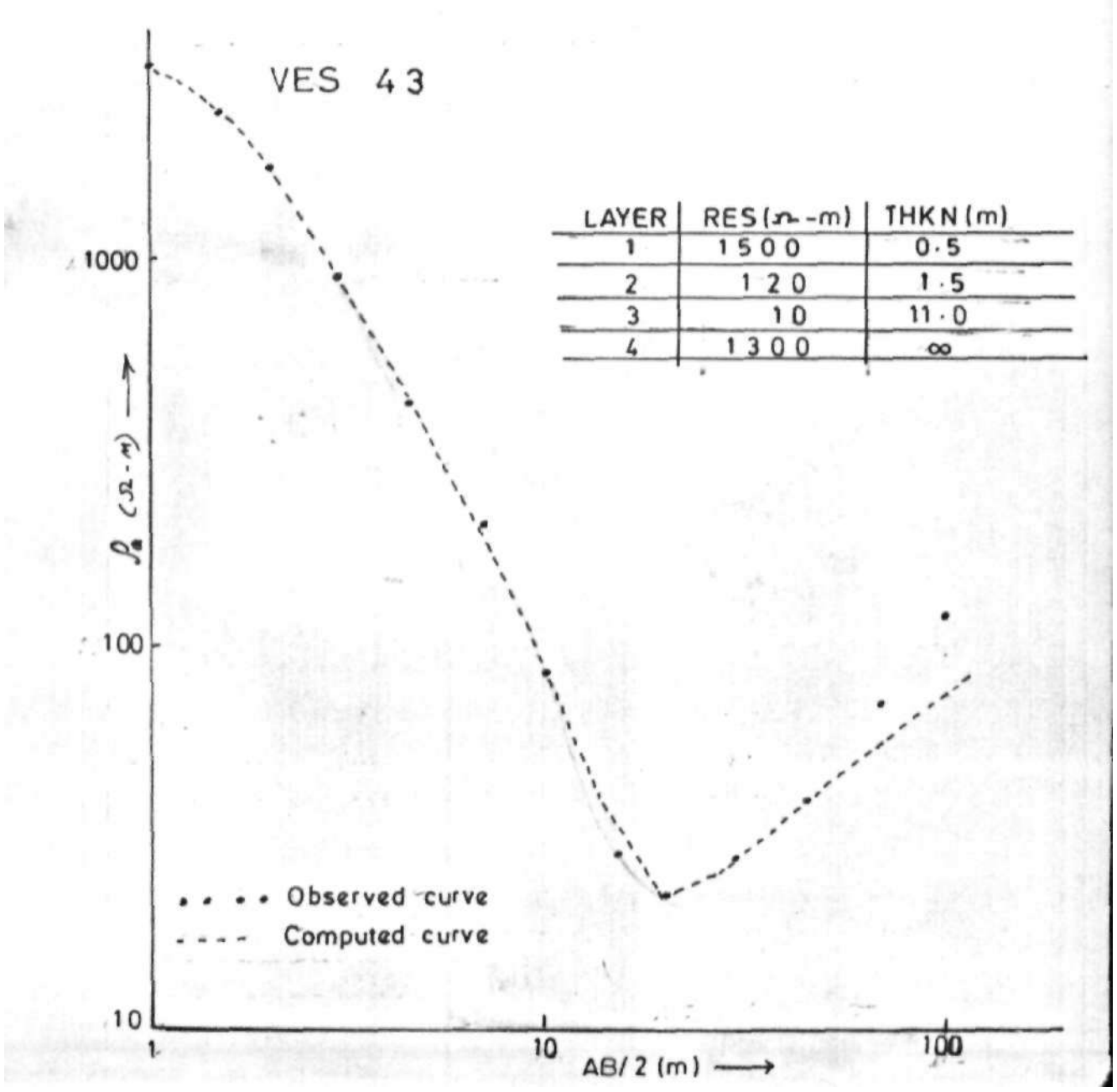
• • • • • Observed curve
– – – Computed curve

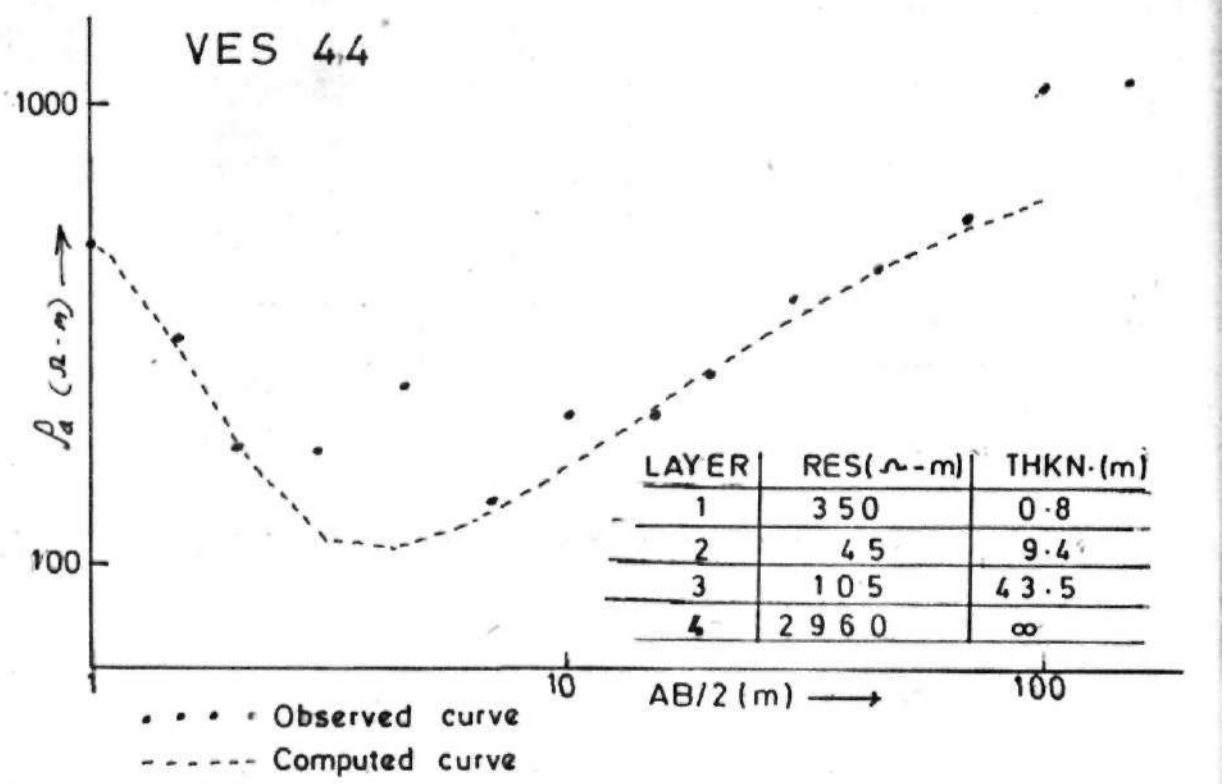
VES 41

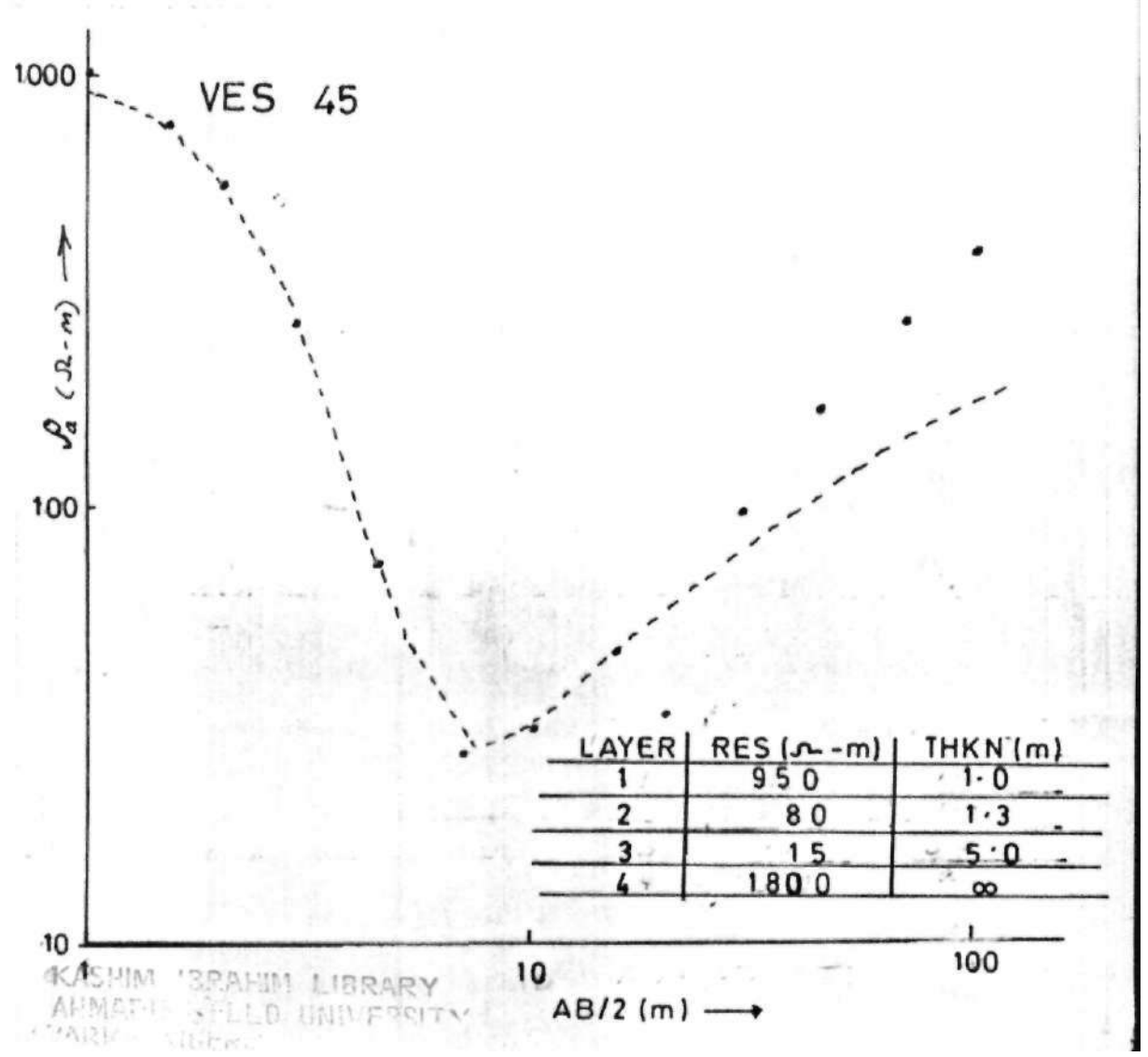


LAYER	RES(Ω-m)	THKN (m)
1	200	0.5
2	50	10·0
3	1200	∞


VES 42
ρ_a (Ω-m) ⟶
100
25
1
10
100
AB/2 (m) ⟶
LAYER | RES (Ω-m) | THKN (m)
1 | 300 | 0·6
2 | 50 | 2·0
3 | 35 | 15·0
4 | 2000 | ∞


VES 43
ρ_a (Ω-m) ⟶
1000
100
10
1
10
100
AB/2 (m) ⟶
LAYER | RES (Ω-m) | THKN (m)
1 | 1500 | 0·5
2 | 120 | 1·5
3 | 10 | 11·0
4 | 1300 | ∞
• • • • Observed curve
- - - - Computed curve





KASHIM IBRAHIM LIBRARY
AHMADU BELLO UNIVERSITY